

Capacitive current interruption with high voltage air-break disconnectors

Citation for published version (APA):

Chai, Y. (2012). *Capacitive current interruption with high voltage air-break disconnectors*. [Phd Thesis 1 (Research TU/e / Graduation TU/e), Electrical Engineering]. Technische Universiteit Eindhoven. <https://doi.org/10.6100/IR728755>

DOI:

[10.6100/IR728755](https://doi.org/10.6100/IR728755)

Document status and date:

Published: 01/01/2012

Document Version:

Publisher's PDF, also known as Version of Record (includes final page, issue and volume numbers)

Please check the document version of this publication:

- A submitted manuscript is the version of the article upon submission and before peer-review. There can be important differences between the submitted version and the official published version of record. People interested in the research are advised to contact the author for the final version of the publication, or visit the DOI to the publisher's website.
- The final author version and the galley proof are versions of the publication after peer review.
- The final published version features the final layout of the paper including the volume, issue and page numbers.

[Link to publication](#)

General rights

Copyright and moral rights for the publications made accessible in the public portal are retained by the authors and/or other copyright owners and it is a condition of accessing publications that users recognise and abide by the legal requirements associated with these rights.

- Users may download and print one copy of any publication from the public portal for the purpose of private study or research.
- You may not further distribute the material or use it for any profit-making activity or commercial gain
- You may freely distribute the URL identifying the publication in the public portal.

If the publication is distributed under the terms of Article 25fa of the Dutch Copyright Act, indicated by the "Taverne" license above, please follow below link for the End User Agreement:

www.tue.nl/taverne

Take down policy

If you believe that this document breaches copyright please contact us at:

openaccess@tue.nl

providing details and we will investigate your claim.

Capacitive Current Interruption with High Voltage Air-break Disconnectors

PROEFSCHRIFT

ter verkrijging van de graad van doctor aan de
Technische Universiteit Eindhoven, op gezag van de
rector magnificus, prof.dr.ir. C.J. van Duijn, voor een
commissie aangewezen door het College voor
Promoties in het openbaar te verdedigen
op woensdag 14 maart 2012 om 16.00 uur

door

Yajing Chai

geboren te Hubei, China

Dit proefschrift is goedgekeurd door de promotor:

prof.dr.ir. R.P.P. Smeets

Copromotor:

dr. P.A.A.F. Wouters

This project was funded by the Dutch Ministry of Economic Affairs,
Agriculture and Innovation in an IOP-EMVT program.

A catalogue record is available from the Eindhoven University
of Technology Library.

ISBN: 978-90-386-3097-7

To Miloš and Ruirui

Promotor:

prof.dr.ir. R.P.P. Smeets, Eindhoven University of Technology/KEMA
Testing, Inspections & Certification

Copromotor:

dr. P.A.A.F. Wouters, Eindhoven University of Technology

Core committee:

prof.ir. L. van der Sluis, Delft University of Technology
prof.dr-ing. V. Hinrichsen, Darmstadt University of Technology
prof.dr. E. Lomonova, Eindhoven University of Technology

Other members:

dr. D.F. Peelo, DF Peelo & Associates
prof.ir. W.L.Kling, Eindhoven University of Technology
prof.dr.ir. A.C.P.M. Backx (chairman), Eindhoven University of Technology

Summary

As low-cost switching devices in high voltage electrical power supply system disconnectors basically have an insulation function only. Nevertheless, they have a very limited capability to interrupt current (below one Ampere), e.g. from unloaded busbars or short overhead lines. The present study is a search for possibilities to increase the current interruption capability with auxiliary devices interacting with the switching arc. In this project the state of the art of disconnector switching is investigated and an inventory is presented of models of the free burning arc in air. A series of experiments were arranged at different laboratories. The switching arc and the interruption process are studied in detail through electrical and optical measurements during the switching process for a disconnector with (without) auxiliary devices under high voltage (0.5 – 30 A, 300 kV) conditions. Three options for auxiliary devices were investigated: (i) arc cooling by forced air flow; (ii) fast interrupting by high-velocity opening contacts; (iii) reduction of arc energy by adding resistive elements. Finally, a qualitative description is provided on the physical nature of the arc and how the evaluated methods affect the arc characteristics. All results are obtained by analysis of high-resolution measurement of arc current (including all relevant transients), voltages across the disconnector and high-speed video observation.

It was found that, depending on the current to be interrupted, the interruption process is governed by the dielectric and/or thermal processes.

In the dielectric regime, the interrupted current is low (roughly below 1 A) and the switching arc is characterized by a high rate of repetition of interruptions and re-strikes that only cease after a sufficient gap spacing has been reached. The re-strikes interact severely with the circuitry in which the disconnector is embedded, exciting transients in current and voltage with frequencies up to the megahertz range. High overvoltages can be generated. Their magnitudes can be limited by a proper choice of the capacitance at supply side of the disconnector. The arc-circuit interaction has been studied and relevant processes have been modelled and verified by experiments in full-power test-circuits.

In the thermal regime, the switching arc behaves less vehemently, interrupting and re-igniting basically occur at every power frequency current zero. Because of the presence of sufficient thermal energy in the switching gap along the arc path, the voltage to re-ignite the arc is limited, and the arc-circuit interaction is less pronounced. Though not producing very severe overvoltages, the arc duration is longer and the current may not be interrupted at every current zero crossing. The ultimate thermal regime is reached when the arc continues to exist after power frequency current zero without any appreciable voltage to re-ignite. This situation

must be avoided because arcing goes on until a higher level breaker interrupts the current. Before this, the arc can reach far away from its roots and can greatly reduce insulation clearance.

The main factors influencing the interruption performance are the level of current to be interrupted, the system voltage, the ratio of capacitances at both sides of the disconnecter and the gap length. These factors influence the energy supplied to the arc upon re-strike. This energy extends the arcing time by lowering the breakdown voltage. It has been observed that the arc in its thermal mode always re-ignites in its former trajectory. Key to the interruption process is the reduction of breakdown voltage in this path, created by hot gases remaining from the former arc. The existing breakdown models are reviewed in order to understand the influence of high temperature air on the breakdown process.

Based on the observed arc behaviour, various methods have been researched to increase the interruption capability.

The most successful methods are those that remove the residual (partially) ionized air from the arc path. Experiments were carried out to demonstrate the effectiveness of air flow directed into the arc's foot point. A substantial gain in interruption capability is demonstrated, but at the cost of generating re-ignition transients at a very rapid succession. Specifically, the experiments showed that 7.5 A could be interrupted successfully at 90 kVrms voltage with a shorter arcing duration (a factor of 0.5 was observed) than without air flow. With application of air flow, the frequency of re-ignitions occurring, and the breakdown voltage are much higher than without air flow.

Another method, the assistance of an auxiliary switch able to produce a very fast opening, was also successful. Herein, the arc is forced mechanically into ambient cool air, thus avoiding accumulation of thermal energy in the arc path. Specifically, it can interrupt currents up to 7 A at 100 kVrms safely and 9 A at 90 kVrms in the experiments with arcing time only a few tens of milliseconds instead of a few seconds. The arc exhibits a "stiff" (linear) character instead of the "erratic" (randomly moving) arc mode with a disconnecter alone. This method reduces the number of re-strikes.

The possible influence of energy absorbing elements (resistors) is investigated through circuit modelling, supported by some laboratory experiments. Other methods, such as the application of series auxiliary interrupting elements (vacuum, SF₆ interrupter and ablation assisted approaches) have been evaluated.

From the practical point of view, the auxiliary fast-opening interrupter is recommended due to its economic, simple and effective merits. Other approaches have certain disadvantages. The method with air flow needs a complex construction in order to introduce the compressed air flow into the disconnecter,

and the hazard for nearby equipments from the overvoltages caused by the interruption is greater. The method of inserted resistor requires very expensive arrangement. Regarding the application of auxiliary interrupters, vacuum interrupters have to be applied in considerable numbers in series and SF₆ interrupters have good performance but at very high cost. An ablation assisted approach seems less promising because the level of the interrupted current is too low to be effective.

Samenvatting

Scheidingsschakelaars, of kortweg "scheiders", zijn relatief eenvoudige schakelaars in hoogspanningsnetten die in principe enkel een isolerende functie hebben. Niettemin bezitten ze een zeer beperkt vermogen stromen (tot ca. 1 A) te onderbreken, zoals bijv. afkomstig van onbelaste railsystemen of korte hoogspanningslijnen. Deze studie bevat een onderzoek naar mogelijkheden het stroom onderbrekend vermogen van scheiders te vergroten met hulpmiddelen die direct ingrijpen in de schakelende lichtboog. Om te beginnen is de stand van de techniek op het gebied van schakelen met scheiders onderzocht en er wordt een overzicht gegeven van het modelleren van vrij brandende lichtbogen in lucht. Tevens is een serie experimenten uitgevoerd in diverse laboratoria. Hierin zijn de schakelende lichtboog en het onderbrekingsproces in detail bestudeerd door middel van elektrische en optische metingen gedurende het schakelen onder hoogspanning (0.5 – 30 A, 300 kV) met en zonder hulpmiddelen. Drie mogelijk hulpmiddelen zijn onderzocht: (i) koeling van de lichtboog door beblazing met een geforceerde luchtstroom; (ii) onderbreking met zeer snelle contact separatie snelheid; (iii) reductie van lichtboog energie door toevoeging van resistieve componenten. Tot slot wordt een kwantitatieve beschrijving gegeven van de lichtboog en hoe de boven beschreven methoden ingrijpen in diverse karakteristieken van de lichtboog.

Alle resultaten zijn verkregen met behulp van metingen met hoge resolutie van lichtboog stroom en – spanning (inclusief hun transiënten) alsmede door observatie met snelle video technieken.

Afhankelijk van de grootte van de te onderbreken stroom, wordt het onderbrekingsproces gekenmerkt door diëlektrische en/of thermische processen. In het diëlektrische regime is de te onderbreken stroom klein (ruwweg beneden 1 A) en de scheider lichtboog wordt gekenmerkt door een zeer snelle opeenvolging van onderbrekingen en herontstekingen. Dit proces stopt wanneer voldoende contactafstand is bereikt. Als gevolg van de herontstekingen is er een heftige wisselwerking met het elektrische circuit waar de scheider deel van uitmaakt. Herontstekingen wekken daarbij transiënten op in zowel stroom als spanning met frequenties tot enkele megahertz. Hoge overspanningen kunnen hierbij optreden. De hoogte hiervan kan worden beperkt door een juiste keuze van capaciteit aan de voedende zijde van de scheider. De wisselwerking tussen lichtboog en circuit is bestudeerd; de relevante processen zijn gemodelleerd en getoetst met experimenten in hoogvermogen beproevingscircuits.

In het thermische regime gedraagt de lichtboog zich minder heftig, onderbreekt de stroom en herontsteekt in principe pas op iedere nuldoorgang van de netfrequente stroom. Vanwege de aanwezigheid van voldoende thermische

energie in het lichtboog pad tussen de contacten is de spanning nodig om de boog te herontsteken beperkt en daarmee is de wisselwerking tussen lichtboog en circuit minder uitgesproken. Hoewel de overspanningen beperkt zijn, is de lichtboogduur langer en wordt de stroom niet bij iedere netfrequente nuldoorgang onderbroken. De meest uitgesproken thermische verschijningsvorm is die waarin (bij verdere verhoging van de stroom) de lichtboog bij elke nuldoorgang herontsteekt zonder meetbare spanning. Deze situatie dient vermeden te worden omdat de lichtboog in deze situatie niet meer dooft en de stroom enkel nog door een vermogensschakelaar onderbroken kan worden. Hieraan voorafgaand kan de lichtboog ver uitwaaiëren en de isolatie afstand tot andere, onder spanning staande delen in het station (te zeer) verkleinen.

De belangrijkste factoren die het onderbrekingsproces beïnvloeden zijn de hoogte van de te onderbreken stroom, de netspanning, de verhouding van capaciteiten ter weerszijden van de scheider en de momentane contactafstand. Deze parameters bepalen de energie die aan de lichtboog wordt toegevoerd op het moment van herontsteking. Deze energie verlengt de lichtboogduur doordat deze de doorslagspanning reduceert. Uit waarneming blijkt dat in het thermisch regime de lichtboog herontsteekt in het voormalige lichtboog pad. Hieruit wordt afgeleid dat de essentie van het onderbrekingsproces de reductie van doorslagspanning langs dit pad is. Deze reductie wordt veroorzaakt door hete gassen en rest-ionisatie afkomstig van de (vorige) lichtboog. Voor het begrijpen van de processen die leiden tot reductie van doorslagspanning bij temperatuur verhoging van de lucht zijn de bestaande doorslag modellen bestudeerd.

Op basis van de boven beschreven waarnemingen van het onderbrekingproces zijn diverse methoden onderzocht die kunnen leiden tot vergroting van het stroom onderbrekend vermogen van scheidingsmiddelen.

Het meest succesvol zijn methoden die de gedeeltelijke geïoniseerde lucht verwijderen uit het voormalige lichtboog pad. Experimenten zijn uitgevoerd waarin de effectiviteit bestudeerd wordt van beblazing van de voetpunten van de lichtboog met koude lucht. Een significante verhoging van stroom onderbrekend vermogen wordt inderdaad vastgesteld, echter ten koste van de generatie van zeer snel opvolgende en hoge herontstekingen die steile spanningfronten genereren. De experimenten tonen aan dat bij een fase-aarde spanning van 90 kV stromen tot ca. 7.5 A succesvol onderbroken worden met een 50% kortere lichtboogduur dan zonder beblazing.

Een andere methode bestaande uit het gebruik van zeer snel opende hulpcontacten om daarmee in zeer korte tijd een grote contactafstand te realiseren, blijkt eveneens succesvol. Op deze wijze worden de lichtboog voetpunten zeer snel naar koele lucht getrokken waardoor een te grote thermische energie dichtheid voorkomen wordt. Op deze manier kunnen stromen van 7 A (bij 100 kV) en 9 A (bij 90 kV) onderbroken worden, terwijl de

lichtboogduur slechts enkele tientallen milliseconden bedraagt in plaats van seconden bij toepassing van conventionele contacten. De uiterlijke verschijningsvorm van de boog verandert hierbij van "dansend" (opwaarts bewegend met vele uitstulpingen) naar "strak" (rechtlijnig brandend als kortste verbinding tussen de contacten). Het aantal herontstekingen blijft hier mee ook beperkt.

Ook de mogelijke invloed van energie absorberende elementen (weerstand) is onderzocht met modellering, ondersteund met enige laboratorium experimenten. Alternatieven, zoals het gebruik van serie geschakelde onderbrekers (vacuüm-, SF₆ onderbrekers en onderbreking gebaseerd op ablatie) zijn geëvalueerd uit de literatuur.

Ter vergroting van het stroom onderbrekend vermogen wordt vanuit praktisch oogpunt de methode met de snelle hulpcontacten aanbevolen vanwege prestatie, eenvoud en prijs. Andere methoden hebben duidelijke nadelen. Beblazing met lucht vereist een ingewikkelde constructie om gecompriëerde lucht in de nabijheid van de schakelende contacten te brengen en heeft als bijkomend nadeel de generatie van steile spanningsfronten tijdens de onderbreking. Het aanbrengen van weerstanden vereist dure aanpassingen. Hulp onderbrekers in vacuüm of SF₆ gas is effectief maar kostbaar en constructief ingewikkeld vanwege de hoogte van de spanning die serie schakeling van elementen vaak nodig maakt. Oplossingen met behulp van ablatie zijn minder kansrijk omdat de stroom hiervoor waarschijnlijk te laag is.

Contents

SUMMARY	I
SAMENVATTING	V
CONTENTS	IX
CHAPTER 1	1
HIGH VOLTAGE AIR-BREAK DISCONNECTORS	1
1.1 DEFINITION OF DISCONNECTORS	1
1.2 TYPE OF DISCONNECTORS	1
1.3 INTERRUPTING CURRENT WITH DISCONNECTORS.....	3
1.4 STANDARDIZATION STATUS	4
1.5 OBJECTIVE OF THESIS	5
CHAPTER 2	9
LITERATURE REVIEW	9
2.1 AWARENESS OF THE CAPACITIVE CURRENT INTERRUPTION WITH DISCONNECTORS.....	9
2.2 FUNDAMENTAL ASPECTS OF CAPACITIVE CURRENT INTERRUPTION.....	14
2.3 TRANSIENTS CAUSED BY CAPACITIVE CURRENT INTERRUPTION	16
2.4 APPROACHES TO ENHANCE THE INTERRUPTION CAPABILITY	17
2.5 ARC MODELS RELATED TO CURRENT INTERRUPTION WITH A DISCONNECTOR	26
2.6 CONCLUSION	29
CHAPTER 3	35
BASIC CIRCUIT ANALYSIS	35
3.1 THE INTERRUPTION PROCESS.....	35
3.2 THREE-COMPONENTS ANALYSIS.....	37
3.3 SIMULATION OF RE-STRIKES.....	41
3.4 RE-STRIKE TRANSIENTS IN DISTRIBUTED ELEMENT LOAD CIRCUITS.....	43
3.5 CONCLUSION	45
CHAPTER 4	47
EXPERIMENTAL SETUP	47
4.1 HIGH VOLTAGE SOURCE.....	47
4.2 MEASUREMENT SYSTEM.....	51
4.3 DISCONNECTOR MAIN BLADES OPENING VELOCITY	57
4.4 CONCLUSION	59

CHAPTER 5	61
CURRENT INTERRUPTION MECHANISM	61
5.1 EXPERIMENTAL OBSERVATIONS	61
5.2 ARC INTERRUPTION CHARACTERISTICS	69
5.3 DISCONNECTOR CONTACTS SPACING	75
5.4 RE-STRIKE VOLTAGE	76
5.5 ELECTRICAL ARC CHARACTERISTICS	80
5.6 ENERGY INPUT INTO THE ARC	82
5.7 TRANSIENTS UPON RE-STRIKE	85
5.8 CONCLUSION	88
5.9 RECOMMENDATION FOR STANDARDIZATION	90
CHAPTER 6	91
INTERRUPTION WITH AIR FLOW ASSISTANCE.....	91
6.1 EXPERIMENTAL SETUP	91
6.2 EFFECT OF AIR FLOW ON ARCING.....	92
6.3 INTERRUPTION DATA ANALYSIS.....	97
6.4 CONCLUSION	103
CHAPTER 7	107
HIGH-VELOCITY OPENING AUXILIARY INTERRUPTER	107
7.1 OPERATING PRINCIPLE	107
7.2 EXPERIMENTAL SETUP	108
7.3 OVERVIEW OF THE EXPERIMENTAL RESULTS	109
7.4 RE-STRIKE VOLTAGE.....	114
7.5 ENERGY INPUT INTO THE ARC	117
7.6 CONCLUSION AND RECOMMENDATION	120
CHAPTER 8	123
INTERRUPTION WITH INSERTED RESISTORS.....	123
8.1 SERIES RESISTOR	123
8.2 PARALLEL RESISTOR	128
8.3 DISCUSSION	130
CHAPTER 9	133
PRE-BREAKDOWN PHENOMENA IN DISCONNECTOR INTERRUPTION.....	133
9.1 CLASSICAL MODELLING OF BREAKDOWN.....	133
9.2 PRE-BREAKDOWN CURRENT IN DISCONNECTOR INTERRUPTION	137
9.3 DISCUSSION	138

CHAPTER 10.....	141
CONCLUSIONS AND RECOMMENDATIONS FOR FUTURE RESEARCH	141
10.1 CONCLUSIONS.....	141
10.2 PROPOSED FUTURE RESEARCH	146
PUBLICATIONS RELATED TO THIS WORK.....	147
NOMENCLATURE	149
ACKNOWLEDGEMENT	153
CURRICULUM VITAE	155

Chapter 1

High Voltage Air-break Disconnectors

1.1 Definition of disconnectors

High voltage disconnectors are commonly used switching devices in power substations. According to the International Electro-technical Vocabulary IEC number 441-14-05 [1], the definition of a disconnector (DS) is: "A mechanical switching device, which provides, in the open position, an isolating distance in accordance with specified requirements". In IEEE standard C37.100-1992 [2], instead of the term "disconnector", the terms "disconnecting", "disconnect switch" or "isolator" are used, defined as "A mechanical switching device used for changing the connections in a circuit, or for isolating a circuit or equipment from the source of power." Both definitions are similar. They define that the principle function of DSs is to provide electrical and visible isolation from the system. In addition, they must open and close reliably, carry current continuously without overheating, and remain in the closed position under fault current conditions [3]. The disconnection generally covers two aspects [4]:

- Disconnection related to ordinary daily operation of the system.
- Disconnection related to maintenance of transmission lines or substation equipment such as transformers, circuit breakers, capacitor banks and so on. For power system, personnel safety practices normally require a visible break as a point of isolation. An open DS meets this requirement.

1.2 Type of disconnectors

DSs in Gas Insulated Substations are out of the scope of this thesis. Only high voltage DSs in the atmospheric air are studied. The HV air-break DS comes in a variety of types and mounting arrangements. The most common four configurations are: vertical-break, centre-break, double-break, and pantograph type. They can be mounted in various orientations, depending on the space offered by the substation [3], [4].

The vertical-break DS is presented in Figure 1.1 (left). This type of DS is highly suitable in icy environments thanks to its rotating blades design. Its contact design allows for application in installations where high fault current situations may occur. The active parts of this type DS are the hinge end assembly, the blade, and the jaw end assembly. The smaller of the two insulators at the left rotates and gives the blade to open or close. It is usually horizontally mounted as shown in



Figure 1.1. (left) A three-phase vertical-break DS mounted horizontally in a closed position (Courtesy of HAPAM B.V.); (right) centre-break DS in a closed position (Courtesy of Siemens).

Figure 1.1 (left). It can also be vertically mounted, i.e. the blade is vertically oriented in closed position. The vertical-break DS requires minimum phase spacing.

An example of a centre-break DS is illustrated in Figure 1.1 (right). This type DS is used mainly in locations with low overhead clearances. However, it requires larger phase spacing than a vertical-break DS. The active parts consist of two blades, disconnecting at the centre. Both insulators rotate in a vertical plane to open or close the DS.

A double-break DS is a variation of a centre-break type and is shown in Figure 1.2 (left). The active parts are two jaw assemblies, one at each end, and a rotating blade. The centre insulator rotates to open or close the DS. They can be installed in minimum overhead clearance locations and require minimum phase spacing. Their field of application includes icy environments due to the rotating blades design and installations in high fault current locations due to the contact design. This design provides for two gaps per phase, allowing to interrupt significantly higher current than the single-break type DSs [3], [4]. This is because the system voltage is distributed across two gaps.

The pantograph DS type, shown in Figure 1.2 (right), is used worldwide (but only occasionally in North America) for Extra High Voltage application, 345-800 kV. The active parts consist of a fixed contacts arrangement attached to the busbar at the top, a scissor type blade and a hinge assembly at the bottom. The smaller one of the two insulators rotates to open or close the DS. This type DS normally provides transitions from high to low busbars, together with providing visible separation at the same time. This method requires the least space.



Figure 1.2. (left) Double-break DS in an open position; (right) pantograph DS in a closed position (Courtesy of HAPAM B.V).

1.3 Interrupting current with disconnectors

Disconnectors disconnect unloaded circuits in order to accomplish visible isolation. However, they are operated under energized conditions and will therefore interrupt some current. The magnitude of this current depends on the specific situations. Although DSs do not have any current interruption rating, they do have a certain interrupting capability, but it is limited due to their slowly moving contacts. Over the years DSs have been applied to interrupt transformer excitation currents, capacitive currents from short lengths of bus, cable or overhead line and small load currents. In this case, very small current is interrupted against full system recovery voltage (RV). Another major application is bus transfer switching. In this case, often the full load current has to be transferred into a parallel path. Because of many different conditions under which the DSs must interrupt currents, no interrupting ratings are assigned [5].

The main applications where a current is to be interrupted are [4]:

- Transformer magnetizing current

It is also called excitation current. The current is usually less than 2 A, often less than 1 A at 100% excitation voltage, for today's transformers. The current is generally described in terms of an equivalent RMS value derived from the core loss measurement by the manufacturer.

- Capacitive current

This current, also called charging current, arises from connected short busbars, short unloaded transmission line, instrument transformers and other elements having stray capacitance. They act as a capacitive load. The typical range of these currents for station air-break equipment is shown in Table 1.1 [6].

Table 1.1 Typical capacitive current range in outdoor substations (50 Hz).

Equipment	Capacitive current (A)					
	72.5 kV	145 kV	245 kV	300 kV	420 kV	550 kV
CT	≤0.04	≤0.04	≤0.04	0.05	0.08	0.1
CVT (4 μF)	0.05	0.11	0.18	0.22	0.3	0.4
Busbars/m	1.7×10^{-4}	0.32×10^{-3}	0.54×10^{-3}	0.66×10^{-3}	0.84×10^{-3}	1.1×10^{-3}

- Loop current

Loops are created when the DS commutes or transfers current from one circuit, such as a busbar or transmission line, to a parallel circuit. The loop current can reach up to the full load current in practice. This current has to be switched against a very low voltage (the voltage across the parallel path) [4].

1.4 Standardization status

A small current interruption capability of the DSs has been recognized by both IEEE and IEC standards. In the IEC standard [7], apart from the definition and basic function of the DS, the current interrupting capability is addressed in three notes:

NOTE 1: A disconnecter is capable of opening and closing a circuit when either negligible current is broken or made, or when no significant change in the voltage across the terminals of each of the poles of the disconnecter occurs.

NOTE 2: "Negligible current" implies currents such as the capacitive currents of bushings, busbars, connections, very short lengths of cable, currents of permanently connected grading impedances of circuit-breakers and currents of voltage transformers and dividers. For rated voltages of 420 kV and below, a current not exceeding 0.5 A is a negligible current for the purpose of this definition; for rated voltage above 420 kV and currents exceeding 0.5 A, the manufacturer should be consulted.

NOTE 3: For a disconnecter having a rated voltage of 52 kV and above, a rated ability of bus transfer current switching may be assigned.

Similarly in the IEEE standard [8], the following note is made:

NOTE: It is required to carry normal load current continuously, and also abnormal or short-circuit currents for short intervals as specified. It is also required to open or close circuits either when negligible current is broken or made, or when no significant change in the voltage across the terminals of each of the switch poles occurs.

An earlier version of the IEEE standard did include the following note and indicated the three types of current without explanation [9].

NOTE: A disconnecting switch and a horn-gap switch have no interrupting rating. However, it is recognized that they may be required to interrupt the charging current of adjacent buses, supports and bushings. Under certain conditions, they may interrupt other relatively low currents, such as:

- 1. Transformer magnetizing current.*
- 2. Charging currents of lines depending on length, voltage, insulation and other local conditions.*
- 3. Small load currents.*

Apart from the above recognition, there are no standards or required ratings for the current interruption by DSs. Both standards only refer to the current capability of the DS, and both use the word "negligible" to qualify the small current. Both point out the potential current types and the possible source, which causes these small currents. The difference between the two standards is that the IEC standard defines the meaning of "negligible current" and quantifies the corresponding current levels, whereas the IEEE standard does not. Reference [6] gave the typical range of these currents for station air-break equipment from 72.5 kV to 1200 kV. This is the newest IEC technical report, released in 2009, which describes the capacitive current switching duty for high voltage air-break DSs for rated voltages above 52 kV and provides guidance on laboratory testing to demonstrate the switching capability. This is also the first time to provide an analysis of the switching duty and to define testing procedures.

1.5 Objective of thesis

Among these three main applications of current interruption using DSs, loop current interruption has been investigated in detail in [4]. As compared to inductive current (excitation current) and resistive current switching, a capacitive current is a more challenging to interrupt because of the trapped charge remaining on the load to be switched (Chapters 3, 5). In the IEEE standard [8], the essential difference between capacitive current and excitation current is pointed out as:

"This type of capacitive interruption is similar to excitation current interruption in which there is a succession of interruptions near zero current, each followed by re-strikes. The difference between the two types of interruptions is that for each capacitive current interruption, a charge is more likely to be retained by the capacitive device. Each of these trapped charges creates an additive bias voltage that increases the probability of re-striking across the open gap of the switch 1/2cycle later when the source voltage has reversed its polarity. Consequently, longer arc reaches have been experienced when switching capacitive currents than when switching excitation currents. "

Certainly compared with switching on the capacitive current with DSs, switching off (interrupting) capacitive current is a more severe task.

It was mentioned that a so-called "negligible current" does not exceed 0.5 A for rated voltages of 420 kV and below. In the past, the current interrupting capability of air-break DSs therefore has been taken as 0.5 A or less. However, at present with the fast development of power networks, user's requirement for small capacitive current interruption using air-break DSs is frequently higher due to complexity of the network or financial reasons. The subject of this thesis "Interruption of capacitive current by HV air-break disconnectors" addresses the challenging task of interrupting relatively large capacitive currents (up to few tens of amperes).

Capacitive current interruption with a DS consists microscopically of a succession of interactive events between the power circuit and the AC arc with a repetitive sequence of interruptions, re-ignitions/re-strikes. The arc re-establishment is characterized in terms of oscillations and transients of current and voltage, recovery voltage. The interruption process is characterized in terms of arc duration, arc reach (perpendicular distance of outermost arc position to a line connecting the contacts), arc type (repetitive or continuous), arc brightness, energy input into the arc, and so forth.

This dissertation will particularly focus on:

- The principle mechanism of the capacitive current interruption using HV air-break DSs. It includes the transient voltage and current, energy input of the circuit, re-strike voltage, etc.
- The phenomena of the switching arc, including different features, such as arc voltage, arc current and other physical characteristics such as arc brightness, arc length, arc duration, arc reach, arc height, based on the analysis of data from optical and electrical experiments.
- Influencing factors on the transient and arc phenomena, which include the ratio of the source and load side capacitances, power supply voltage, current level to be interrupted and re-strike voltage from the electrical side. From the physical side, the influences of (forced) arc cooling and (forced) elongation are analyzed experimentally.
- The breakdown voltage and the pre-breakdown mechanism in the air during the numerous re-ignitions and re-strikes.
- Approaches to enhance the interruption capability.
 - i. An air flow system assisting arc quenching
 - ii. Auxiliary high-velocity contacts
 - iii. Insertion of resistors into the circuit
 - iv. Other approaches (discussion only)

The research is carried out based on experiments in different laboratories. Development and preliminary experiments are done at the high voltage laboratory of Eindhoven University of Technology. Full scale tests are performed at KEMA High Power Laboratories in Arnhem and Prague. The test object DSs are supplied by HAPAM B.V., the Netherlands.

References

- [1] IEV number 441-14-05, [online].
Available:<http://std.iec.ch/iev/iev.nsf/display?openform&ievref=441-14-05>.
- [2] *IEEE Standard Definitions for Power Switchgear*, IEEE Standard C37.100-1992, Oct. 1992.
- [3] J. D. McDonald, *Electric Power Substations Engineering*, London: CRC press, 2007.
- [4] D. F. Peelo, "Current interruption using high voltage air-break disconnectors", Ph.D. dissertation, Dept. Electrical Engineering, Eindhoven Univ. of Technology, Eindhoven, 2004.
- [5] *IEEE Guide to Current Interruption with Horn-Gap Air Switches*, American National Standard (ANSI) IEEE Standard C37.36b-1990, Jul. 1990.
- [6] IEC Technical Report IEC/TR 62271-305, "High voltage switchgear and controlgear-Part 305: Capacitive current switching capability of air-insulated disconnectors for rated voltages above 52 kV", Nov. 2009.
- [7] *IEC Standard on "High voltage switchgear and control gear-Part 102: Alternating current disconnectors and earthing switches"*, IEC 62271-102, Dec. 2001.
- [8] *IEEE Standard Definitions and Requirements for High Voltage air switches, insulators, and bus supports*, American National Standard (ANSI) IEEE Standard C37.30h-1978, Jun. 1978.
- [9] *American National Standard Definitions and Requirements for High voltage Air Switches, Insulators, and Bus Supports*, American National Standard (ANSI) IEEE Standard C37.30-1971, Apr. 1971.

Chapter 2

Literature Review

From the huge number of publications on devices applied in power systems, there appears to exist only a limited amount of papers on air-break DSs. Especially, only a few of them are actually concerned with the phenomena related to fairly small capacitive current interruption with DSs in high voltage systems. The review presented in this chapter is based on selected papers (partly) related to interruption of small capacitive current. In particular this chapter will involve five topics:

- Engineering guidelines on current interruption with air-break DSs.
- Fundamental aspects of capacitive current interruption with a stand-alone DS (i.e. without any auxiliary devices to aid interruption).
- Transients caused by DS switching.
- Approaches to improve capacitive current interrupting capability of the DS.
- Possible arc models related to the current topic.

2.1 Awareness of the capacitive current interruption with disconnectors

F. E. Andrews et al. belonged to the earliest authors on the field of current interruption with air-break DSs. They carried out numerous laboratory tests on transformer excitation current, loop current switching at 33 kV level and line dropping at 132 kV using DSs with horn-gap on the Public Service Company of Northern Illinois, USA, in the 1940s. The results were published in a thesis [1] and in a subsequent paper [2]. A typical horn gap device (also called arcing horn) is shown in Figure 2.1. The horn gap normally acts as the last point of metal-to-metal contact on the DS when opening. Thus the arc burns between the arcing horn rather than between the main blades of the DS. The goal of these tests was to find the correlation between the voltage across the DS after switching off and the interrupted current on one hand, and the arc length, reach on the other hand. The arc length was defined as the complete length of the irregular path followed by the arc. The arc reach was defined as the distance from a point midway between the blade ends to the most remote point of the arc at the time of its maximum length (see Figure 2.2). It was recognized that the arc length scaled proportional to the arc voltage. The main attention was paid to "arc reach", since it was considered to be more significant than the "arc length" in switching operations if the phase-to-phase and phase-to-ground clearance were considered [2]. For this reason the arc reach has been taken as a measure to provide a criterion for switching clearance.

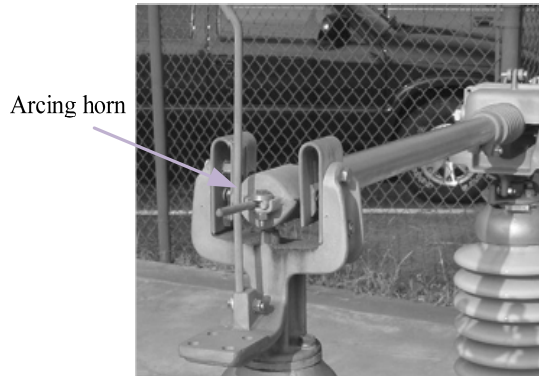


Figure 2.1. Arcing horn mounted on a vertical-break DS (copied from [50]).

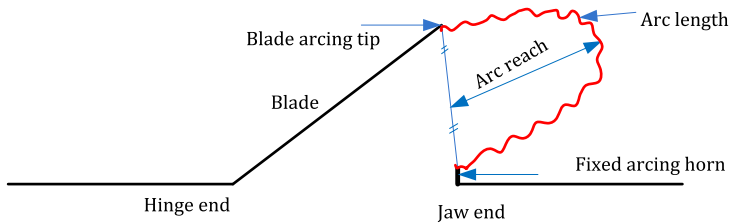


Figure 2.2. Definition of arc reach and length according to Andrews et al. [2].

The overall results plotted in Figure 2.3, copied from [2], present the arc reach in terms of "feet per kilovolt" as a function of initial interrupted current. From the results, the critical limits described the "Limit of the Probable Reach" (LPR) of the arc, were derived for excitation current and loop current interruption:

$$\begin{aligned} LPR &= 5.03U_{oc}I, \text{ when } 0 < I < 100 \text{ A} \\ LPR &= 503U_{oc}, \text{ when } 100 \leq I < 320 \text{ A} \end{aligned} \quad (2.1)$$

where LPR is in millimetres, U_{oc} the voltage across the DS after switching off is in kilovolts of rms, and I is the initial interrupted current in ampere of rms. The LPR for current levels below 100 A was confirmed by later literature [3]-[6]. In particular, [3] and [4] confirmed that (2.1) was valid for interrupting a magnetizing current of 1.73 A at 242 kV, and for currents of up to 9 A at voltages up to 735 kV respectively. In [5] and [6] it was stated that there was good agreement between the results and (2.1). Equation (2.1) has been frequently cited by utilities and DSs manufactures later on, and is also included in the Standard IEEE C37.36b-1990 [7].

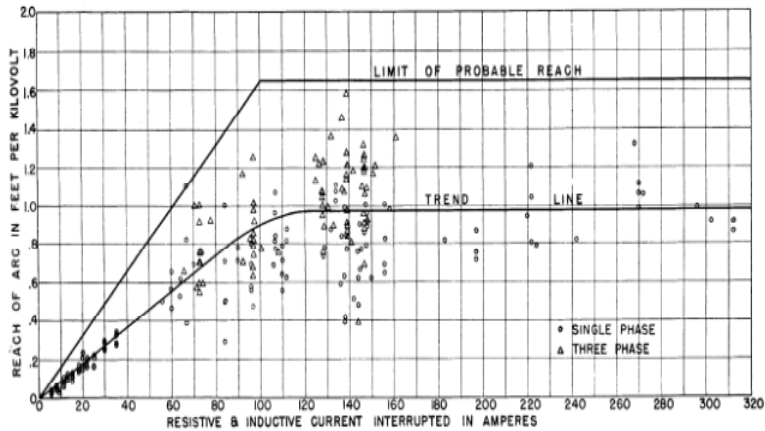


Figure 2.3. Arc reach per kilovolt as a function of the interrupted current, copied from [2].

The test on the capacitive current interruption, performed in [2], showed it was safe to drop a 27 km line (about 7 A charging current) at 132 kV for a 5 m horizontal phase spacing owing to a favourable oblique wind. In addition, it was pointed out the arc reach from the capacitive current interruption was clearly larger than that from the excitation and loop current interruption observed in the laboratory tests. Consequently, for the voltage used for the calculation of the arc reach from interrupting capacitive current probably value twice of the actual voltage was taken. No further information on this issue was provided.

Two AIEE committee reports, which are cited frequently, are of interest [8], [9]. The initial goal of the study reported in [8] was to investigate the transformer magnetizing current and its effect on relaying and DS operation. In addition, the interruption of (capacitive) overhead line charging current by a horn-gap was surveyed in 1949 by distribution of a questionnaire to 250 utilities, of which 59 responded. The main results are presented in Figure 2.4. About 70% of the responses indicated 100% success with a limited current range (e.g. 22 A at 66 kV, 13 A at 118 kV).

A more recent survey on line and cable charging current interruption with DSs was made in 1962 amongst 71 utilities to collect the operating practice and experience of utilities [9], the results of which are shown in Figure 2.5 and 2.6.

In Figure 2.5 the utility responses were divided into three categories, stating 100% successful, 90-99% successful, and less than 90% successful operations in line charging current interruption. For cable charging interruption (Figure 2.6) all operations reported were successful, but the total number of operations was very small (only 12 operations were reported).

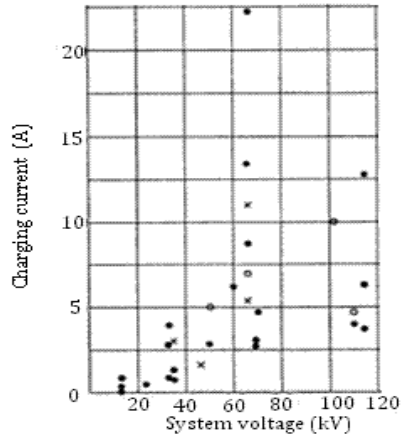


Figure 2.4. Interruption of overhead line charging current by a horn-gap DS (copied from [8]). Note: ●: signifies 100% successful operation; ○: signifies 90%-99% successful operation; ×: signifies 75%-80% successful operation.

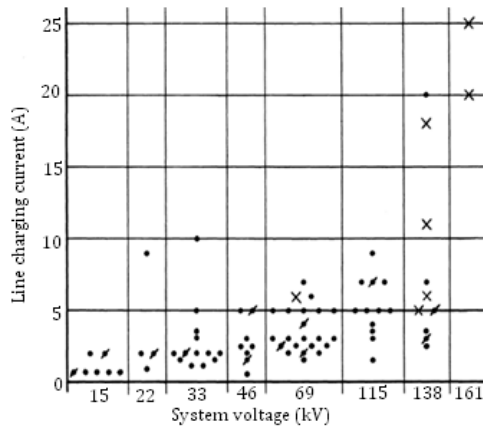


Figure 2.5. Company experiences reported on the use of air-break DS for interruption of line charging current. Note: ●: grounded-100% successful, ◐: grounded-90%-99% successful, X: companies using quick-break or other similar devices. (Quick-break, or "whip" is an auxiliary device to aid arc quenching, see Chapter 7). "grounded" means grounded wye system (copied from [9]).

The AIEE reports were the earliest thorough surveys, which were carried out so far to the best knowledge of the author of this thesis. It was found that most of the utilities and companies did use the air-break DSs to interrupt capacitive current at system voltage lower than 138 kV in the 1950s. It was reported that most companies did not have any guide for general use except previous experiences. Some of them used manufacturer's data, and others used (2.1) as a guide.

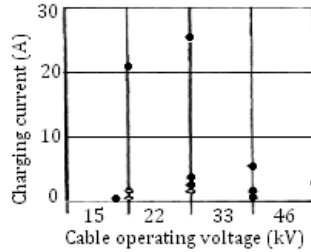


Figure 2.6. Company experiences reported on the use of air-break DSs for interruption of cable charging current. Note: \bullet : grounded-100% successful; \circ : ungrounded-100% successful (copied from [9]).

As from the mid 1980s most important contributions are from Peelo [6], [10]-[13]. In his earlier papers [10] and [11], the current interrupting capability of DSs was analyzed by considering the given phase spacing, arc reach (based on the equation from F.E Andrews et al. [2]).

$$LPR = 2.75 \times 5.03 \times U_{oc} \times I \quad (2.2)$$

Here LPR is the arc reach in mm , U_{oc} is the voltage in kilovolt (rms) across switch after interruption, and I is the interrupted current in ampere (rms). Compared with (2.1), a factor of 2.75 was introduced. This value came from the test results reported in [2] and [4]. Based on (2.2), safe maximum capacitive current levels that can be interrupted were calculated and compared with actual currents to be interrupted. A criterion for the application of DSs from a current interrupting point of view was also provided in Table 2.1.

Based mainly on the results from Andrews [2] and Peelo [10], the IEEE guide for DS to interrupt capacitive current ratings was published in 1990 [7]. In this guide,

Table 2.1: Maximum capacitive current levels for safe interrupting by air-break DSs. Note: d_{ϕ} is the difference between the minimum metal-to-metal phase-to-phase clearance, d_r is the maximum allowable arc reach, I_c is maximum current to be interrupted safely (copied from [11]).

Maximum system voltage (kV)	d_{ϕ} (m)	d_r (m)	I_c (A)
15.0	0.31	0.22	1.84
27.5	0.38	0.22	1.02
72.5	0.79	0.37	0.65
145.0	1.35	0.52	0.45
253.0	2.26	0.81	0.40
550.0	4.30	2.20	0.50

recommendations for system voltage up to 362 kV are given related to: minimum phase spacing to grounded objects (or horn-gap switch-phase spacing), calculated arc reach and maximum operation voltage, safe capacitive currents to be interrupted with vertical-break DS equipped with arcing horns and mounted in horizontal upright position.

In addition, in 2001 IEC also published a standard [14], where it defines that the DS is supposed to be able to disconnect a "negligible" current (i.e. less than 0.5 A) at system voltage below 420 kV. Based on the work of Peelo and Smeets, IEC 62271-305 (2009) High voltage switchgear and controlgear–Part 305: Capacitive current switching capability of air-insulated DSs for rated voltages above 52 kV was released. Two alternatives circuits for test are recommended for capacitive current interruption with a DS in the laboratory.

Summarizing this subsection, already tens of years ago it was recognized through field experience, surveys of utilities and power companies that a DS is able to interrupt the capacitive current. Principally, based on the work of Andrews and Peelo, the IEEE guide includes the maximum capacitive current to be interrupted safely by vertical DSs (see Table 2.1). The IEC standard, however, also states the current limitation, being 0.5 A for below 420 kV, but without supporting information. A test circuit for DS on the capacitive current interruption is proposed.

2.2 Fundamental aspects of capacitive current interruption

Most literature sources referred in the previous subsection deal with current interruption from the point of view of the interrupted current level through experiments and surveys. The literature cited in this subsection describes the involvement of the circuit, e.g. by investigating the factors affecting the interruption capability [15]-[20].

The laboratory experiments of Knobloch on interrupting capacitive currents described in [15] were carried out using a pantograph DS with rated voltage 245 kV. It was concluded that both the source and load side capacitances play a role during the operations. During the interruption, in the voltage and current wave shapes, transients of two distinct frequencies were observed, i.e. a low frequency (specific data was not provided) and a high-frequency (750 kHz approximately). In [15] all DS tests succeeded in switching off 1 A capacitive current reliably.

A paper by Boehne [16] was probably the first to be specifically related to small capacitive current interruption using a DS to study transients in EHV systems. This paper analyses the field performance of EHV DS operations at 400 kV and 505 kV in the Pennsylvania Electric Company, through computer simulation. It presents modelling study of various phenomena associated with interrupting

small capacitive currents in air with a DS. Particular attention was given to the current and voltage transient magnitudes as a function of bus MVA rating, switch resistance (a resistor in series with the DS) and the capacitive load. Specifically, the simulations covered nine MVA-values (500-2500 MVA), seven values of the interrupted current (0.25 A, 0.5 A, 1 A, 2 A, 3 A, 4 A, 5 A), and four separate resistor values (250 Ω , 500 Ω , 1000 Ω , 2000 Ω). The results included the line current, bus voltage and its rate of change, line voltage, and the arc voltage. The main conclusions were: the overvoltage was higher for disconnecting a smaller bus bar (in terms of MVA) than a larger bus bar; the rate of switching overvoltage rise could reach values in the order of 300 kV/ μ s; two natural frequencies were present in the voltage and current during the interruption; the arc voltage and the switching resistance can readily assist to reduce the overvoltage below 2.0 p.u. (the ratio of the transient voltage and amplitude of the phase-to-ground voltage).

A project was initiated in 1984 at Georgia Power Company [17] to determine the influence of parallel lines and line/conductor configuration on the charging current of 115 kV lines, which were switched off with an air-break DS. A total of five types of centre-break and pole-mounted DSs, to de-energize a section of 115 kV lines were investigated by computer simulation as well as by field tests. Several line/conductor configurations and parallel line arrangements were included. The results indicated that parallel lines had a negligible effect on values of the charging current. However, the conductor configurations affected the charging current significantly.

In Peelo's Ph.D dissertation [6] and subsequent papers [12], [13] capacitive current interruption was studied through a series of experiments. The main results can be summarized as follows:

- The interrupted current and the ratio of source and load side capacitance play a key role.
- The overvoltage was highest and the arcing duration was longest when the ratio of source and load side capacitance was smallest.
- Two types of appearance of the switching arc (so called "erratic" and "stiff" mode) were recognized during the interruption with different ratios of source and load side capacitances.

As a conclusion, according to the consulted literature, transient phenomena, together with high-frequency oscillations, on re-ignitions or re-strikes during the interruption were found. The capacitances at both sides of the DS play a crucial role. The level of the current to be interrupted influences the interruption capability as well. However, the details are still not clear. For instance, how do the capacitance values affect the arcing time, the transient overvoltage and transient current? How do the high-frequency phenomena arise and how to quantify them? In this thesis, these issues will be dealt with in detail.

2.3 Transients caused by capacitive current interruption

Research during the last two decades has confirmed that interruption of capacitive currents by DSs can be a major source of interference in secondary circuits of HV substations [21], [22]. DS operation generates high-frequency transients, which may endanger sensitive secondary components of the network through electromagnetic coupling. Due to the slow motion of the DS main blades during operation, an arc of long duration (up to several seconds) arises. The arc is characterized by numerous interruptions and re-strikes and is associated with high-frequency phenomena. These voltage and current transients have been reported to interfere with or even damage secondary systems [23]-[28]. Reported examples are: (i) PG&E Company in the USA experienced problems with switching off the DSs leading to an equipment damage [23]; (ii) transients in substations have been identified to interfere with the control signal wiring and power supply units for protection relays burned down during DS operation in Europe [24]-[26]; (iii) a faulty relay performance occurred because of the DS operation in a 500 kV switching operation in China [27]; (iv) computer simulations and field measurement confirmed the possibility that normal operation of air DSs could result in a damaged current transformer in Argentina [28].

The literature related to transient phenomena mainly focuses on system voltages above 220 kV. A major part of the publications either describes field tests in HV substations directly, or was related to investigation of expected surge levels by computer simulation after having observed faults in secondary systems [29]-[32], [40].

Due to various factors such as switchyard configuration and bus length, the range of overvoltage levels caused from operations by air-break DS is broad. For example, series of test were done at 362 kV, 787 kV and 1200 kV substations, with an overvoltage level of maximum 1.9 p.u. during switching off operations of EHV buses in Russia [30]. An earlier field test done in a 500 kV substation in Shanghai, China revealed an overvoltage level of 1.81 p.u. when disconnecting an unloaded bus with an interrupted current of 0.75 A [31]. A maximum overvoltage level of 1.4 p.u. was observed in two 220 kV substations in Bosnia [21], [32], [33]. A laboratory test showed that the overvoltage is about 2.3 p.u. while interrupting a capacitive current up to 2.3 A at 170 kV phase voltage [13]. Overvoltage reached 2.6 p.u. at the termination of the bus, and 3.1 p.u. value at a secondary service circuit in the station appeared, during de-energizing a 396 m long bus with a DS at 345 kV in the USA [40].

The dominant high-frequency transient was also one of the factors of concern in previous references. Frequency values reported were in the order of a few hundred kilohertz. For instance, it reached 720 kHz at 138 kV while de-energizing the transmission line [34]; it was found that dominant frequency was in the range

of about 400-500 kHz at 200 kV and 500 kV substation field tests reported in [21], [31], [35].

In conclusion, most of the work related to transient phenomena associated with capacitive current interruption using air-break DS focused on the overvoltage level in a specific substation and also focused on methods to protect secondary systems. However, the origin of the transients from disconnecting capacitive currents has hardly been studied yet. The influential factors on overvoltage are also not considered systematically and in detail. In addition, the transient current was hardly investigated at all. Regarding the dominant frequencies, none of the literature gave detailed analysis of the fast mechanisms involved. Therefore, the fundamental phenomena resulting in high-frequency behaviour during the switching process will be studied in this thesis.

2.4 Approaches to enhance the interruption capability

Several approaches to enhance the ability to interrupt the capacitive current with air-break DSs are addressed in the related literature. Up to now, main attention is paid to high-velocity contact opening devices, inserted damping resistors and gas-blast devices.

2.4.1 Fast contact separation

A high-velocity contact opening device (also called whip type quick-break) can be attached to the DS. It assists in extinguishing the arc by achieving a large air gap within a short time. An example of such device is shown in Figure 2.7.

In 1989, a series of laboratory tests was conducted based on 10 different whip type quick-break devices mainly attached at vertical-break DSs by the U.S. Department of Energy [36]. The goal was to determine the maximum interrupting capacitive current capability of 115 kV DSs with this type of device. The results showed successful interruptions up to 11 A at 115 kV, managed by the device having the highest tip speed. It was found that the interrupted current magnitude played a more prominent role than the RV across the DS main blades. However, there were no further details reported on the design of the device itself.

In a study reported in [17] a total of five types of DS/quick-break devices, together with a centre-break and pole-mounted DS to de-energize a section of 115 kV line, were tested. The results showed that one of the quick-break DS designs could successfully drop a 29 km line at 115 kV (corresponding to 6.5 A). It was also stated that high tip speed and minimum bounce of quick-break devices significantly enhance the charging current interruption capability, without mentioning any supporting details.

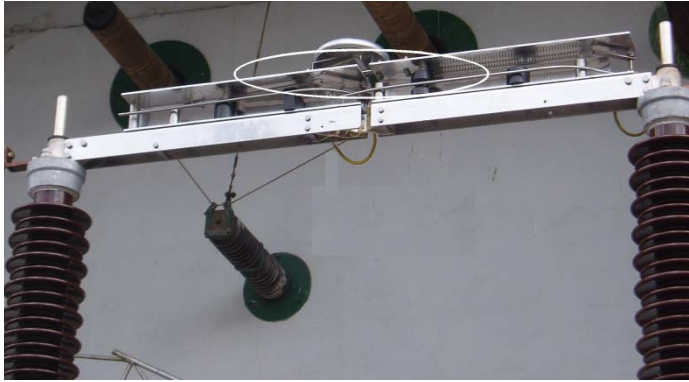


Figure 2.7. A centre-break DS with a high-velocity auxiliary device (indicated within the ellipse, from the test in this thesis).

Reference [37] also confirmed that a high-velocity device was able to successfully interrupt a capacitive current of 8 A at 138 kV. In [38] both laboratory and field tests were carried out in the Allegheny Power System. The result showed that the high-velocity opening device succeeded interrupting 17.6 A at 80 kV.

The cited literature revealed that a fast-opening device usually is employed at 138 kV or below, and it was mainly installed with the vertical-break DS type. It can be concluded that a high-velocity opening device extends significantly the capability of interrupting capacitive current of a DS. The interruption mechanism with this high-velocity interrupter on a centre-break DS will be further investigated in Chapter 7 of this thesis.

2.4.2 Resistive transients suppression

A resistor inserted into the circuit can reduce the transients imposed on the system [5], [39]-[44]. In [39], it was reported that the resistance in series or in parallel to the arc can limit the amplitude and the duration of the transients.

In order to evaluate the switching surge level by disconnecting capacitive currents and magnetizing currents, reference [5] described a series of tests on an American EHV experimental line. The switching surge was studied while disconnecting was achieved with a conventional switch with and without surge voltage suppressing resistors. Charging currents of 2.4 A at 400 kV and 3.0 A at 505 kV were interrupted. Compared to the situation without resistor, the surge level decreased by about 15%, which means the inserted resistor was beneficial for disconnecting a capacitive current.

In Figure 2.8 three remedial approaches to reduce the surge level in a 345 kV substation, according to [40], are shown. These methods are: (i) a resistor in

series with the DS during opening; (ii) a porcelain-enclosed resistor placed at the same vertical position as the stationary contact of the vertical-break DS, which was inserted automatically step by step during the operation; (iii) a parallel combination of line traps (a device that blocks the high-frequency carrier (24 kHz to 500 kHz) and lets power-frequency (50 Hz - 60 Hz) pass through) and a resistor connected in series with the DS. It appeared that method (iii) did not prove very effective in limiting overvoltages, but methods (i) and (ii) were effective. The overvoltage at the station service (secondary) circuit dropped to 1.7 p.u. and to one third, respectively, compared with 3.1 p.u. from the interruption without any remedial devices. The resistor, which was bypassed whenever the DS was in closed position, also appeared to be the most effective way to reduce overvoltages.

A similar method to gradually insert a resistance was again employed in [41]-[43]. A computer simulation of a three-phase 550 kV system using distributed parameters was carried out to investigate the re-strike transients upon disconnecting unloaded transmission line. The simulations indicated that the surge-suppressing resistors were effective in limiting the surge current and significantly contributed to damping of the re-strike transients [41], [42]. Reference [43] reports a series of field tests, in which a 0.5 M Ω resistor was installed in parallel to the main blades of the DS including a small arcing horn, conducted at a 220 kV power station (Figure 2.9). The results at switching off a busbar showed that the arcing duration was reduced from 2.5 s without resistor to the value between 1.1 s and 1.5 s with parallel resistors. It was also reported that the high-frequency component of the voltage wave shapes measured nearby was damped. The overvoltage in the antenna of the secondary system in the vicinity reduced from 3.1 p.u. without resistor to only 1.6 p.u. with resistor. From these results it can be concluded that the damping resistor has a strong suppressing effect on the transient overvoltages caused by interrupting small capacitive current.

Further, in [44] the effect of the arc resistance on transients suppression due to DS switching was studied and it was confirmed that arc resistance reduced transient overvoltages.

In summary, most of the work on employing resistive devices focuses on the surge or overvoltage level. However, still the conclusion can be drawn that a resistor enhances the capacitive current interruption capability of the DSs. For instance, a 396 m long bus of 345 kV was successfully interrupted according to [40]. Reference [43] showed that arcing time was reduced greatly by a resistor in parallel to the main blades of the DS. In addition, it was mentioned that with an inserted resistor currents up to 4 A at 230 kV, 3 A at 345 kV and 1.5 A at 500 kV were interrupted. However, no specific details were provided [45].

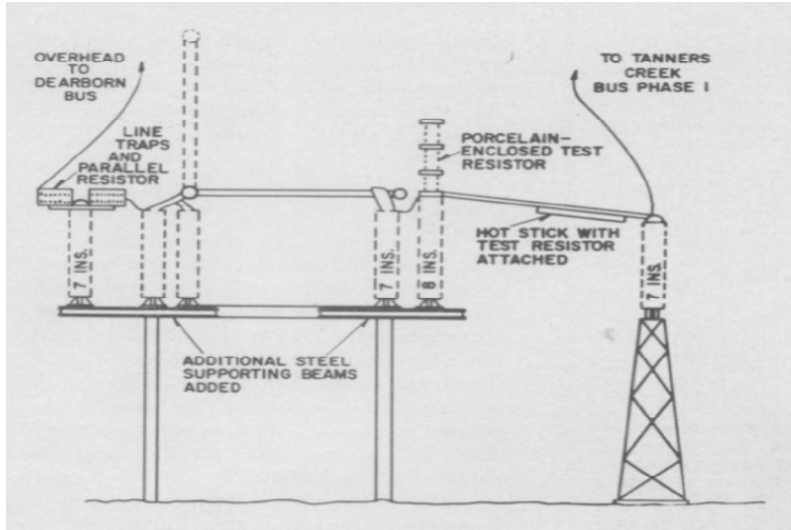


Figure 2.8. Sketch of 345 kV DS with various remedial devices mounted in place (copied from [40]).

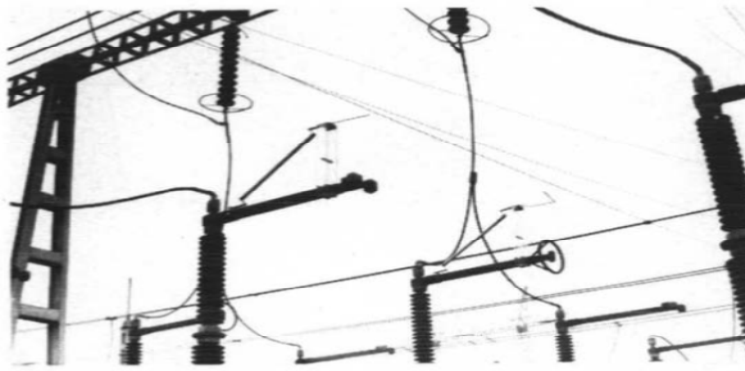


Figure 2.9. Installed DS with damping resistor in a 220 kV substation (copied from [43]).

In this thesis, a resistor in series or in parallel to a centre-break DS will be studied through simulation and laboratory experiments. The pros and cons will be discussed.

2.4.3 Arc cooling

A gas-blast device, as a method to improve the DS capability, is not used frequently. Such gas-blast interrupting attachment was mounted on a vertical-break DS as indicated in Figure 2.10. Each pole unit was equipped with a porcelain

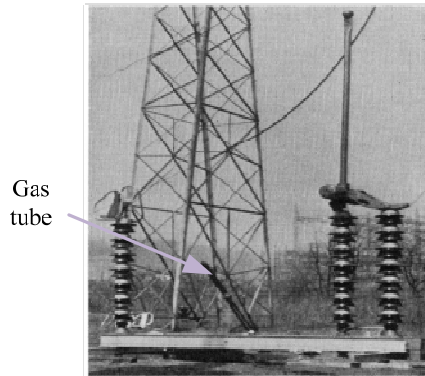


Figure 2.10. Gas-blast interrupter test at Tidd test site (copied from [47]).

tube mounted between the blade insulator stacks, and each porcelain tube had a convergent-divergent nozzle, aiming to deliver the high-speed jet of gas into the arc. This method was found to be a most effective means to interrupt capacitive currents according to [5], [37], [46]-[48]. It was stated that gas-blast has strong effect in reducing the arc reach and arc length by visual observation, but without quantitative data support [5]; Tests showed that a vertical-break DS with gas-blast device could drop 20 A at a U.S. 138 kV station [37]; a 135 km line was dropped successfully at 230 kV (estimated current 25 A) with the support of the gas-blast as reported by a test program on a vertical-break DS at the U.S. Bureau of Reclamation [46]; a 330 kV vertical-break DS with gas-blast device was designed as shown in Figure 2.10 [47]. Specifically the porcelain tube was connected to a gas tank, which was mounted under each single-pole switch unit. The test in the American Gas and Electric 500 kV Tidd test site showed that it was capable to interrupt capacitive current up to 8.5 A at 220 kV successfully. Further, a nitrogen puffer was used in an effort to facilitate the DS in the interruption of magnetizing current [48].

The work related to gas-blast is relatively old. Exclusively, an extra tube was applied under the vertical-break DS. Since it was proved this method to be most effective, in this thesis, this approach will be continued to study, but mainly focus on the arc extinguishing mechanism and interruption performances.

2.4.4 Vacuum and SF₆ interrupter

Due to the extraordinary arc interruption performances, vacuum and SF₆ interrupters (see Figure 2.11) are also implemented in conjunction with an air gap DS in some designs [45]. However, in these cases, the costs involved are high and the construction is complex, because the interrupters must be able to withstand the full RV. Most commonly, only vertical-break DSs are provided with such an auxiliary interrupter. In principle, during the opening operation of the DS



Figure 2.11. (Left) multiple vacuum interrupters and (right) a single gap SF₆ interrupter per phase (copied from [45]).

the current is transferred into a loop with the SF₆ or vacuum interrupter that performs the switching. The SF₆ or vacuum interrupters are out of circuit during the closed position of the DS. The working principle of this sort of approaches will be described below in detail using vacuum medium as an example. The SF₆ interrupter does in a similar manner.

Arcs in vacuum are easier to interrupt than in air, because the vacuum has an electrical strength of typically 30 kV/mm in case of well polished contact surfaces. This high electric field withstand strength and very fast recovery ensure that once the arc is extinguished, usually at the first current zero, no re-ignition occurs and dielectric recovery is achieved within a few microseconds [51]. The idea of combining the DS with vacuum interrupters is to commutate the current path through the vacuum interrupters first and then open the contacts within the vacuum. In general, multiple series vacuum interrupters are needed for high voltage since a single vacuum interrupter can only function at medium voltage level [52]. The working principle of an inserted single vacuum bottle with vertical DS is plotted in Figure 2.12. It works according to the following steps:

- Step 1: the DS is in closed position. The vacuum interrupter is out of the circuit. The current flows between jaw (metal part connected with main blades at the right side) and blade contacts. The vacuum contacts are closed.
- Step 2: the DS contacts separate but the circuit is maintained through the moving arc horn and the fixed arc horn. As the blades continue opening, the moving arc horn engages the vacuum interrupter's actuating arm. The vacuum contacts remain still in a closed position.
- Step 3: as the blade movement continues, the fixed and moving horns separate. The current is transferred to a path through the closed vacuum contacts. After an adequate clearance distance is established, the current is interrupted inside of the vacuum interrupter with no external arcing as the contacts open.

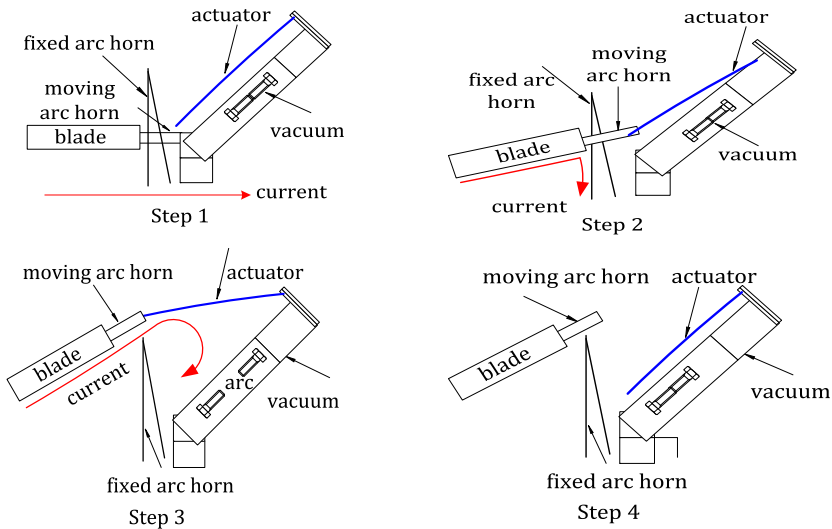


Figure 2.12. Interruption for DS with inserted vacuum bottle(s), (obtained from [52]).

- Step 4: the DS moves to the fully open position releasing the actuator arm, which is spring loaded to return to its original position and close the vacuum contacts.

This approach is actually closer to a load-break switch than to a DS switch. The main advantage is that it can interrupt higher currents than an air-break DS alone. The level of the current to be interrupted is determined by the number of the vacuum modules connected in series. For instance it is capable to interrupt up to 70A capacitive current for up to rated system voltage 230 kV [45]. The drawbacks of a vacuum interrupter are:

- There is no visual indication of the dielectric integrity prior to operation, creating a potential safety hazard to personnel when operating the DS.
- Each vacuum bottle in a DS with a multi-bottle stack can handle only the MV voltage level (up to 30 kV). Grading capacitors are required to divide the voltage evenly across the multiple gaps for successful performance. A vacuum interrupter stack can only be installed on a vertical-break or a single-side break DSs due to its complex construction.

Since most of the literature is related to the vertical-break DS as a test object, the potential interrupting capability of the vertical-break DS with the aid of various approaches and their corresponding costs are summarized in Table 2.2. Vacuum interrupters can be used to interrupt higher current. Issues to be considered are the costs and the need for grading capacitors. SF_6 may interrupt the highest level current compared with the other approaches, but with highest cost.

Table 2.2. Potential interruption ratings of vertical-break DSs with different auxiliary devices. Note: the costs are taken from [45], assuming the cost of the arcing horn is "1".

Type of auxiliary devices	Interrupting capability (I_{rms})	Cost
Arcing horn	Interrupts very small current, refer to [7]	1
High-velocity devices	Higher than with arcing horn (e.g. up to 8 A at 138 kV [37])	1.2
Gas-blast	Higher than with high-velocity break devices	No literature
Multiple vacuum interrupters	70 A at up to 230 kV	2.8
SF ₆ interrupters	Up to 300 A at up to 230 kV	3.6
Resistors	4 A—230 kV 3 A—345 kV 1.5 A—500 kV	No information

2.4.5. Ablation assisted approaches

The use of arc cooling through ablation, i.e. evaporated materials from compounds like polyvinyl chloride, polymethylmethacrylate, etc. is a method commonly applied in load break devices [53], [54]. The working principle is confinement of the hot arc in a narrow tube causing a high pressure and fast flowing gas, which facilitates rapid arc extinction. Based on this method, a special arcing horn has been developed [55]. This device was designed originally to prevent lightning damage on overhead line, capable of interrupting ground fault currents. It was confirmed experimentally that it can interrupt ground fault current up to 1 kA within half cycle at 77 kV system voltage. Figure 2.13 shows the arrangement and working principle. There is a narrow tube, made of polyvinyl chloride, mounted at the tip of the arcing horn electrode in order to interrupt the current. The interruption portion, located in the ground side horn, is a tube with an intermediate electrode. This electrode is a small column, which pierces at a spot in the tube wall. When excessive voltage is applied between the horns at line and ground side, a breakdown occurs between their tips through the intermediate electrode. Then, the arc arises between the horns. The gas during arcing in the interruption tube has gained a high-velocity and a high-pressure. The device was not able to interrupt a short-circuit current above 10 kA. No further information about the interruption performance below 445 A was reported. Pressure and velocity of the gas inside the tube, and the ablation of the tube material at current levels around 10A might be too low for effective operation.

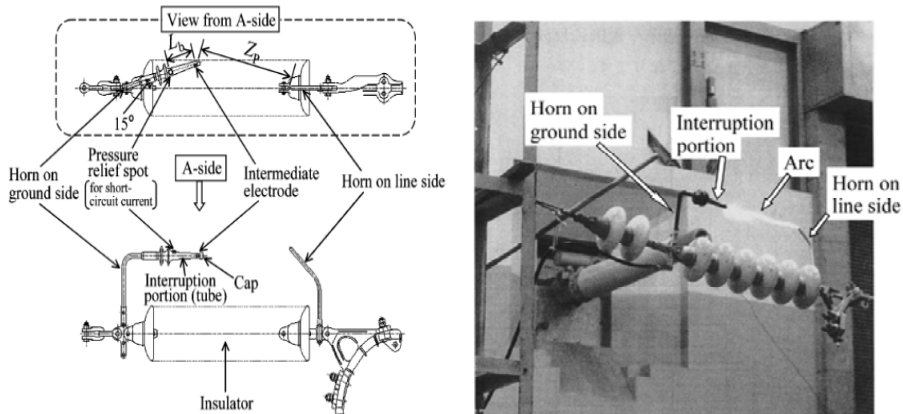


Figure 2.13. Working principle of ablation assisted arcing horn with PVC tube (copied from [55]).

Arc interruption through ablation is very successfully applied in medium voltage load break switches. One application is discussed here [56]. Figure 2.14 shows the structure and working mechanism. Upon disconnecting, the main contacts "1" open first and the current is briefly taken over by the parallel connected lagging pins "2". During this breaking motion, the opening springs "3" acting on the lagging pin are tensioned. On reaching a stop, the lagging pin leaves the holding contact "4". The arc occurring between the arcing tip of the holding contact and the tungsten tip of the lagging pin is extinguished in the arcing chamber "5". The arcing chamber itself is closed. This device contains four sections and has a pressure chamber "6" and an expansion chamber "7". Two extinction plates "8", arranged in the pressure chamber, are forced into the path of the arc by lateral spring pressure. At low currents the arc is extinguished due to the cooling effect of the walls. In the higher current range arc extinction is achieved by the ablated gases produced in the pressure chamber flowing out of this chamber into the expansion chamber. Owing to this complementary combination of several extinction principles a wide current interruption range is effectively covered. This device is capable to interrupt cable charging currents up to 20 A at low voltage level 38.5 kV. For higher current and higher voltage levels, no information was provided.

Based on using ablation assisted arc extinction as commonly used in load break switches was considered. Present designs require high current (for sufficient ablation) or are limited to relatively low voltage level. Their applicability on high voltage air-break DSs may be questionable because the long length of the arc and the lower energy density. In addition, confining the DS arc in a small space may have adverse effects because cooling from ambient air is obstructed. This may be considered for further investigation.

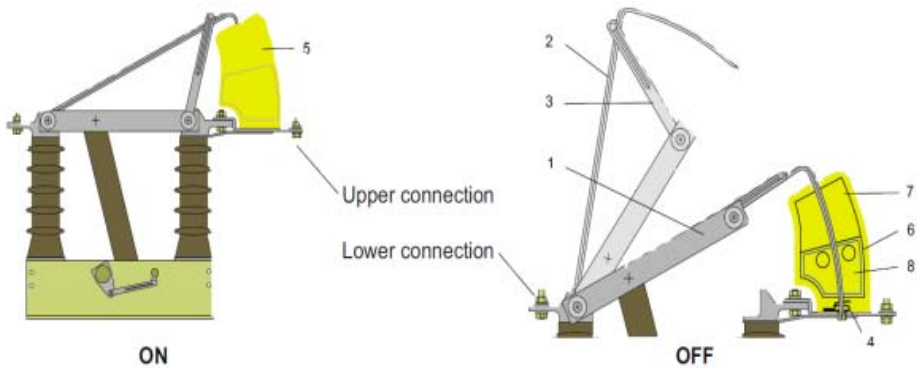


Figure 2.14. Working principle for an indoor load break switch with two chambers (copied from [56]).

2.5 Arc models related to current interruption with a disconnect

An electric arc is a discharge, characterized by a high current flow (as compared to other gas discharges, like glow discharge), resulting in a current flowing through a usually non-conductive medium such as air. Understanding the phenomena associated with the electric arc requires combined knowledge of electromagnetism, thermodynamics and plasma physics.

The electric arc related to current interruption with a DS is a so called free burning AC arc with relatively low current (up to a few tens of amperes) in the atmosphere. It behaves differently from the well-studied and well-documented fault arc in circuit breakers because of its much higher length (metres vs. centimetres), its much lower current (amperes vs. kilo-amperes) and its unconfined ("free-burning") nature. Compared with the short arc, where the influence of anode and cathode roots is significant [57], the arc length of DS arc may reach up to a few metres depending on the system voltage and current. Compared to the confined arc, the free burning arc behaves more randomly and is influenced by external conditions as wind, humidity, and surrounding electromagnetic fields. An overview of the free burning arc literature was presented in [6].

Arc modelling may be an effective computational tool when field experiments are difficult to manage. Selected models from literature are therefore discussed in relation with their applicability for the arc from a low current interruption or free burning arc in the air.

Due to the random nature of the free burning arc, it is practically not possible to duplicate the genuine arc characteristics by a computer model. Sometimes the arc is represented by a resistor or as a voltage source with periodic rectangular wave form, changing its sign at each arc current zero crossing; sometimes a more

complicated model with piecewise characteristics is adopted to present the arc at variable length, resulting in a variable arc voltage. However, these arc models do not take into account the actual interaction of the arc and the electromagnetic transients in the circuit [58], [59]. No model exists, taking into account the discontinuous character of the arc, which is observed in the present study to be the main feature of the low-current DS arc. Therefore, only models, more distantly related to the arc in DS current interruption will be introduced here.

An arc model simulating the behaviour of arcs driven by magnetic force in a gas [57], [60]-[62], was proposed first in [62]. The arc is assumed to be a chain of small rigid cylindrical current elements. Each element experiences the Lorentz force from the magnetic field and a fluid drag force from the surrounding gas. Each element moves with the velocity determined by these forces. The arc behaviour is determined by the position and the motion of each element. Consequently, the behaviour and the shape of the entire arc may be constructed. Experiments in [62] with current of 1 kA at 50 Hz in SF₆ showed good agreement between model and the observed arc in practice.

In overhead line, generally, an arcing horn is used to protect the insulators against damage from arcs after switching, or by lightning induced breakdown to earth. The arcing horn is installed in parallel with the insulator. The arc between the arcing horns behaves as a free burning arc in the air. Based on the model [60], it can be estimated how far the arc is from the column of the insulator. A situation for a current of 160 A was studied in [61], resulting in a good match between the simulation and experiments. Such an arc model can potentially be used to describe arc movement related to DS current interruption, and to evaluate the risk of endangering the surrounding equipment. However, the current related to the DS interrupting has much lower values and their arc movement is much more influenced by convection processes than by electro-magnetic interaction.

Compared with all other types of arc mentioned before, the secondary fault arc from EHV power overhead line resembles most closely the arc from capacitive current interruption with a DS because of a comparable length and similar environmental (unconfined) conditions. A secondary fault arc follows the primary fault current in single phase tripping and reclosing schemes due to capacitive and inductive coupling with the sound phases [63]. The value of the secondary current may reach up to a few hundred amperes and is determined by the structure of the overhead line, such as line arrangement, length, earthing, etc.

The Cassie arc model [64], frequently cited, assumes that the arc channel has the shape of a cylinder and is filled with highly ionized gas with a constant temperature, but with a variable diameter. Cassie developed his arc model based on the assumption that a high current arc is governed mainly by convection losses. One of the most common used Cassie arc equation formulations is:

$$\frac{d[\ln(g)]}{dt} = \frac{1}{\tau} \left(\frac{u_a^2}{u_0^2} - 1 \right) \quad (2.3)$$

where u_0 is the static arc voltage, u_a is the momentary arc voltage, τ is the arc time constant, g is the instantaneous arc conductance.

Through study of experimental u - i characteristics of arcs, having peak arc current values from 68 A to 21 kA, it was found that the Cassie model may be used to model the behaviour of the secondary arc [59]. Knowing u_a , u_0 , τ from specific experiments, the arc conductance g can be determined to represent the arc for computer simulation [66], [67].

Based on the Cassie model, Kizilcay defined the arc behaviour according [53], [68]-[70] as:

$$\begin{cases} \frac{dg}{dt} = \frac{1}{\tau}(G - g) \\ G = \frac{|i_a|}{(u_0 + r_0|i_a|) \cdot l_a} \end{cases} \quad (2.4)$$

where i_a is the instantaneous arc current, l_a the instantaneous arc length, u_0 is the arc voltage per unit length, r_0 is the arc resistance per unit length, G is the stationary arc conductance. Parameters τ , u_0 , r_0 depend on arc length, and can be obtained over a certain time interval due to the required high accuracy of measured arc current and voltage from specific measurements, as described in detail in [59]. This model not only considers the heat of the arc, but also takes into account the secondary arc elongation. The experiments with a current up to a few hundred amperes matched the simulated results well. It may be feasible to describe the arc with lower current (from capacitive current switching as well).

Terzija took considerable effort to model long arcs in free air [71]-[75]. The arc in his experiments was initiated between two electrodes with a distance of 60 cm, the current ranged from 100 A to 20 kA at a system phase voltage of 20 kV. The

equation used is a generalization of (2.3): $\frac{dg_a}{dt} = f(g_a, u_a, i_a, t)$. By observing the arc voltage waveform, presented roughly as a rectangular shape in phase with the arc current, the arc was modelled through the following nonlinear equation:

$$u_a(t) = \left(U_a + U_b \frac{I_0}{i_b(t)} + R_\delta |i_b(t)| \right) \text{sgn}(i_a) + \zeta \quad (2.5)$$

where $u_a(t)$, $i_a(t)$ are arc voltage and arc current,

$$i_b(t) = \begin{cases} I_0 & |i_a(t)| < I_0 \\ |i_a(t)| & |i_a(t)| \geq I_0 \end{cases} \quad (2.6)$$

U_a , U_b , R_δ are parameters defining the shape of the arc voltage, ζ is to account for Gaussian noise with. $U_a = E_a l_a$, the average of E_a was taken between 1.2 kV/m and 1.5 kV/m for the chosen experimental current range. The term $U_b \frac{I_0}{i_b(t)}$ models the arc re-ignition voltage, and $R_\delta |i_b(t)|$ is an additional term, which is determined by the arc current i_a , R_δ , is part of the arc resistance, at the chosen current range, in the order of tenths of ohm. The author added the effect of the arc elongation in [75] by multiplying (2.5) with a suitable elongation function $L(t)$ in [73]. The arc current from the experiments was in the range taken of fault current. For instance, the model was applied to a secondary arc in overhead line [74]. However, the method may also be considered to describe the arc related to capacitive current operation with a DS.

Except for the arc model based on magnetic forces, the other models introduced in this section are exclusively based on the Cassie arc model. Most model parameters must be obtained from specific field experiments. As a conclusion, although there is no detailed arc model connected to current interruption with a DS, the arc models mentioned above may be considered as a first step. Because of the random, inhomogeneous and time dependent nature of the conducting medium, it has not been attempted to design an arc model in the present study.

2.6 Conclusion

Capacitive current interruption using an air-break DS has not attracted too much attention, and the existing literature provides only a limited insight into the mechanism. However, certain literature sources do exist, which are more or less related to this subject. Each from different points of view and with different application purposes, such as surges imposed on secondary systems, disconnection of magnetizing currents, loop currents and so forth.

It is recognized that DS requirements should include the capability to interrupt small capacitive current. Based on field tests and computer simulations at different system voltage levels, it was found that interrupting even of small capacitive currents can cause large transients, which potentially can damage nearby equipment. Also, arcs with unacceptable duration and/or reach can arise.

Among many factors, which influence the capability of interruption in practice, such as clearance distance, atmospheric condition (wind, humidity), conductor configurations and so on, a few factors were recognized and investigated. The role of bus length (source and load side capacitance), parallel lines, line configurations were pointed out. In addition, high-frequency transients were recognized only to a practical extent, but neither fundamentally nor systematically investigated.

In this literature survey, it was found that there are no interruption ratings for DSs except those given by IEEE [7]. The IEC standard [14] also fails to clarify this topic. On the other hand, the present power systems are rapidly increasing in size, requiring performances but also enhancing cost-effectiveness. In certain locations, low-cost DSs having an enhanced current interruption capability could in some situations of de-energization of unloading the short line/cable/busbar to replace the circuit breakers.

It is indispensable to understand the phenomena of capacitive current through free burning arcs in air profoundly and to find approaches to improve the ability of the switching device: the disconnecter. This consideration is the motivation of the work in this thesis.

References

- [1] P. A. Abetti, "Arc interruption with disconnecting switches", Master thesis, Illinois Institute of Technology, Jan. 1948.
- [2] F. E. Andrews, L. R. Janes, M. A. Anderson, "Interrupting ability of horn-gap switches", *AIEE Trans.*, vol.69, pp. 1016-1027, Apr. 1950.
- [3] M. W. Anderson, "Power autotransformer current interruption with an air-break disconnect switch", *IEEE Trans. on Power Apparatus and Systems*, vol.74, pp. 1157-1163, Jan. 1955
- [4] CEA Project 069-T-102 report, "The interrupting capability of high voltage disconnect switches", Canadian Electrical Association, Jul. 1982.
- [5] A. Foti and J. M. Lakas, "EHV switch tests and switching surges," *IEEE Trans. on Power Apparatus and Systems*, vol.83, pp. 266-271, Mar. 1964.
- [6] D. F. Peelo, "Current interruption using high voltage air-break disconnectors", Ph.D. dissertation, Dept. Electrical Engineering, Eindhoven Univ. of Technology, Eindhoven, 2004.
- [7] *IEEE Guide to Current Interruption with Horn-Gap Air Switches*, IEEE Standard C37.36b-1990, Jul. 1990.
- [8] AIEE Committee Report, "Report on transformer magnetizing current and its effect on relaying and air switch operation", *AIEE Trans.*, vol.70, pp. 1733-1740, Jul. 1951.
- [9] IEEE Committee Report, "Results of survey on interrupting ability of air-break switches", *IEEE Trans. on Power Apparatus and Systems*, vol.PAS-85, pp. 1008-1019, Sept. 1966.
- [10] D. F. Peelo, "Current interrupting capability of air-break disconnect switches", *IEEE Trans. on Power Delivery*, vol.1, pp. 212-216, Jan. 1986.

- [11] D. F. Peelo, "Current interrupting capability of air-break disconnect switches", *IEEE Power Engineering Review*, vol.PER-6, pp. 53-54, Jan. 1986.
- [12] D. F. Peelo, R. P. P. Smeets, L. van Der Sluis, S. Kuivenhoven, J. G. Krone, J. H. Sawada and B. R. Sunga, "Current interruption with high voltage air-break disconnectors", in *Proc. Cigre Conf.*, paper nr. A3-301, 2004.
- [13] D. F. Peelo, R. P. P. Smeets, J. G. Krone, "Capacitive current interruption in atmospheric air", in *Proc. Cigre A3/B3 Colloquium*, 2005.
- [14] *IEC Standard for High voltage Switchgear and Control Gear -Part 102: Alternating Current Disconnectors and Earthing Switches*, IEC 62271-102, Dec. 2001.
- [15] H. Knobloch, "Switching of capacitive currents by outdoor disconnectors", in *Proc. Fifth International Symposium on High Voltage Engineering Conf.*, Aug. 1967.
- [16] E. W. Boehne, "EHV surge suppression on interrupting light currents with air switches I- capacitive currents", *IEEE Trans. on Power Apparatus and Systems*, vol.PAS-84, pp. 906-923, Oct. 1965
- [17] S. G. Patel, W. F. Holcombe, D. E. Parr, "Application of air-break switches for de-energizing transmission lines", *IEEE Trans. on Power Apparatus and Systems*, vol.4, pp. 368-374, Jan. 1989.
- [18] A. Schutte, H. Rodrigo, "Transient phenomena due to disconnect switching in high voltage substation", in *Proc. 11th International High Voltage Engineering Symposium Conf.*, London, Aug. 1999
- [19] I. B. Johnson, A. J. Schultz, N. R. Schultz, R. B. Shores, "Some fundamentals on capacitance switching", *IEEE Trans. on Power Apparatus and Systems*, vol.74, pp. 727-736, Aug. 1955.
- [20] W. M. Leeds, R. C. van Sickle, "The interruption of charging current at high voltage", *AIEE Trans.*, vol. 66, pp. 373-382, Jan. 1947.
- [21] S. Carsimamovic, Z. Bajramovic, M. Ljevak, M. Veledar, "Very fast electromagnetic transients in air insulated substations and gas insulated substations due to disconnecter switching", in *Proc. International Symposium on Electromagnetic Compatibility*, vol.2, pp. 382-387, Aug. 2005.
- [22] C. M. Wiggins, D. E. Thomas, F. S. Nickel, S. E. Wright, "Transient electromagnetic interference in substations", *IEEE Trans. on Power Delivery*, vol.9, pp. 1869-1883, Oct. 1994.
- [23] R. J. Gavazza, C. M. Wiggins, "Reduction of interference on substation low voltage wiring", *IEEE Trans. Power Delivery*, vol. 11, pp. 1317-1329, Jul. 1996.
- [24] M. A. van Houten, E. J. M. van Heesch, A. P. J. van Deursen, "General methods for protection of electronics against interference, tested in high voltage substations", in *Proc 8th International Symposium on Electromagnetic Compatibility Conf.*, pp. 429-434. Zürich, Mar. 1989.
- [25] A. Rodewald, "Interference generated by switching operations and its simulation", in *Proc. IEEE International Symposium on EMC Conf.*, pp. 133-138, 1984.
- [26] S. Carsimamovic, R. Gacanovic, Z. Bajramovic, "Switching overvoltages in air-insulated substation (AIS) due to disconnecter and circuit breaker switching", paper nr. C4-301, *Cigre Conf.*, Paris, 2006.
- [27] W. Mao, "Analysis for malfunction of CBF relay insulating switch operation", *Automation of Electric Power Systems*, vol. 26, pp. 74-76, Apr. 2002.
- [28] A. Funes, A. Ledesema, "Field measurements and modelling of high-frequency transient during disconnect switch operations in EHV substations, assessment of their effects on Current Transformers", paper nr. A3-207, *Cigre Conf.*, Paris, 2010.
- [29] G. Carrasco, "Electromagnetic interference in substation Jose up to 400/115 kV", in *Proc. IEEE Transmission & Distribution Conference and Exposition*, pp. 1-6, Aug. 2006.

- [30] V. S. Rashkes, L. D. Ziles, "Very high-frequency overvoltages at open air EHV substations during disconnect switch operations", *IEEE Trans. on Power Delivery*, vol.11, pp. 1618-1623, Jul. 1996.
- [31] Z. Liu, "The test of switching no-load bus with 500 kV disconnecter", *High Voltage Engineering*, vol.4, pp.58-61, 1990.
- [32] S. Carsimamovic, Z. Bajramovic, M. Ljevak, M. Veledar, N. Halilhodzic, "Current switching with high voltage air disconnecter", in *Proc. International Conference on Power Systems Transients*, paper nr. IPST05-229, Jun. 2005.
- [33] S. Carsimamovic, Z. Bajramovic, M. Veledar, O. Hadzic, A. Carsimamovic, "Computer simulation of transients due to disconnecter switching in air-insulated substations", in *Proc. International Conference on Computer as a Tool*, pp. 2051-2053, Sept. 2007.
- [34] S. G. Ludwig, C. C. Scheutz, "Coupling to control cables in HV substations", in *Proc. IEEE International Symposium on Electromagnetic Compatibility*, vol.1, pp. 249-253, Aug. 2001.
- [35] Z. Lu, C. Wang, "The switching transient electric field measurements in a 500 kV substation", in *Proc. the 3rd International Symposium on Electromagnetic Compatibility*, pp. 194-197, May 2002.
- [36] R. J. Denis, "Tests to determine the interrupting capabilities of 115 kV quick-break devices", Division of laboratories report from U. S. Department of Energy, Tech. Rep. Bonneville Power Administration, Mar. 1989.
- [37] E. C. Rankin, "Experience with methods of extending the capability of high voltage air-break switches", *AIEE Trans. on Power Apparatus and Systems*, vol.78, pp. 1634-1636, Dec. 1959.
- [38] T. J. Jackson, "138 kV air switch interrupting device tests", presented at *PEA Electrical Equipment Meeting*, Hershey, Pennsylvania, May 1977.
- [39] R.C. van Sickle, "Influence of resistance on switching transients", *AIEE Trans*, vol.58, pp. 397-404, Aug. 1939.
- [40] H. L. Rorden, J. M. Dils, S. B. Griscom, J. W. Skoglund, E. Beck, "Investigations on switching surges caused by 345 kV disconnecting-switch operation", *AIEE Trans. on Power Apparatus and Systems*, vol.77, pp.838-844, Oct. 1958.
- [41] D. L. Lott, "Surge-suppressing resistors applied to EHV disconnecter switches", *Allis-Chalmers Engineering Review*, vol.40, pp. 24-27, 1975.
- [42] K. B. Stump, D. L. Lott, "Controlling system transients with surge-suppressing resistors in air disconnect switches", *Electric Power Systems Research*, pp. 269-277, Feb. 1979.
- [43] M. S. Savic, "Suppression of the high-frequency disturbances in low voltage circuits caused by disconnecter operation in high voltage open-air substations", *IEE Proceedings Generation, Transmission and Distribution*, vol.133, pp. 293-297, Jul. 1986.
- [44] S. Carsimamovic, Z. Bajramovic, "Influence of resistance of electric arc on transients due to disconnecter switching in air-insulated substations", *IEEE Trans. on Plasma Science*, vol.36, pp. 2560-2565, Oct. 2008.
- [45] D. Childress, "Disconnect switch mounted interrupting devices how to choose what to use when and where", [Online]. available: www.southernstatesllc.com.
- [46] P. E. Richardson, A. Foti, "Gas-blast switch tests on 230- kV system", *Electrical Engineering*, pp. 712-717, Aug. 1956.
- [47] I. W. Gross, C. Killian, J. M. Sheadel, "A 330- kV air switch", *AIEE Trans. on Power Apparatus and Systems*, vol.73, pp.264-270, Jan. 1954.
- [48] A. J. Mcelroy, W. S Price, H.M. Smith, D. F. Shankle, "Field measurement of surge when switching in 345- kV stations", *AIEE Trans. on Power Apparatus and Systems*, vol.83, pp. 250-263, Mar. 1964.

- [49] B. J. Berner, J. R. Rostron, "New improvement in transmission switching using SF6 interrupter technology", in *Proc. IEEE/PES Transmission and Distribution Conference and Exposition*, vol.1. pp. 317–322, Oct. 2001.
- [50] J. D. McDonald, "Electric power substations engineering", CRC Press, ISBN-10: 0849317037, Jun. 2003.
- [51] H. M. Ryan, *High voltage engineering and testing*, 2nd edition, Bungay Suffolk: RefineCatch Ltd, p. 121, 2001.
- [52] [online]. Available: <http://www.southernstatesllc.com/>.
- [53] L. Niemeyer, "Evaporation dominated high current arcs in narrow channels", *IEEE Trans. Power Appl. Syst.*, vol. PAS-97, pp. 950–958, Jun. 1978.
- [54] E. Z. Ibrahim, "The ablation dominated polymethylmethacrylate arc", *J. Phys. D: Appl. Phys.*, vol. 13, pp. 2045–2065, 1980.
- [55] T. Chino, M. Iwata, "Development of arcing horn device for interrupting ground-fault current of 77 kV overhead lines", *IEEE trans. on power delivery*, vol.20, pp.2570-2575, Oct. 2005.
- [56] [online]. Available: <http://www.driescher.com/home/index.htm>.
- [57] S. Gu, J. He. "Motion characteristics of long ac arcs in atmospheric air", *Applied Physics Letters*, vol.90, pp. 0515011-0515013, 2007.
- [58] A. T. Johns, R. K. Aggarwal, Y. H. Song, "Improved techniques for modelling fault arcs on faulted EHV transmission systems", *IEE Proceedings Generation, Transmission and Distribution*, vol.141, pp. 148-154, Mar. 1994.
- [59] L. Prikler, M. Kizilcay, G. Ban, "Improved secondary arc models based on identification of the arc parameters from staged fault test records", in *Proc. 14th Power Systems Computation Conf.*, paper nr. 3, p. 1-7, Jun. 2002.
- [60] G. Meunier, A. Abri, "A model for the current interruption of an electric arc", *IEEE Trans. on Magnetics*, vol.20, pp. 1956–1958, Sept. 1984.
- [61] S. Gu, J. He, B. Zhang, G. Xu, S. Han, "Movement simulation of long electric arc along the surface of insulator string in free air", *IEEE Trans. on Magnetics*, vol.42, pp. 1359-1362, Apr. 2006.
- [62] K. Horinouchi, Y. Nakayama, M. Hidaka, "A method of simulating magnetically driven arcs", *IEEE Trans. on Power Delivery*, vol.12, pp. 213-218, Jan. 1997.
- [63] A. Al-Rawi, M. Devaney, "Measurement of secondary arc current in transmission lines employing single phase switching", in *Proc. IEEE Instrumentation and Measurement Technology: Sensing, Processing, Networking Conf.*, vol.1, pp. 297-301, May. 1997.
- [64] L. van der Sluis, *Transients in Power Systems*, England, John Wiley & Sons Ltd, p.70, 2001.
- [65] A. P. Strom, "Long 60-cycle arcs in air", *AIEE Trans.*, vol. 65, pp.113–118, Mar. 1946.
- [66] A. S. Maikapar, "Extinction of an open electric arc", *Elek trichestvo*, vol.3, pp. 64-69, Apr. 1960.
- [67] G. Song, J. Ling, "Research on secondary arc in 1000 kV UHVAC two-circuit transmission lines and its control", in *Proc. of Chinese Society for Electrical Engineering*, vol.31, pp.138-143, Jun. 2011.
- [68] M. Kizilcay, G. Ban, L. Prikler, P. Handl, "Interaction of the secondary arc with the transmission system during single-phase autoreclosure", in *Proc. IEEE Power Tech Conf, Bologna*, vol.2, p. 1-7, Jun. 2003.
- [69] M. Kizilcay, P. La Seta, "Digital simulation of fault arcs in medium-voltage distribution networks", in *Proc. 15th Power Systems Computation Conf.*, paper nr. 3, p. 1-7, Aug.2005.
- [70] M. Kizilcay, T. Pniok, "Digital simulation of fault arcs in power systems", *European Trans.on Electrical Power*, vol.1, pp. 55-60, Jan. 1991.

-
- [71] V. Terzija, H. Koglin, "Long arc in free air: testing, modelling and parameters estimation: part I", in *IEE Proc. Generation, Transmission and Distribution*, vol.2, pp. 404-409, May 2002.
 - [72] V. Terzija, H. Koglin, "Long arc in free air: testing, modelling and parameters estimation: part II", in *IEE Proc. Generation, Transmission and Distribution*, vol.2, pp. 481-486, May 2002.
 - [73] V. Terzija, Z. M. Radojevic, "Numerical algorithm for adaptive autoreclosure and protection of medium-voltage overhead lines", *IEEE Trans. on Power Delivery*, vol.19, pp. 554-559, Apr. 2004.
 - [74] V. Terzija, H. Koglin, "Laboratory testing and dynamic modelling of long arc in free air", in *Proc. International Conference Power System Technology*, vol.2, pp. 897-902, Dec. 2000.
 - [75] V. Terzija, G. Preston, M. Popov, N. Terzija, "New Static "AirArc" EMTP model of long arc in free air power delivery", *IEEE Trans. on Power Delivery*, vol.26, pp. 1344-1353, Jul. 2011.

Chapter 3

Basic Circuit Analysis

Capacitive current interruption by a DS is considered as a topology with capacitances at either side of the DS. The capacitance at the supply side may come from (instrument) transformers, busbars or also from the other conductors that are connected to the busbar. The capacitance at the load side of the DS, may come from unloaded transmission line, busbar, etc. The capacitance values range from less than one nanofarad, e.g. for short lines, to hundreds nanofarad in case of large capacitor banks. Switching of DSs is basically governed by charge exchange between these capacitances. This thesis is concerned with switching between capacitances that can be considered as lumped elements capacitances that have values up to 300 nF. Capacitor banks, having much larger value, are not switched with DSs.

3.1 The interruption process

Capacitive current interruption with a DS consists of the interaction between the circuit and the arc. This interaction results in a repetitive sequence of breaks (interruption of current) and re-strikes and/or re-ignitions. Re-strike is a breakdown of the insulating medium – the air between the DS blades - resulting in re-establishment of the arc, more than one quarter of a cycle after interruption. Re-ignition is the same physical event, but within one quarter power-frequency cycle. Re-strikes and re-ignitions are characterized in terms of transients in current and voltage due to oscillations in the circuit. The arc is macroscopically characterized in terms of its duration, reach (perpendicular distance of outermost arc position to a line connecting the contacts), type (repetitive or continuous), the energy input from the circuit during the re-strike, arc voltage, arc brightness, and so forth. Understanding the basic phenomena upon re-strike or re-ignition is essential in the understanding of capacitive current interruption. It will therefore be addressed in detail in this chapter.

The equivalent circuit for capacitive current interruption is shown in Figure 3.1 [1]. The DS is marked with D ; R_s , C_s and C_l stand for resistance, capacitance at supply and load side respectively; i_d is the current; u_s is the phase-to-ground supply voltage of the network. u_d , u_{cs} and u_{cl} are voltage across the D , C_s and C_l respectively. The short-circuit inductance is based on the short-time withstand current for which the DS is rated: $L_s = U_{line}/(\sqrt{3}\omega I_{sc})$ with I_{sc} is the short-time withstand current; U_{line} is the rms of the source phase-to-phase voltage. For example, $I_{sc}=40$ kA, $U_{line}=145$ kV, $\omega = 2\pi f$ ($f = 50$ Hz), L_s is about 7 mH.

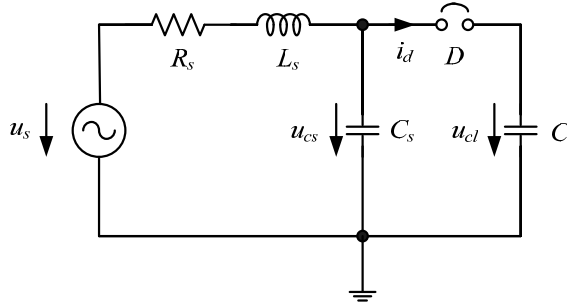


Figure 3.1. Basic circuit diagram for capacitive current interruption with a DS.

Before the interruption starts, the DS is closed. The circuit of Figure 3.1 is energized by a harmonic source $u_s = E_m \sin(\omega_p t + \theta)$, with ω_p the angular power-frequency, E_m the amplitude, and θ the initial phase angle. The current i_d and the voltage across the capacitances C_s and C_l (denoted as u_{cp}) are:

$$\begin{cases} u_{cp} \approx E_m \sin(\omega_p t + \theta) \\ u_{cs} = u_{cl} = u_{cp} \\ i_d \approx C_l \omega_p E_m \cos(\omega_p t + \theta) \end{cases} \quad (3.1)$$

It is assumed that the impedances R_s and $\omega_p L_s$ are much smaller than $1/(\omega_p C_{s,l})$, meaning that the voltage u_{cp} is very close to u_s . Theoretically, if C_s is very large, then i_d is reduced because of a voltage drop across R_s and L_s (C_s is normally in the order of a few tens of nanofarad in practice).

When the DS interrupts the current, the circuit in Figure 3.1 is separated into two parts abruptly. The supply circuit (left of the DS, consisting of R_s , L_s , C_s) remains energized with u_s . Since the impedance of C_s is much larger than the impedances of R_s and L_s , u_{cs} remains close to the source voltage u_s . The right part of the DS, i.e. C_l , has no discharge path and the voltage u_{cl} across C_l remains 1 p.u. due to trapped charge. After the arc extinguishes at current zero, the RV starts to rise. The RV across the DS u_d , is the difference between u_{cs} and u_{cl} arising after interruption ($u_d = u_{cs} - u_{cl}$). The dielectric strength of the air gap, denoted as u_r , starts to recover simultaneously. When the increasing value of u_d exceeds u_r , the gap re-ignites or re-strikes and the arc re-establishes. This process is shown in Figure 3.2.

In principle the arc lasts no longer than half a power cycle and extinguishes temporarily when the arc current crosses zero. The circuit is separated into two parts again until the next re-strike or re-ignition occurs, but generally at a higher voltage because the contacts have separated further after a half cycle. The interruption process therefore consists of repeated arc extinctions and re-strikes/re-ignitions. Finally, this sequence comes to an end and the arc

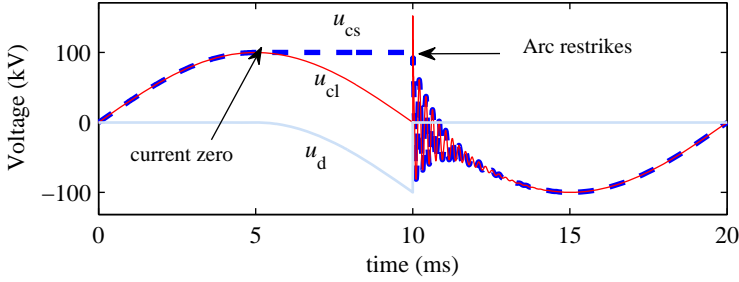


Figure 3.2. Illustration of the moments when the arc extinguishes and re-strikes.

extinguishes completely when the distance between the DS contacts has become sufficiently large and the RV remains below the dielectric strength of the gap [2]. When this is not the case, the arc lasts as long as the power supply is active or as long as external influences (wind) do not extinguish the arc. In practical situations, normal interruption should be achieved before the blades reach a 90 degree angle with respect to the original closed position of the main blades. After this moment, due to excessive elongation and reach, the arc may endanger the insulation of the station arrangement.

3.2 Three-components analysis

Upon each re-strike, the voltages u_{cs} , u_{cl} , u_d and the current i_d have oscillations at distinct frequencies. A high-frequency (HF) component arises after re-strike when the voltages across source and load side capacitances are equalizing. After this process, the voltages u_{cl} , u_{cs} are equal and a voltage drop arises across L_s , which causes a medium-frequency (MF) oscillation in the circuit. As the HF and MF oscillations are damped out, the power-frequency (PF) remains. These frequency components will be analyzed as follows.

3.2.1 High-frequency (HF) component

At the instant of re-strike the voltages u_{cs} and u_{cl} will equalize through a high-frequency oscillation. The voltage U_E , remaining across both C_s and C_l after equalization is calculated from conservation of charge stored in both capacitances:

$$U_E = \frac{U_{cs}C_s + U_{cl}C_l}{C_s + C_l} [3], \text{ where } U_{cs}, U_{cl} \text{ are the initial voltages across } C_s, C_l \text{ at the}$$

moment of the restrike respectively. In the HF circuit model shown in Figure 3.3, the power supply is neglected since it is decoupled by the high impedance of inductance L_s for the HF oscillation. R_H , L_H represent the high-frequency resistance and inductance of the circuit formed by the capacitances, the DS and the arc

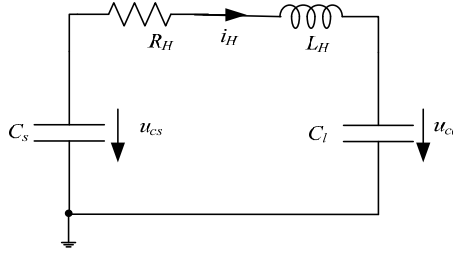


Figure 3.3. High-frequency equivalent circuit diagram.

within the HF loop. u_{cs} , u_{cl} and i_H denote the voltage across C_s , C_l and the current in the high-frequency loop circuit respectively. The HF oscillation lasts only a short time (typically less than a few tens of microseconds), during which it can lead to a high transient current through circuit and arc and moderate to transient voltages across both capacitances.

The voltage across the air gap just before re-strike at time approaching $t = 0$ is denoted as $U_r (= U_{cs} - U_{cl})$. At this voltage the air gap breaks down. Assuming for the total circuit resistance $R_H < 2\sqrt{\frac{L_H}{C_H}}$, and the equivalent capacitance as seen by

the arc: $C_H = \frac{C_s C_l}{C_s + C_l}$, it is found:

$$\begin{cases} u_{cl} = -\frac{U_r}{1 + C_l/C_s} \frac{\omega_{0H}}{\omega_H} e^{-\delta_H t} \sin(\omega_H t + \beta_H) + U_E \\ i_H = \frac{U_r}{L_H \omega_H} e^{-\delta_H t} \sin(\omega_H t) \end{cases} \quad (3.2)$$

Similarly, the voltage u_{cs} across the source side capacitance at HF can be calculated:

$$u_{cs} = \frac{U_r}{1 + C_s/C_l} \frac{\omega_{0H}}{\omega_H} e^{-\delta_H t} \sin(\omega_H t + \beta_H) + U_E \quad (3.3)$$

where $\delta_H = \frac{R_H}{2L_H}$, $\omega_{0H} = \frac{1}{\sqrt{L_H C_H}}$, $\omega_H^2 = \omega_{0H}^2 - \delta_H^2$, $\beta_H = \arctan \frac{\omega_H}{\delta_H}$.

The parameter δ_H is the HF damping constant. The HF oscillation angular frequency ω_H depends mainly on the inductance and the series connection of both capacitances. This frequency can be up to several megahertz. The current magnitude can reach values up to 7 kA in the tests. The oscillation across the

capacitances eventually ceases and settles at a quasi steady state value U_E . The maximum voltage across C_s and C_l , which occurs in case of negligible HF damping,

$$\text{is: } \max(u_{cs}) = \left| \frac{U_r}{1 + C_s/C_l} \right| + |U_E| \text{ and } \max(u_{cl}) = \left| \frac{U_r}{1 + C_l/C_s} \right| + |U_E|, \text{ respectively. The}$$

rise speed of the current depends on the breakdown voltage and the inductance in HF loop: $\max(di/dt) = U_r/L_H$.

At the smaller capacitance, C_s or C_l , arises the higher maximum voltage and both voltages across the capacitances are proportional to the re-strike voltage U_r . Further, U_r increases with increasing contacts distance, which means the HF voltages across the capacitances will primarily become largest just before the arc extinguishes completely. The maximum HF voltage that can occur is $3E_m$, in case $U_r = 2E_m$ and either $C_s \ll C_l$ or $C_s \gg C_l$. The maximum current through the DS in the HF loop is $U_r \sqrt{C_H/L_H}$ (neglecting HF damping). Obviously, i_H increases with increasing U_r and C_H and decreases with increasing L_H . Thus U_r and C_s/C_l (or C_l/C_s) are key parameters that affect the HF transient behaviour on re-strikes. The HF transients in the current are candidates to cause electro-magnetic interference in secondary systems, as it will be reported in Chapter 5. Given the high-frequency and amplitude derivatives of the current, up to a few kiloamperes per microseconds in later tests, it can couple inductively with neighbouring circuitry. Also, it provides a significant power input into the re-striking arc, albeit during a limited time.

3.2.2 Medium-frequency (MF) component

Upon re-strike, also a "medium-frequency" (MF) oscillation starts. The MF component, which lasts about a few milliseconds, also causes a transient voltage and current. At this stage the voltage across the arc is neglected and the analysis starts after decay of the HF transient, with voltage of each capacitor equalized to U_E . L_H in Figure 3.3 is neglected as well, because its equivalent impedance is much smaller than the capacitance's impedance at MF. Therefore, C_s and C_l with an identical initial voltage U_E are in parallel and the equivalent circuit of Figure 3.1 at MF applies. Because of the charge redistribution during the HF oscillation, the voltages across C_s and C_l have changed, and will discharge via L_s and R_s during the duration of the MF oscillation.

The instant of re-strike is again taken as $t = 0$. On the time scale of the MF oscillation, u_s can be treated as a constant ($E_m \sin\theta$). Similarly as for the HF analysis, u_{CM} (the voltage across C_s and C_l), and i_M (the current through the DS) can be determined:

$$\begin{cases} u_{CM} = E_m \sin \theta - \frac{U_r}{1 + C_s/C_l} \frac{\omega_{0M}}{\omega_M} e^{-\delta_M t} \sin(\omega_M t + \beta_M) \\ i_M = \frac{1}{(1 + C_s/C_l)^2} \frac{U_r}{L_s \omega_M} e^{-\delta_M t} \sin(\omega_M t) \end{cases} \quad (3.4)$$

where $\delta_M = \frac{R_s}{2L_s}$, $\omega_{0M} = \sqrt{\frac{1}{L_s(C_s + C_l)}}$, $\omega_M^2 = \omega_{0M}^2 - \delta_M^2$, $\beta_M = \arctan \frac{\omega_M}{\delta_M}$.

The oscillation frequency ω_M mainly depends on the sum of both capacitances and the inductance L_s . In general the frequency of this oscillation is in the order of several kilohertz. Similarly as for the high-frequency transient, the voltages during the MF oscillation across both capacitances with initial voltages U_E are damped due to the equivalent resistance in the loop and finally reach the value u_s . The

maximum voltage across the capacitances is $|E_m \sin \theta| + \left| \frac{U_r}{1 + C_s/C_l} \right|$. It increases with

increasing U_r , ratio C_l/C_s and E_m . Similar to the HF oscillation, the maximum theoretical voltage is $3E_m$. The maximal current during the MF oscillation is:

$\max(i_M) = \left| \frac{1}{(1 + C_s/C_l)^2} \frac{U_r}{L_s \omega_M} \right|$, which depends on U_r , C_s/C_l and L_s as well, and scales

with U_r .

3.2.3 Three-components synthesis

After HF and MF components have damped out, only the PF component remains. Since the time constants involved are highly distinct, the HF component vanishes on the timescale for the MF oscillation and the MF oscillation has disappeared on the timescale for PF. The initial voltage, at which the MF oscillation starts, is the final steady state voltage after HF oscillation decay and the initial voltage for the PF oscillation is the final steady state voltage of the MF oscillation.

In order to quantify the complete transient behaviour, the three-components are combined. The voltage u_{cl} across the load side capacitance and the current i_d flowing through the DS on re-strike can be written as:

$$\begin{cases} u_{cl} = -\frac{U_r}{1 + C_l/C_s} \frac{\omega_{0H}}{\omega_H} e^{-\delta_H t} \sin(\omega_H t + \beta_H) - \frac{U_r}{1 + C_s/C_l} \frac{\omega_{0M}}{\omega_M} e^{-\delta_M t} \sin(\omega_M t + \beta_M) + E_m \sin(\omega_p t + \theta) \\ i_d = \frac{U_r}{L_H \omega_H} e^{-\delta_H t} \sin(\omega_H t) + \frac{1}{(1 + C_s/C_l)^2} \frac{U_r}{L_s \omega_M} e^{-\delta_M t} \sin(\omega_M t) + C_l \omega_p E_m \cos(\omega_p t + \theta) \end{cases} \quad (3.5)$$

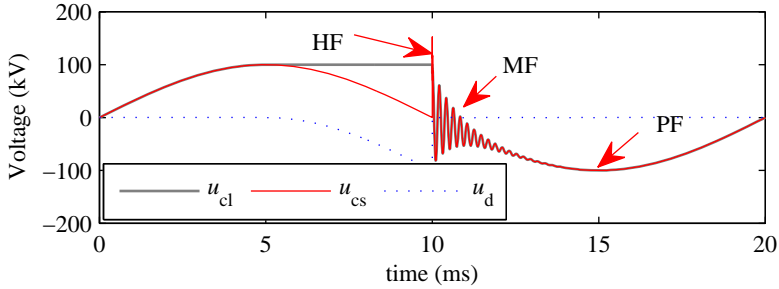


Figure 3.4. Simulated wave shapes of u_{cs} , u_{cl} , u_d during one power frequency cycle upon re-strike.

Equation (3.5) contains the three frequency components in the voltage across the load side capacitance and in the current through the DS arc. The voltage across the source side capacitance can be calculated in a similar manner. It turns out that the transient voltages and currents depend on the air gap breakdown voltage, voltage supply level, the ratio of C_s/C_l and so forth. In the following sections the distinct frequency contributions to overvoltages and currents will be discussed on the basis of the analysis above and compared with experimental data.

3.3 Simulation of re-strikes

For illustrating the re-strike phenomena in voltage and current waveforms a simulation is performed using MATLAB Simulink (SimPowerSystems). The parameters taken are: $E_m = 70\sqrt{2}$ kV, $L_s = 10$ mH, $C_s = 10$ nF, $C_l = 100$ nF, the resistance for arc at re-strike is taken as 20Ω and $L_H = 15 \mu\text{H}$. Initially, the DS is in closed position. The DS gap starts to recover at $t = 5$ ms, and re-strikes at $t = 10$ ms. The simulated wave shapes for the current i_d , voltages u_{cl} , u_{cs} and u_d together with their zoomed in of the HF and MF components, are plotted in Figures 3.4-3.6. In Figure 3.4, the three-components are indicated with arrows. According to Section 3.2, the charges of the source and load side capacitance C_s and C_l exchange during the high-frequency period until the equalization voltage U_E is reached, shown in Figure 3.5. The medium-frequency component, after the high-frequency oscillation has disappeared, is depicted in Figure 3.6. In a similar way, the wave shapes of the current i_d and its high and medium-frequency components are shown in Figures 3.7-3.9.

It can be observed that the high and medium-frequency components last about $10 \mu\text{s}$ and 2-3 ms respectively in this simulation. During the oscillation, there is a transient current with a peak value up to 2 kA upon re-strike at $t = 10$ ms. The observed overvoltage across the source side capacitance C_s is 1.5 p.u.

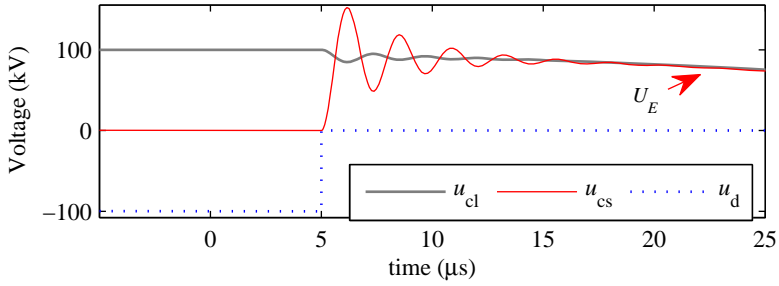


Figure 3.5. Simulated wave shapes of u_{cs} , u_{cl} , u_d at high-frequency (zoomed in from approximately 9.96 ms to 10.06 ms in Figure 3.4).

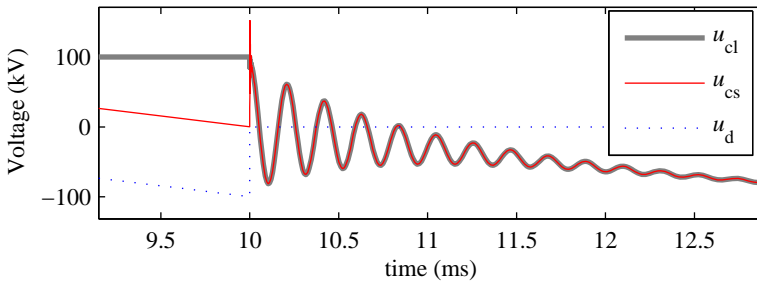


Figure 3.6. Simulated wave shapes of u_{cs} , u_{cl} , u_d at medium-frequency (zoomed in from approximately 9.5 ms to 12.5 ms in Figure 3.4).

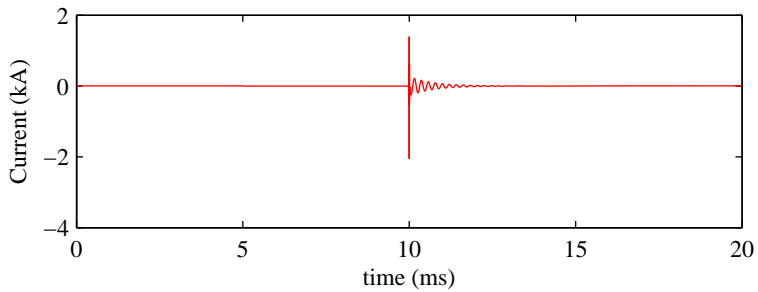


Figure 3.7. Simulated wave shapes of i_d over one power frequency cycle upon re-strike.

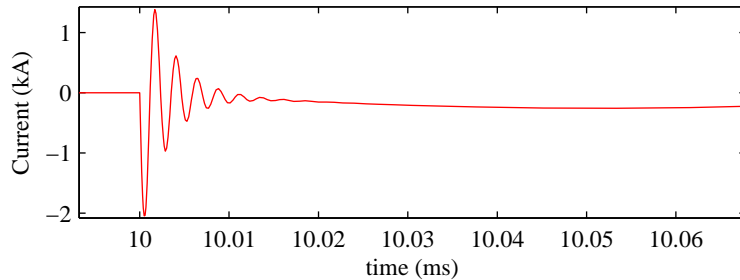


Figure 3.8. Simulated wave shapes of i_d at high-frequency (zoomed in from approximately 10.00 ms to 10.06 ms in Figure 3.7).

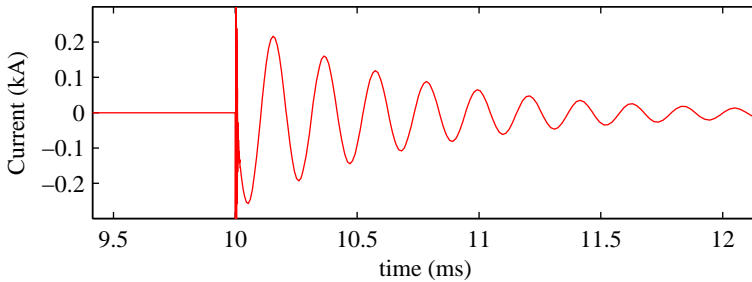


Figure 3.9. Simulated wave shapes of i_d at medium-frequency (zoomed in from approximately 9.5 ms to 12.0 ms in Figure 3.7).

3.4 Re-strike transients in distributed element load circuits

In the circuit of Figure 3.1 only lumped components are considered. As mentioned in Chapter 1, the capacitive current to be interrupted arises from substation components, such as current transformer, capacitive voltage transformer, but also from distributed elements, such as busbars, overhead line, and power cables.

If the physical dimensions of the considered components are much shorter than the wavelength corresponding with the current and voltage oscillations, lumped parameters can be used to model the power system. Otherwise, a distributed parameter approach has to be adopted. The transmission line specific (per unit length) parameters L , C and R (G is omitted since the air is considered a perfect insulator) are uniformly distributed over the length of the line. For the steady state operation (power-frequency, 50 Hz or 60 Hz), the transmission lines can be represented by lumped parameters. But for transient behaviour the lines it may be necessary to be represented by distributed parameters.

During the capacitive current interruption by a DS, transient phenomena occur with high-frequency content, due to the repeated breaks and re-strikes. Therefore, a distributed parameter simulation for transmission lines is considered in this section. The simulated results of a lumped parameter and a distributed parameter approach of a transmission line are compared.

The value of the lumped element parameters in Figure 3.10 are taken to produce the same power-frequency results as those in Figure 3.1. The unloaded overhead line is simulated with distributed parameters. A line length of 50 km is taken to match the interrupted current I_d (PF current of 9 A) of the lumped circuit (line capacitance and inductance are 8.48 nF/km and 1.33 mH/km, matching a lumped load side capacitance of $C_l = 424$ nF). The simulated results are shown in the Figures 3.11-3.13, where the wave shapes of the interrupted current i_d and the voltage across the DS u_d , are presented respectively: i_{d1} , u_{d1} are simulated results from simulation with distributed elements, and i_{d2} , u_{d2} are simulated results are obtained from simulation with lumped elements.

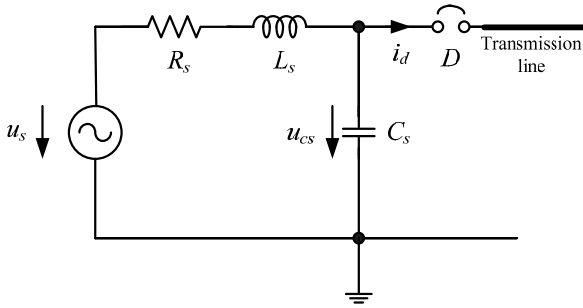


Figure 3.10. Simulated circuit for capacitive current interruption with a transmission line represented by distributed parameters.

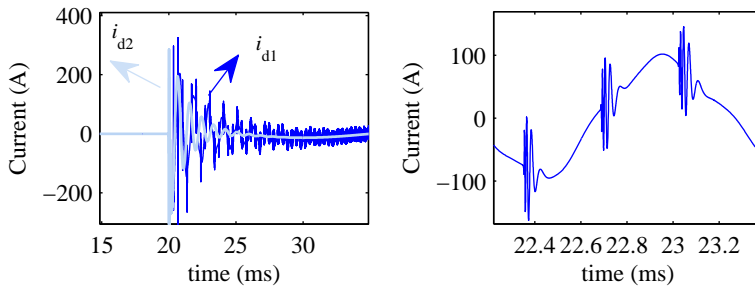


Figure 3.11. (Left) wave shapes of the current i_{d1} , i_{d2} through the DS with distributed lines and lumped capacitance respectively and (right) expansion of i_{d1} between 22.4 ms and 23.2 ms.

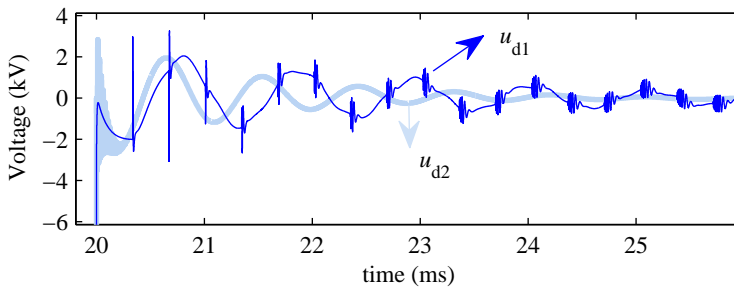


Figure 3.12. Wave shapes of the voltage u_{d1} , u_{d2} across the DS with distributed lines and lumped capacitance respectively.

The wave shapes of current and voltage show that the travelling waves are reflected within 0.33 ms. There are transient phenomena on each reflection moment (see Figure 3.11, 3.12). Nevertheless, there is hardly any high-frequency component at re-strikes in the voltage and current waveforms with the distributed parameters, which consequently reduces the total amount of energy

input into the circuit upon re-strike. This is because the high surge impedance of the line (in this example 390Ω) limits the HF re-strike current compared to the much lower surge impedance of the lumped capacitor. Therefore, to interrupt a circuit with lumped parameters is a more severe task as compared to a configuration with distributed parameters. In the analysis in this chapter, and also in the experimental arrangement described in the following chapters, circuits with lumped elements are applied. This point should be paid attention to, because of its impact on testing, where normally (lumped) capacitor banks are used.

3.5 Conclusion

The main observations with respect to calculations and simulations on capacitive current interruption with high voltage air-break DSs are:

Capacitive current interruption by a DS consists of repeated breaks and re-strikes as a consequence of the interaction between arc and circuit.

The transient upon re-strike consist of three-components: high, medium and power-frequency component. During the high-frequency component, the transient period is in the order of a few tens of microseconds. The medium-frequency component is in the order of a few milliseconds. The overvoltage across the capacitances at both sides of the DS can be up to 3 p.u. theoretically. The peak of the transient current may be up to a few kiloamperes within a few microseconds.

The ratio of source and load side capacitance, the re-strike voltage and the current to be interrupted are the key factors that influence the transient voltage and current magnitudes upon re-strike.

The circuit with lumped elements, which is adopted in this thesis, is a worst case approach. Capacitive current interruption of transmission lines where a distributed parameter approach applies is less severe.

References

- [1] IEC Technical Report IEC/TR 62271-305, "High voltage switchgear and controlgear-Part 305: Capacitive current switching capability of air-insulated DSs for rated voltages above 52 kV", Nov. 2009.
- [2] L. van der Sluis, "*Transients in Power Systems*", Chichester: John Wiley & Sons, 2001.
- [3] D. F. Peelo, "Current interruption using high voltage air-break DSs", Ph.D. dissertation, Dept. Electrical Engineering, Eindhoven Univ. of Technology, Eindhoven, 2004.

Chapter 4

Experimental Setup

Experiments in this thesis are performed at several locations employing different types of voltage sources. The basic circuit diagram for all test sites was presented in Figure 3.1. Figure 4.1 depicts the general setup including the measuring system schematically.

The voltage supply is represented by an ideal voltage source u_s with series resistance R_s representing losses and inductance L_s . Their values depend on the source type being used (see Section 4.1). Capacitances C_s and C_l stand for the source and load side capacitor banks with a DS in between. The capacitance values can be varied for the test series. The voltages u_{cs} , u_{cl} are the voltages across C_s and C_l , respectively. These voltages are measured by the capacitive voltage dividers D_1 and D_2 in combination with the high voltage probes D_3 and D_4 (Section 4.2.1). The differential signal is used to determine the voltage across the DS (Section 4.2.2). The current through the DS is indicated by i_d . Current transformers CT_1 and CT_2 measure the current through C_l (Section 4.2.3). Two current transformers are applied to cover the dynamic range of different frequency components simultaneously (below 1 A to several kiloamperes and from 50 Hz to several megahertz), denoted as i_{pf} and i_{hf} , respectively. Voltages and currents are recorded by a data acquisition system including four digitizers, CH_{1-4} , each having a single input channel (Section 4.2.4). In addition to the electrical signals, arc images are recorded by means of a high-speed camera, which is installed on the same height as the DS blades (Section 4.2.5). The opening characteristics of the DS is determined in Section 4.3.

4.1 High voltage source

Two different types of high voltage source are employed. Depending on the test sites, a power transformer or a resonance high voltage source is used.

A short-circuit generator plus a transformer are available in large scale laboratories, such as KEMA High Power Laboratories in Arnhem and Prague. The equivalent test circuit is shown in Figure 4.2. A source inductance L_s is used with a value up to a few hundreds of millihenry. Air gaps are used to protect the capacitors bank, but are not shown in Figure 4.2. These setups supply up to 173 kVrms phase-to-ground voltage, and up to 27 A current during the experiments. The specific test configurations employed for different series of experiments will be presented in Chapters 5, 6 and 7.

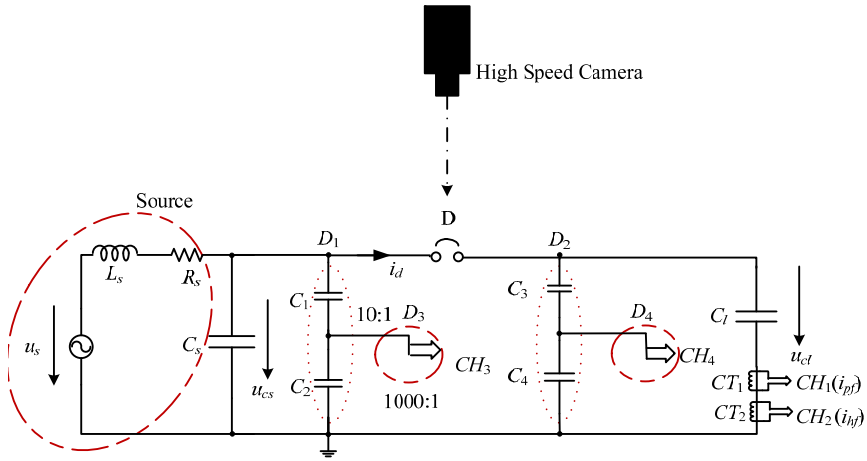


Figure 4.1. Experimental circuit including electrical and optical transducers.

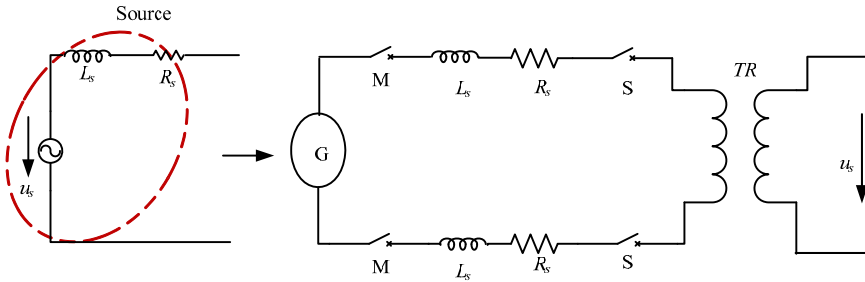


Figure 4.2. Test circuit with source in KEMA HPL. *G*: short-circuit generator; *M*: master breaker; L_s , R_s : reactor and resistor at source side; *S*: make switch; *TR*: short-circuit transformer.

In the high voltage laboratory at the Eindhoven University of Technology a resonant system (Hipotronics) is available as high voltage supply. Its top view and equivalent scheme are shown Figure 4.3 (left and right, respectively).

The resonant system includes an adjustable high voltage reactor L_s , a capacitor C and an exciter transformer. The variable auto transformer T_1 controls the transformer T_2 , which supplies power to the resonant circuit, and it isolates the test specimen from the line. Two tuneable reactors, which can be connected either in series or in parallel, make up the source inductance. Each of them has an inductance with a value in the range of 400 H-10 kH, and resistance (measured at DC) of about 1 k Ω . Each reactor is designed for a voltage of 300 kVrms. The AC

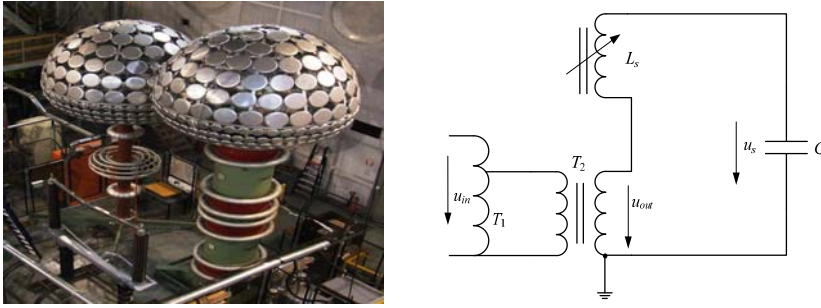


Figure 4.3. (left) Laboratory source for capacitive current interruption with a DS at TU/e; (right) simplified schematics of Hipotronics high voltage source.

source powering the resonant circuit, indicated with u_{out} in Figure 4.3 (right) is at maximum 22 kVrms. The capacitance C_s is chosen either 2 nF or 4 nF by series connections of four or two 8 nF, 150 kV capacitors. Different combinations of ten available 16 nF high voltage capacitors can be made to adjust the (load) capacitance C_l to the desired current. Each of these capacitors has a rated voltage of 150 kVrms and $\tan\delta < 5 \times 10^{-3}$. The total capacitance (denoted as C in Figure 4.3 (right)) before opening the DS includes the capacitances at both sides of the DS, including capacitances from voltage dividers, bushings, etc. The reactor L_s is adjusted to compensate the total capacitive reactance and thereby tuning the circuit. The quality factor Q of this system can reach values of 50-80 for high quality capacitive loads. The system is capable to supply a 50 Hz high voltage up to 300 kV. Ideally, a maximum current of 2 A or 4 A can be achieved, depending on whether the reactors are in series or in parallel. During the experiments, first the system is energized with the closed DS at a low level of u_s . Next, the inductance L_s is tuned until L_s and C become resonant at 50 Hz. Once the system is in resonance, the desired voltage level is chosen and the interruption experiment can commence.

A drawback of the resonant system is that it can be tuned into resonance at power-frequency while the DS is in closed position only. When the DS starts opening, the resonant condition still remains because the load capacitor is connected through the conductive arc at the very beginning. The quality of the circuit drops, however, due to the arc resistivity. Since the arc extinguishes repeatedly at each current zero, the resonance is lost during the voltage recovery period. After re-strike/re-ignition, the resonance condition is met again but the source voltage has started dropping. Figure 4.4 shows the decay of measured source voltage at different initial high voltage levels. It demonstrates that the system voltage decays rapidly after 10 to 20 power-frequency cycles.

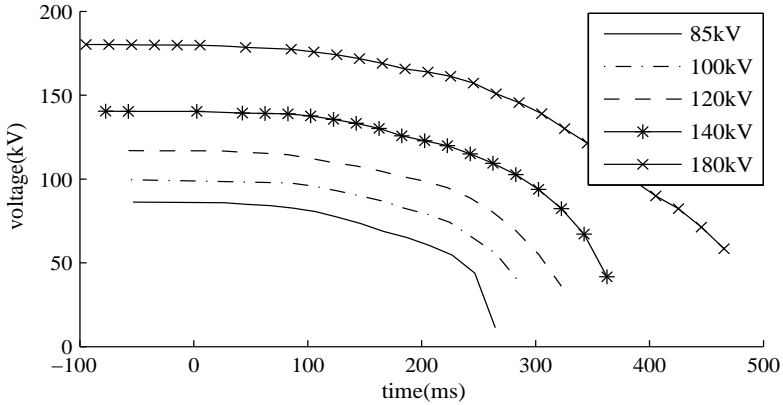


Figure 4.4. Source voltage decay by loss of resonance and energy dissipation by the arc, measured results.

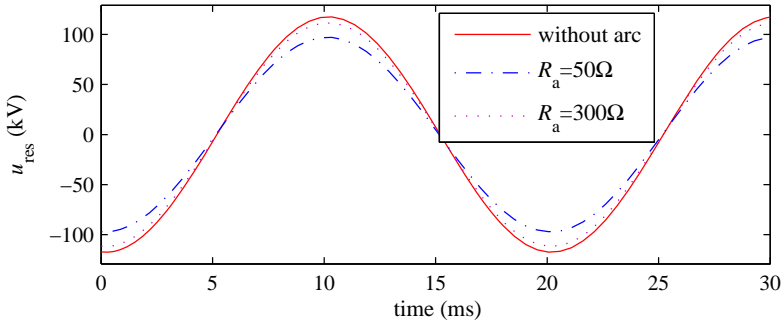


Figure 4.5. Resonant voltage reduction for different values of the arc resistance, simulated results.

The arc resistance is in the order of several hundred ohms (Section 5.5.3), i.e. only in the order of 10-30% of the dc resistance of the resonant circuit (1 k Ω). As simulated in Figure 4.5 this is expected to reduce the source voltage with the same amount, since the circuit quality is inversely proportional to the total circuit resistance. The initial voltage reduction can be ascribed to the energy dissipation in the arc, since the arc interruption time is still negligible. The voltage drops after ten cycles is larger than can be expected based on the arc energy dissipation. This reduction must mainly be ascribed to the longer arc interruption periods with increased air gap distance between the DS blades resulting in loss of resonance.

Another drawback of the resonant circuit is that this circuit deviates strongly from the practical situation in which circuits have a low value of source inductance (or a high short-circuit power). This causes the medium-frequency component during the transients to be virtually absent. In this situation, the experiments definitely

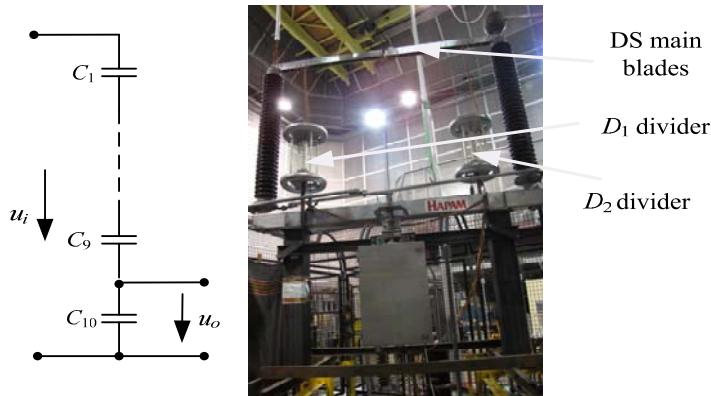


Figure 4.6. Scheme of the voltage dividers (D_1 or D_2), $u_i:u_o = 10.7:1$ and their mounting positions in parallel to the DS insulators.

do not match practical situations. Specifically, compared to the experiments performed in the large test laboratories, the arc duration and length is shorter and the arcing/switching is accompanied with lower overvoltage levels. The experiments done at the TU/e high voltage laboratory therefore are used for study of the principal (microscopic) phenomena, but are not suitable to give realistic macroscopic results, e.g. arc duration.

4.2 Measurement system

The electrical signals and optical arc image recording system are described in this section.

4.2.1 Voltage measurement

The voltage measuring systems at both DS sides are identical from design. Each capacitive divider consists of ten Murata 2 nF, 40 kV capacitors in series (D_1 or D_2), and a 1000:1 North Star high voltage probe (D_3 or D_4), see Figure 4.1 [1], [2]. The ten divider capacitors for both dividers are carefully selected to realize a division ratio being as close as possible to each other. The capacitive dividers (C_1 – C_{10}) are shown in Figure 4.6 with division ratio $u_i:u_o = 10.7:1$. The dividers are mounted in parallel to the DS insulators. The determination of the divider response up to the cut-off frequency is accomplished by injecting a unit step voltage with a rise time of 20 ns. The wave shapes of the input and output signals and their transfer function (u_i/u_o) are shown in Figure 4.7 and 4.8, respectively. The results show that the capacitive voltage dividers have bandwidths up to about 5.5 MHz. In the experiments, the highest transients (HF oscillation, see Chapter 3) have frequencies up to 1 MHz (see Figure 5.6), which has attenuation of less than 2% (for cut-off frequency of 5.5MHz).

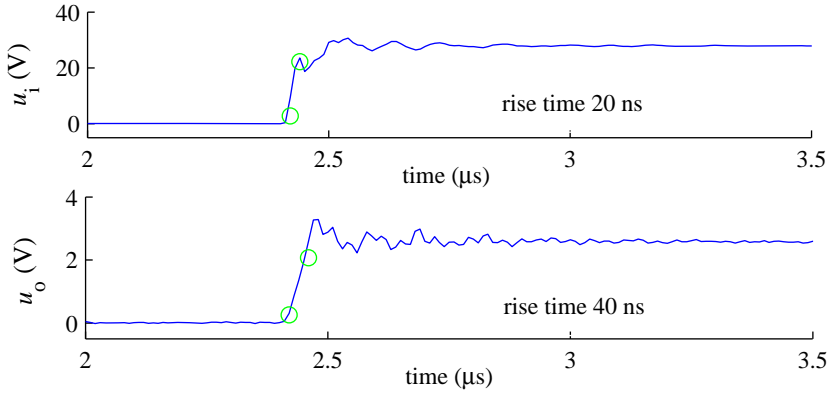


Figure 4.7. Injected step function (top) and response (bottom) of the divider.

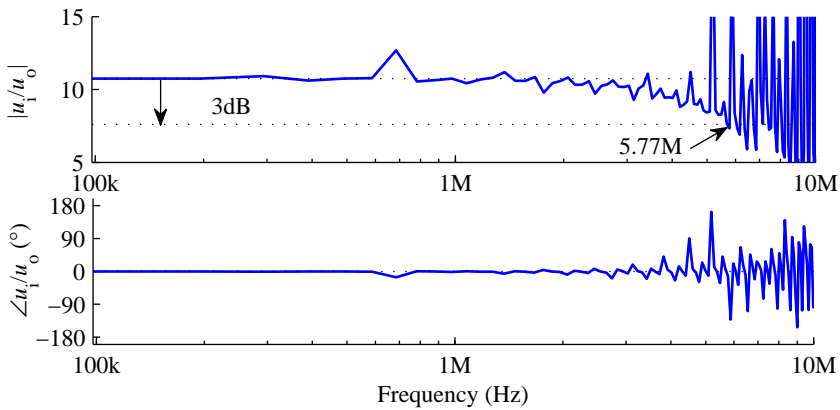


Figure 4.8. Frequency response of the capacitive voltage dividers (u_i/u_o).

In order to lower the output voltage from the Murata capacitor stack divider further to be able to supply it to the digitizer system, commercial voltage dividers (probes) are used. The high voltage probe, (type North Star, PVM-5), is basically a parallel RC voltage divider designed to produce precisely attenuated signals over a wide bandwidth. The circuit diagram is shown in Figure 4.9. The divider network contains a high voltage branch consisting of a parallel capacitor and resistor and a low-voltage network, which consists of a parallel RC network and a compensation circuit. The high voltage section of the voltage divider is contained in an oil-filled housing. The low-voltage section is contained in a separate box underneath the divider's base. Its main characteristics are: max DC/pulse voltage: 60/100 kV; bandwidth: 80 MHz; cable impedance: 50 Ω ; input R/C: 400 M Ω /13 pF; divider ratio: 1000:1.

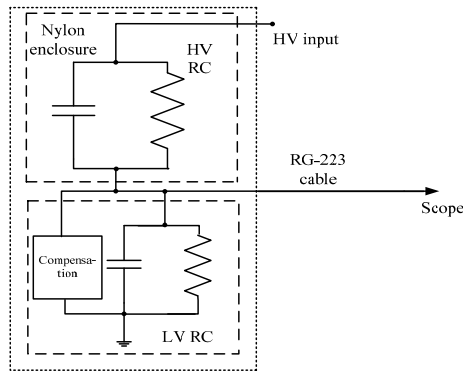


Figure 4.9. Circuit diagram of the voltage divider.

4.2.2 Differential voltage accuracy

Accurate voltage measurements of the voltage across the DS (u_d) are essential for arc voltage and re-strike voltage analysis. Therefore, the differential voltage $u_d = u_{cs} - u_{cl}$ must be available with the highest possible precision. This is achieved by comparing the voltages u_{cs} and u_{cl} in closed position of the DS. The relative voltage divider ratios can be adjusted by comparing the divider outputs before DS opening for each measurement, where the two outputs should be equal.

Figure 4.10 shows the wave shapes of voltages u_{cs} , u_{cl} and u_d together with the expansions of amplitude and phase of u_{cs} , u_{cl} before interruption. Ideally, they should be completely identical, but due to tolerances in the division ratios of dividers and probes minor differences occur. The zoomed waveforms in Figure 4.10 of u_{cs} and u_{cl} show that the peak amplitudes and the phase angles differ. An amplitude correction with a factor 0.9961 and a phase shift of 0.021 ms is applied to match the wave shapes of u_{cs} , u_{cl} to obtain u_d . Voltage wave shapes u_{cs} , u_{cl} and u_d expansions near voltage peak and near zero-crossing of u_{cs} , u_{cl} after calibration are plotted in Figure 4.11. The error in voltage magnitude of u_d has dropped from 1 kV to about 0.1 kV.

4.2.3 Current measurement

Instead of measuring i_d directly, the current through C_l is measured with the high-frequency current transformers CT₁, CT₂. Because the impedance of C_l (capacitance in the range several nanofarad up to hundreds of nanofarad) is much lower than the impedance of the voltage divider (with a total capacitance in the order of 200 pF), the error for current difference therefore is maximum 2.5% for $C_l = 8$ nF for the TU/e laboratory setup. At the other experimental sites, this effect is usually smaller because of the larger capacitor values (up to 900 nF).

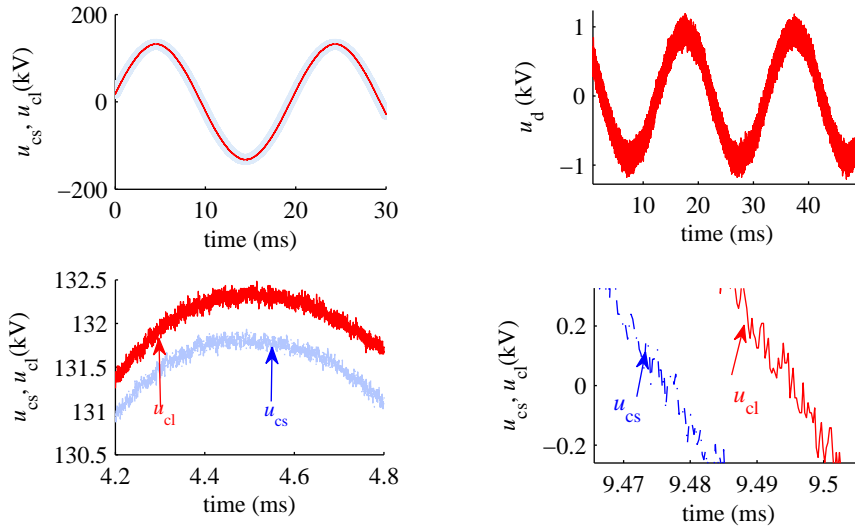


Figure 4.10. Voltages u_{cs} , u_{cl} and u_d and zoomed in near voltage peak and near zero-crossing of u_{cs} , u_{cl} before interruption without adjustment.

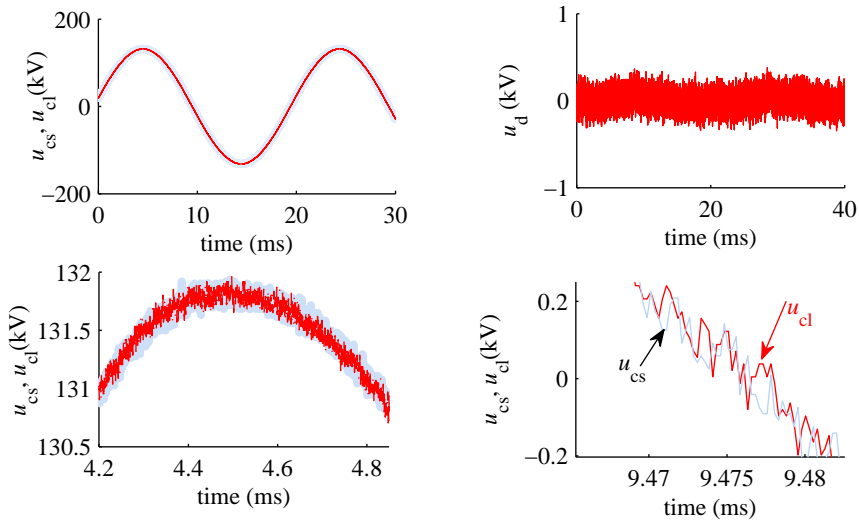


Figure 4.11. Voltages u_{cs} , u_{cl} and u_d zoomed in near voltage peak and near zero-crossing of u_{cs} , u_{cl} after adjustment of amplitude and phase shift.

Two similar current transformers (CT₁, CT₂, each connected to a separate digitizer) are employed for measuring both power-frequency and high-frequency components. Each transformer (type: Pearson 110) has the following properties (according to [3]): sensitivity: 0.1 V/A; output resistance: 50 Ω; maximum peak current: 5 kA; maximum rms current: 65 A; rise time 20 ns; -3 dB cut-off



Figure 4.12. Location of current transformers.

frequencies: approximately 1 Hz and 20 MHz. Figure 4.12 shows both current transformers and their location around the lead connecting C_1 to the ground.

4.2.4 Isolated digitizer and data acquisition

The voltage and current signals are supplied to four channels of a high resolution data acquisition system (LDS Nicolet HV 6600 digital system). It consists of isolated digitizers ("FrontEnd"), optical fibre, Genesis mainframe and software "Perception" (see Figure 4.13). The FrontEnds can be used in a heavily EM polluted high voltage environment owing to their shielding and electrical insulation. Each FrontEnd has an input impedance of $1\text{ M}\Omega/38\text{ pF}$, and its analogue bandwidth ranges up to 25 MHz. The sampling frequency is up to 100 MS/s with a vertical resolution of 14 bit. The optical fibre link transmits the signals in real time to the Genesis (central unit) mainframe, avoiding EM interference in the connection between transducer and central data storage unit and allowing the installation of transducers on locations of any potential. Each FrontEnd is remotely programmable. The Genesis mainframe and a PC are connected via an IP network address. The software "Perception" controls the hardware, records data, allows viewing of the signals, and performs basic signal post-processing. Final data analysis is carried out with programs in MATLAB script.

4.2.5 High-speed camera

A high-speed camera (Model Centurio C100, from Lot-Oriel Europe, shown in Figure 4.14) with frame memory 2 GB is employed to record the arc images [4]. It is based on a large format CMOS detector with a maximum resolution of 1280×1024 pixels. A CMOS sensor converts the photons from the light coming through the lens into electric charges, which are then processed by the electronic circuitry. The resolution ranges from 64×12 pixels, with a maximum recording time of 27 s, at a rate of 10^6 frames/s to 1280×1024 pixels, with a maximum recording time of 3.6 s, at a rate of 424 frames/s. The sensitivity is adjustable

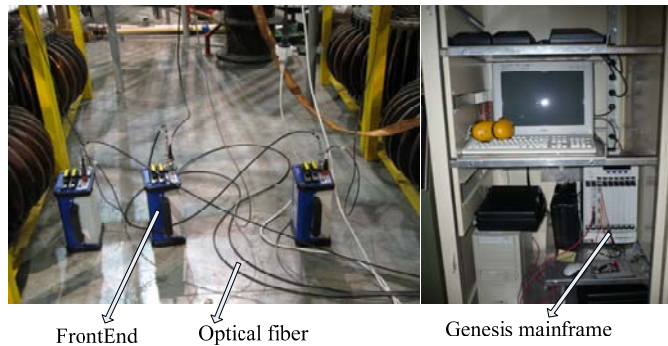


Figure 4.13. Data acquisition system with isolated FrontEnds, optical fibre links, Genesis mainframe and PC.

between 50 and 2000 ASA. The exposure time is adjustable from 2 μ s to 520 ms. The camera works in connection with a PC using the USB2.0 interface through software, which allows precise triggering, recording, and post-processing. The optical format is 17.9x4.3 mm. An F-mount Sigma lens is applied, with filter size 82 mm, lens construction 13-14, angle of view 84.1 $^{\circ}$ -34.3 $^{\circ}$, minimum aperture 32, minimum focusing distance 40 cm, magnification 1:3.8 and focal length 24-70 mm.

During measurements, electrical and optical signals are recorded simultaneously. The electrical and optical signals are synchronized through carefully matching the frame with the highest brightness with the most severe re-strike moment in the measured current or voltage waveforms. Normally, the final re-strike is chosen.

The duration of the electrical transient signals accompanying the bright frame is a few tens of microseconds, much shorter than the exposure time of the frame, usually taken 1 ms for a 1000 frames/s recording speed. The timing clock accuracy of the camera is checked by measuring its sync output and is found to deviate 0.06%, i.e. clearly less than variation in the 50 Hz power-frequency. The synchronization between framing rate and power-frequency therefore is limited by the momentary value of the power-frequency.

The arc length is estimated based on two dimensional projection of recorded arc images. In space the arc propagates in all three dimensions due to the blades moving, air flow, magnetic field, presence of objects in the environment. The single high-speed camera can capture only two dimensions. Ignoring the third dimension leads to certain estimation error. This error can be minimized with prudent camera positioning. The camera is positioned facing the central axis of the frontal view of the DS, in the same height as the main blades. The camera's position secures that the most dominant directions of arc propagation are captured.



Figure 4.14. High-speed camera for recording the arc image in a shielding box.

4.3 Disconnecter main blades opening velocity

The opening characteristics, such as the opening velocity of the main blades, are based on measured the time dependent distance between the DS contacts. This distance depends on the angle between the moving blades and the blades' original closed position. The elapsed time is determined by the rotation speed of the driving shaft of the DS (approximately 40 turns/s). On the shaft a cylindrical sheet is mounted with 25 reflective slots generating 25 pulses per turn (about 1 kHz). The reflected light from a small light source is detected by a sensor. It takes about 210 rotations (5 s) to open the DS main blades from zero to ninety degrees. The light sensor pulses are recorded and related to the mechanical movement of the blade contacts calculated from the driving mechanism of the DS.

The top view of the DS is shown in Figure 4.15. The movement of the arms of the rotating parts is indicated in Figure 4.16. The opening mechanism is attached to the shaft via a gearbox and is driven by an electromotor. The rotation of the shaft relates linearly to the central rotating strip, indicated as '1' in Figure 4.15. The angle θ_2 is the rotation angle of the strip related to the position parallel to the DS blades. The left end of this strip is mounted to a pipe indicated as '2', which is mounted to a frame at the left side with on top the insulator indicated as '3'. θ_1 is the rotation angle of this frame related to the position parallel to the DS blades. The pipe pulls this frame of the left insulator and rotates the insulator and meanwhile the DS blade. The right insulator is mounted with another pipe to the left insulator frame and therefore rotates similarly in opposite direction. All distances and the initial angles (for closed position) $\theta_{1,0}$ ($\frac{1}{4}\pi$ rad), $\theta_{2,0}$ (0.186rad) are measured.

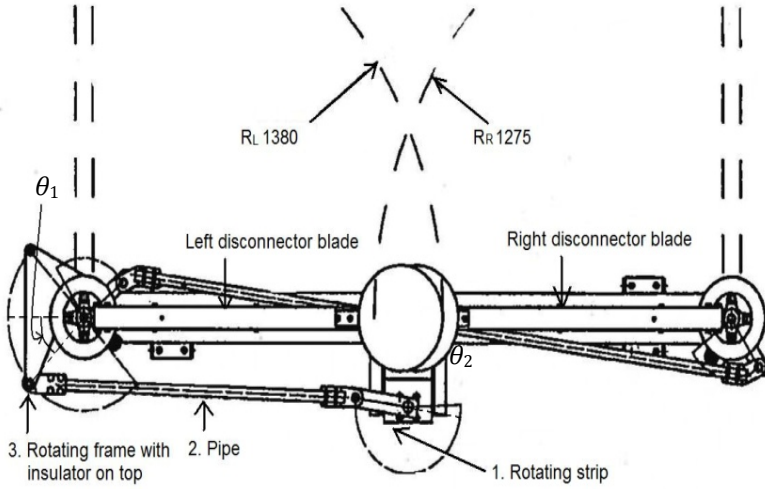


Figure 4.15. Schematic of the top view of the DS.

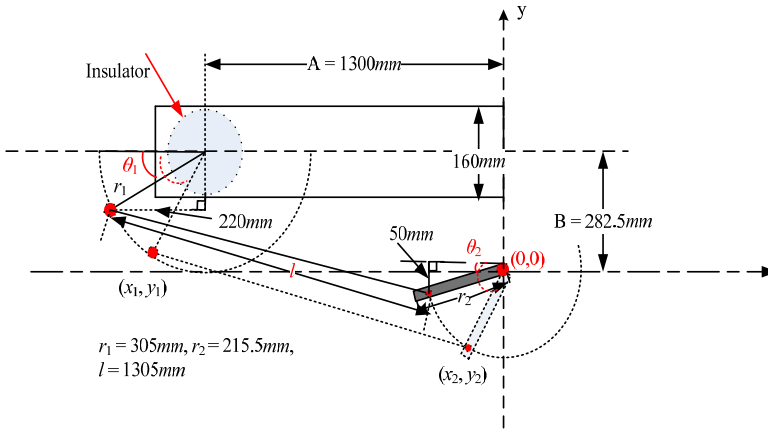


Figure 4.16. Rotating angle of the left blade in Figure 4.16.

The centre of the rotating strip is chosen as the origin of the coordinate system. The position of the connection point to the pipe is:

$$(x_2(p); y_2(p)) = \left(-r_2 \cdot \cos\left(\frac{\pi \cdot p}{5250} + \theta_{2,0}\right); -r_2 \cdot \sin\left(\frac{\pi \cdot p}{5250} + \theta_{2,0}\right) \right) \quad (4.1)$$

In this equation 'p' is the number of pulses, with a total of 5250 pulses to open the DS completely. A similar expression can be obtained for the position of the connection between the pipe and the rotating frame '3' in Figure 4.15:

$$(x_1(p); y_1(p)) = \left(-A - r_1 \cdot \cos(\theta(p) + \theta_{1,0}); B - r_1 \cdot \sin(\theta(p) + \theta_{1,0}) \right) \quad (4.2)$$

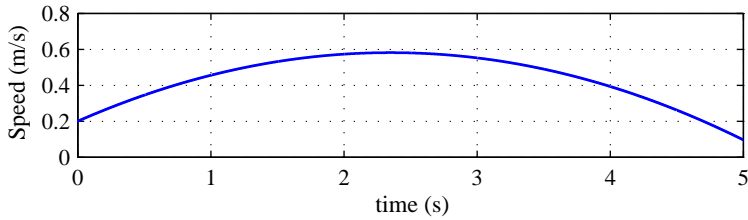


Figure 4.17. Opening speed of the DS in TU/e HV laboratory.

Here $(-A, B)$ indicates the centre of rotation with respect to the chosen origin. The length of the pipe between (x_1, y_1) and (x_2, y_2) is fixed, $l = 1305$ mm:

$$l = \sqrt{(x_2(p) - x_1(p))^2 + (y_2(p) - y_1(p))^2} \quad (4.3)$$

Because this holds for every pulse number p this must hold also for every angle $\theta(p)$. In this way the rotation of the insulator is calculated. From the position at every pulse and the time between the pulses the velocity of the DS blades is calculated. Figure 4.17 shows that the contact separation speed is initially 0.2 m/s and increases up to 0.6 m/s after 2 s (this result is based on the 245 kV rated voltage centre-break DS from Hapam [5]).

4.4 Conclusion

The experimental setups with two different power supplies (resonant generator and short-circuit generator) are described for different test locations. The measuring system includes voltage divider, current transformer, digital data acquisition system, and high-speed camera. Two identical voltage dividers with 5.5 MHz bandwidth are designed for the purpose of measuring voltage across the main contacts of the DS. After correction their division ratio is equal within 0.07%. The bandwidth of the current measurement is up to 20 MHz. Transient current up to 7 kA is measured simultaneously with power-frequency with sensitivity of 5 mA. A high-speed camera is employed and its taking frame up to 5000 frames/s, and a resolution of 256x254 pixels. The DS employed in the tests, opens with typical speed 0.4 m/s.

References

- [1] [Online]. Available: <http://www.murata.com/products/capacitor/index.html>.
- [2] [Online]. Available: <http://www.highvoltageprobes.com/faq.html>.
- [3] [Online]. Available: <http://www.pearsonelectronics.com/>.
- [4] [Online]. Available: <http://www.lot-oriel.com>.
- [5] [Online]. Available: <http://www.hapam.nl/>.

Chapter 5

Current Interruption Mechanism

The current interruption of an air-break HV DS is investigated experimentally by observation of electrical and optical signals in this chapter. From these observations the interruption is characterized in terms of arc duration, arc mode, arc movement, arc brightness, and decay of afterglow. The electrical characteristics related to the free burning arc are derived as well. The major factors that control the DSs' capability to interrupt capacitive current, such as blade contacts spacing, the re-strike voltages, arc energy, and transient phenomena are studied in detail. In the end, based on experimental data, the principal transient process is described, and the transient voltages and currents are studied.

Experiments are carried out in different laboratories (see Chapter 4.1) with a centre-break DS. Three DSs are tested with a rated voltage of 145 kV, 245 kV and 300 kV respectively. Usually at each current level, the operation is repeated at least three times. The level of the current to be interrupted is controlled by C_l (see Figure 3.1). The main configurations of the capacitors C_s and C_l are listed in Table 5.1 with light, medium and dark shaded regions respectively. The experiments from 8 A to 27 A (at 90 kV and C_s fixed at 50 nF, C_l ranging from 170 nF to 935 nF) in the dark shaded region are performed with an external fast opening contacts (see Chapter 7), indicated by the italic and bold font style. Some of these interruptions failed. They are included in this table in order to illustrate different arc characteristics for this chapter.

5.1 Experimental observations

Based on electrical signals and optical images, a global characterization is made. The interruption process is studied based on voltages across both capacitances and the DS, and the current through the DS. The optical observation includes the development of the arc, resulting in arc motion, arc shape, and arc brightness. The correlation of the electrical and optical signals is also presented.

5.1.1 *Electrical arc signal observation*

Typical wave shapes of the relevant transient phenomena during the interruption process are shown in Figures 5.1-5.8. Specifically, information of u_{cs} (the voltage across the source side capacitance), u_{cl} (the voltage across the load side capacitance), i_d (the current through the DS), $u_d (= u_{cs} - u_{cl}$, the voltage

Table 5.1. Interrupting current for source and load side capacitance combinations.

$\begin{matrix} C_s \\ C_l \\ I_d \end{matrix}$	2.0	4.0	1.5	6.0	20.0	60.0	50.0	100.0
4.3			0.23					
8.0	0.6							
10.7			0.60			0.60		
16.0		1.2						
17.0							0.5	
19.3			1.0	1.0	1.0	1.0		
32.0		2.4						
38.6				1.1/ 2.1		1.1/ 2.1		
40.0			2.1	2.1	2.1	2.1		2.1
48							1.4	
88							2.6	
121							3.5	
133							3.9	
170							5.0	
183							5.3	
218							6.3	
277							8	
312							9	
346							10	
433							12.5	
519							15	
588							17	
692							20	
796							23	
865							25	
935							27	

Note: C_s and C_l are in nanofarads and I_d is the current in amperes. The light shaded region is performed with a DS rating of 245 kV at the TU/e laboratory setup at voltages up to 170 kV; the medium shaded region corresponds to a DS rated for 300 kV tested at 90 kV or 173 kV; "1.1/2.1" at $C_l = 38.6$ nF means 1.1 A at 90 kV and 2.1 A at 173 kV; the dark shaded region corresponds to a DS rated for 145 kV tested at 90 kV. For the dark shaded region, the interruptions up to 6.3 A are successful. The experiments indicated by the medium and dark shaded region are carried out at KEMA laboratories.

across the DS) is plotted. The current i_d is simultaneously measured with a bandwidth of 50 kHz (i_{pf} , covering power-frequency) and a bandwidth of 20 MHz (i_{hf} , covering high-frequency transient signals). The experimental parameters for the illustrations in Figures 5.1-5.8 are: $E_m = 90\sqrt{2}$ kV, $C_s = 1.5$ nF, $C_l = 40$ nF, $I_d = 1.1$ A. Time $t = 0$ is taken as the moment when the DS blades start opening.

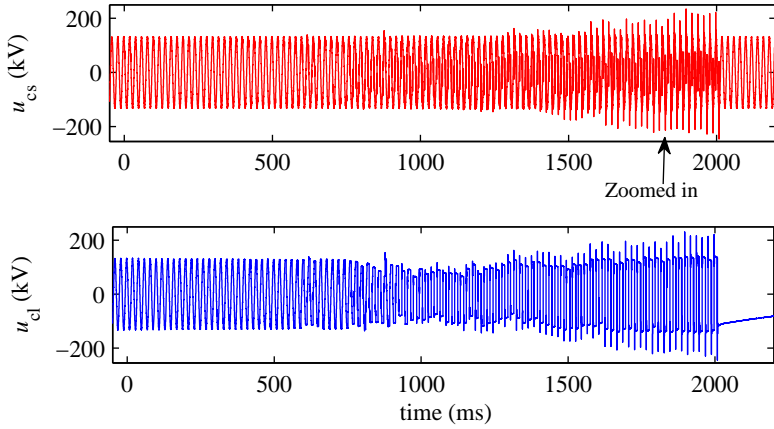


Figure 5.1. Voltages (u_{cs} , u_{cl}) cross the capacitors.

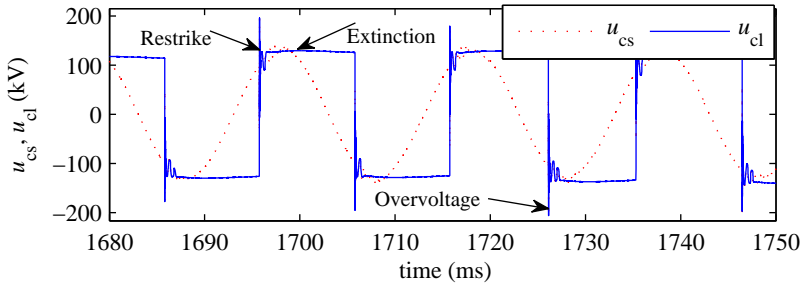


Figure 5.2. Zoomed in between 1680 ms and 1750 ms of Figure 5.1.

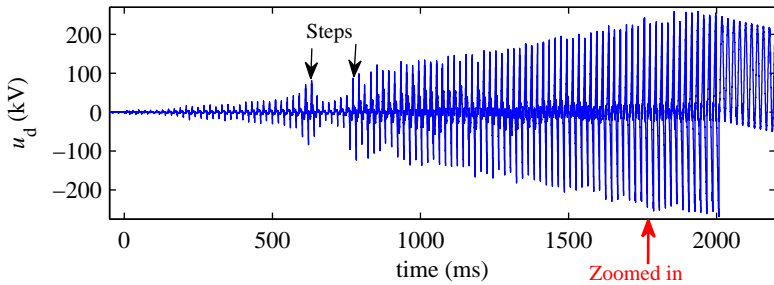


Figure 5.3. Wave shape of the voltage across the DS: $u_d = u_{cs} - u_{cl}$.

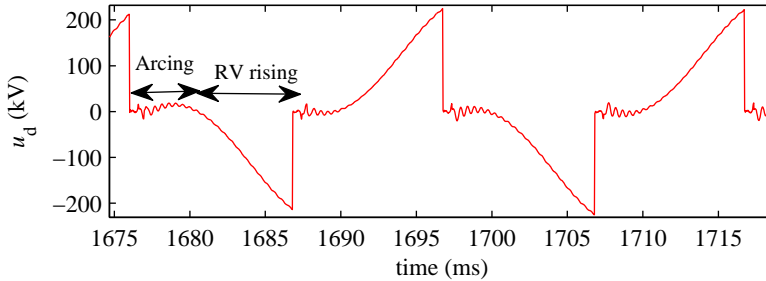


Figure 5.4. Zoomed in between 1675 ms and 1720 ms of Figure 5.3.

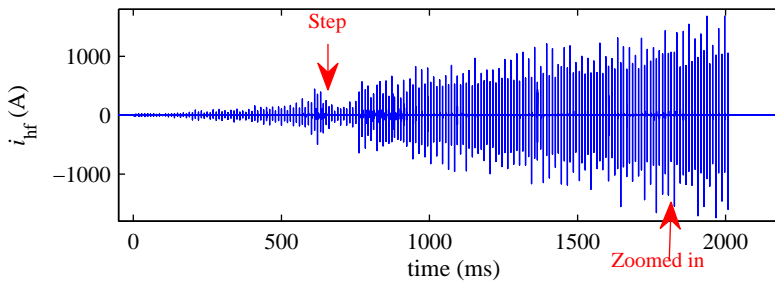


Figure 5.5. Wave shape of the current i_a scaled to allow full coverage at HF component.

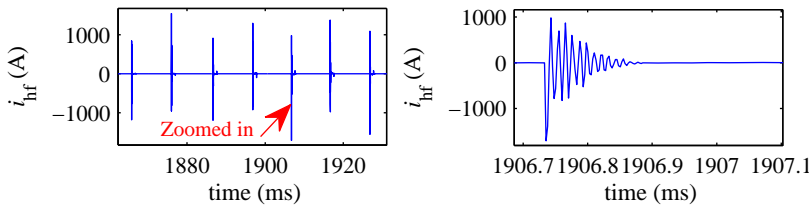


Figure 5.6. (left) zoomed in between 1860 ms to 1930 ms of Figure 5.5, and (right) zoomed in a single high-frequency component.

From the waveforms in these figures the following general phenomena are observed:

- The entire interruption process lasts about 2 s. During this process the capacitive current interruption consists of multiple, periodical arc extinctions and re-strikes, which are clearly observed in the expanded wave shapes (Figures 5.2, 5.4, 5.6 and 5.8). The arc extinguishes as the arc current crosses zero and re-establishes during the succeeding half power cycle due to the collapse of the (power-frequency) RV. Transient phenomena occur upon each re-strike. First the HF component appears, followed by the MF and PF components (see Chapter 3). For example, the high-frequency component shown in Figure 5.6, with frequency approximately 100 kHz.

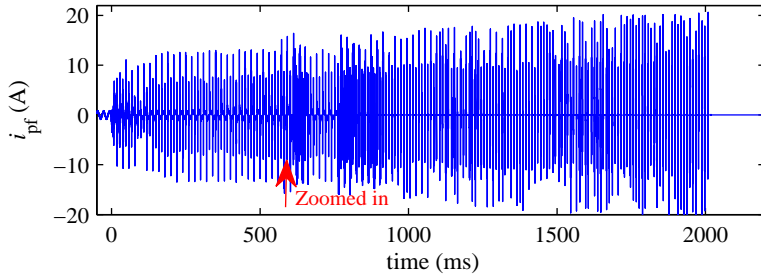


Figure 5.7. Wave shape of the current recorded at lower frequency in order to filter out HF transients.

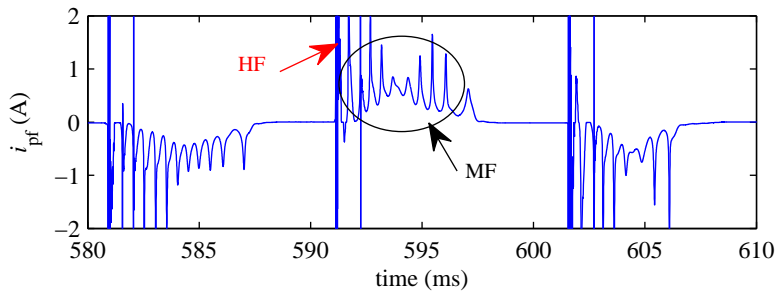


Figure 5.8. Zoomed in between 580 ms and 610 ms of Figure 5.7 arc current i_{pf} .

It lasts about 0.1 ms. The medium-frequency component, shown in Figure 5.8, has a frequency of about 2 kHz, lasting approximately 6 ms. After the high and medium-frequency oscillations have decayed, only the power-frequency component remains.

- During the interruption, overvoltages across the capacitor banks at both DS sides and between the DS main blades arise. Upon re-strike a high peak current through the DS occurs. In the example, the maximum overvoltage of u_{cl} , u_{cl} is 1.86 p.u. and the maximum HF transient current is about 1.6 kA (see Figures 5.5 and 5.6).
- The expansion of the voltage u_d (Figure 5.4), and the power-frequency component of the current (Figure 5.8) show the periods with arc and intervals in between, where the RV builds up at each half power-frequency cycle. The arc re-strikes whenever the RV exceeds the dielectric strength of the air gap. It extinguishes completely when sufficient air gap distance between the main blade contacts of the DS has been reached to withstand the RV.
- Values of u_d and i_d (Figures 5.3 and 5.5) on each moment of re-strike do not rise monotonously with the increasing contacts distance, but "steps" are observed. The re-strike voltage is not only determined by the gap distance

between two contacts of the DS, but apparently depends on other influences as well. For example, thermal effects in the air gap can reduce the gap breakdown voltage, which will be discussed in detail later on in this chapter.

5.1.2 Optical arc image observation

The arc extinctions and re-strikes/re-ignitions are also visible through arc imaging. The arc length increases due to the increasing distance of the contacts, and the arc moves upwards gradually mainly due to the rising hot air. The arc usually has a single re-strike resulting in the highest brightness during a short period of time within each half cycle. Both electrical signals and arc images are exemplified in Figure 5.9 for an entire interruption. The instances in the electrical signals, where the image frames are taken, are indicated by time inside the optical images. The arc images show the gradual upward movement as a 2 dimensions projection of the complex 3 dimensional shape. The arc length is increasing until its final extinction. In the shown example, the arc extinguishes prematurely

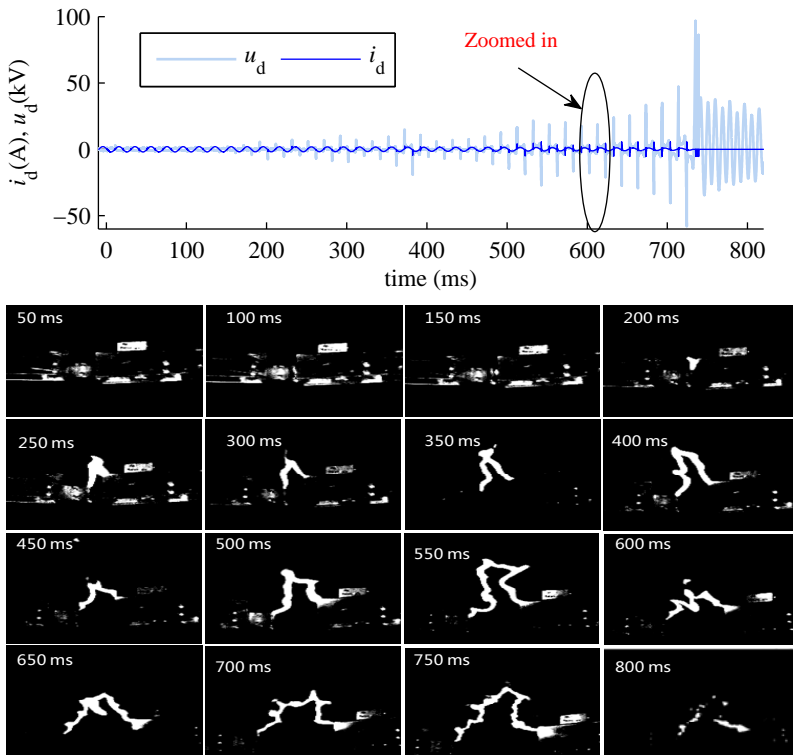


Figure 5.9. Wave shapes of u_d and i_d , and arc image frames at different time instances for 140 kV, 2 A measured at the TU/e HV laboratory.

because of the decaying resonant source voltage (see Chapter 4, Figure 4.4). The expansion over a full cycle taken between 674 ms and 694 ms of Figure 5.9, together with arc images taken every 1.1 ms, is shown in Figure 5.10. Time t_1 is the moment that the re-strike occurs; t_2 is the moment of the re-strike one power cycle later. As already observed from the electrical signals, also from the brightness of the arc images, it is confirmed that re-strike occurs each half cycle. The arc brightness drops drastically from the frame at re-strike to the subsequent frame because the high-frequency component lasts only a fraction of the camera exposure time of 0.99 ms for 1000 frames/s. The arc images show that a re-established arc follows closely the path of the preceding arc before re-strike.

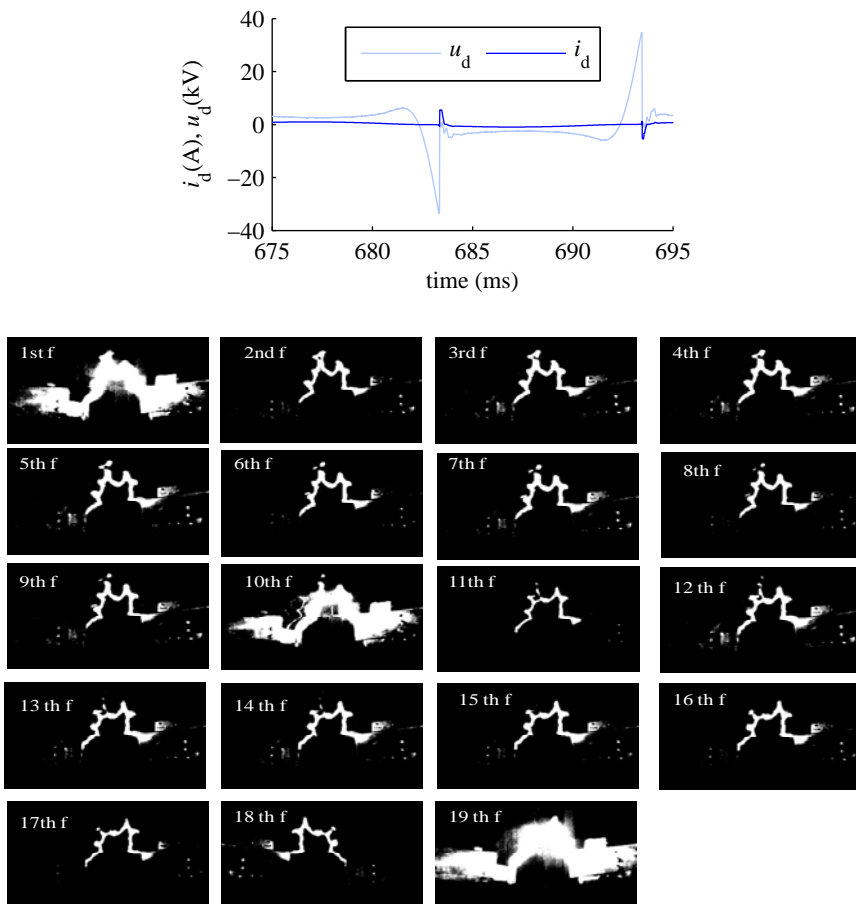


Figure 5.10. Arc images recorded within 20 ms of Figure 5.9 including three re-strikes (1st, 10th and 19th image).

5.1.3 Combined optical and electrical signals

The changes in the arc over time are characterized with two types of measurements. The electrical measurements provide information about changes in the arc current and voltage. On the other hand the optical measurements provide a visual perception of the arc properties through the recorded images. The presence of the arc in an image results in the increased image brightness. In order to investigate the correlation between optical and electrical arc information qualitatively, a method is sought to quantify the brightness of a single arc image frame, which are extracted from high-speed arc video recording.

Brightness is an attribute of visual perception in which a source appears to emit a given amount of light. In order to quantify brightness in this application, it is defined here as the normalized integrated greyscale value of all pixels in a certain image of the high-speed video camera output file. The greyscale value of a pixel in the digital image has a value in the range of 0-255. The value 0 corresponds to the black, while the value 255 represent white. Such definition has no verified/calibrated relationship to any physical quantity of the light emitting properties of the arc. Therefore, brightness measurement results thus have only indicative value.

The brightness of a pixel with coordinates (i, j) in frame k of a digital image recording is denoted as $B_{i,j}^{(k)}$, where $1 \leq i \leq n$ and $1 \leq j \leq m$ ($n \times m$ is the spatial resolution of the camera). The image brightness of the k^{th} frame is defined as the sum of brightness from all pixels:

$$B_k = \sum_{i=1}^n \sum_{j=1}^m B_{i,j}^{(k)} \quad (5.1)$$

The values of B_k of different images can only be compared directly if they are taken with identical camera settings. In order to compare and evaluate each image in a recording, the brightness is normalized to the brightness N_k of a full white image:

$$N_k = \frac{1}{N_w} \sum_{i=1}^n \sum_{j=1}^m B_{i,j}^{(k)}, \quad (5.2)$$

where N_k is the brightness after normalization on $N_w = n \times m \times 255$ (255 being the maximum 8 bit pixel intensity value). The arc brightness is estimated as an increase in the image brightness due to appearance of arc. Thus, it is calculated as a difference between the brightness of the image with the arc and the image without arc (background image): $N_{arc} = N_k - N_0$. The background brightness N_0 is taken from a recorded frame just before opening the blades.

Practical imaging systems have a limited dynamic range, i.e., the range of luminosity that can be reproduced accurately is limited. Parts of the subject (in this case arc) that are too bright are represented as white, with no details which is often referred to as saturation; parts that are too dark are represented as black. The levels of the luminosity in the recorded arc were too high for the dynamic range of the camera. Therefore, certain level of the saturation is present in almost all images. The number of saturated pixels is higher in the images corresponding to the moment of the restrikes, especially for the images with dark environment. In the greyscale, pixels which exhibit saturation effect are represented with a pixel intensity of 255. The presence of the saturation effect in the images prevents quantitative analysis. However, the recorded images can provide an indication about arc behaviour and allow that the most important trends are observed.

An example of arc brightness as a function of time is shown in Figures 5.11 and 5.12 for $I_d = 1.3$ A with a resolution of 256×254 pixels, recorded with 5000 frames/s. The arc image is synchronized with the measured waveforms for voltage u_d and current i_d (refer Section 4.2.5). In Figure 5.11 the arc brightness and its expansions of three time periods (120 ms-160 ms, 440 ms-490 ms, 650 ms-780 ms) together with the synchronized u_d and i_d traces are shown. Figure 5.12 is a further expansion taken between 670 ms and 716 ms to show the precise synchronization.

The following observations are made:

- High arc brightness occurs each half power-frequency cycle, directly at the moment of re-strike. Figure 5.12 shows that the bright arc only covers 2-3 images corresponding to a few tenths of a millisecond. The fast decay is related to the duration of the high-frequency oscillations.
- The arc brightness varies synchronously with the arc current. It implies that in a steady burning arc (between re-strikes) the arc current is the dominating factor, which determines the arc brightness.

5.2 Arc interruption characteristics

The arc characteristics of the interruption include arc duration, appearance, brightness, movement and remnant decay. The electrical parameters influencing on the arc characteristics will be analyzed. Besides the electrical circuit parameters, environmental condition such as wind, humidity plays a role as well. But their effect is not considered in this thesis.

5.2.1 Arc duration

Arc duration is a key factor in evaluating the interruption performance. The arc duration is defined as the duration from the moment when the arc ignites between the two contacts of the blades until the moment when it extinguishes

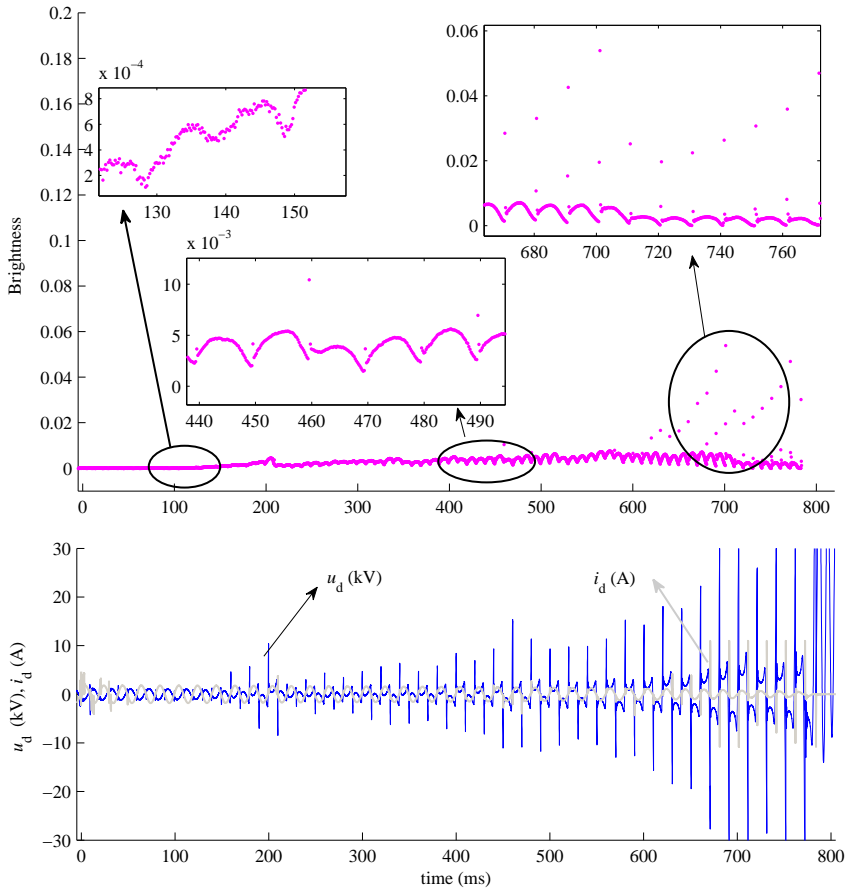


Figure 5.11. Arc brightness with the synchronized voltage u_d and current i_d waveforms for $I_d = 1.3$ A.

completely. The glow emitted by hot air remnants after the final arc current zero crossing is not taken into account. Figures 5.13 and 5.14 chosen from the medium shaded region in Table 5.1 show the arc duration as a function of the interrupting current I_d and C_s/C_l , respectively. The arc duration depends on I_d (with equal C_s and u_s) as indicated by the regression lines in Figure 5.13. It decreases with increasing ratio C_s/C_l at fixed u_s and I_d , see the regression lines in Figure 5.14. Furthermore, it increases with the system voltage when the current I_d and the ratio C_s/C_l are taken constant. The results confirm that the system voltage, interrupting current and ratio of the capacitances at source and load side are indeed the main factors affecting the arc duration.

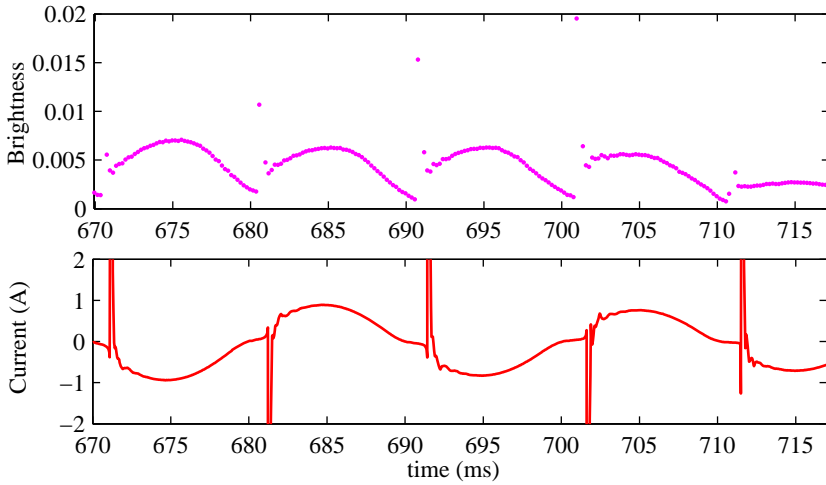


Figure 5.12. Expansion of both electrical (lower) and optical (upper) signals between 670 ms and 716 ms from Figure 5.11.

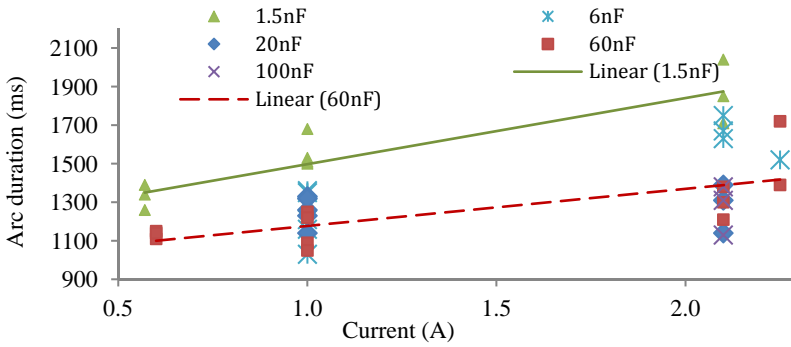


Figure 5.13. Arc duration versus interrupting current I_d with C_s as a parameter at 173 kV.

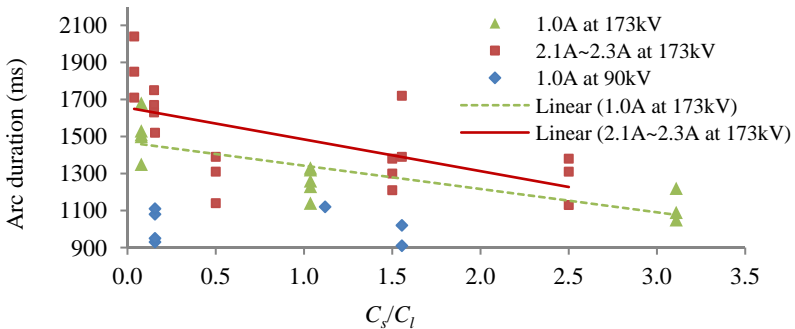


Figure 5.14. Arc duration versus the ratio C_s/C_l at 90 kV and 173 kV with I_d as a parameter.

5.2.2 Arc appearance

For the experiments up to 2.3 A the arc exhibits two distinct visual appearances, or "modes", as shown in Figure 5.15. These modes are denoted as "erratic" and "stiff" mode in [1]. For the erratic mode the arc develops in a complex shape and its length is much longer than the blade tip spacing (Figure 5.15a). The stiff mode is a contraction from the erratic mode to a more or less straight path between the contacts (Figure 5.15b). It is observed that the arc shape remains erratic during the complete interruption for $C_s/C_l < 1.5$ in the experiments. The erratic arc mode is associated with longer arcing time. The arc changes from erratic to stiff mode after a certain time, and remains stiff till the end for $C_s/C_l > 1.5$. This is associated with shorter arcing time. The experimental results show no convincing relationship between the arc mode and I_d or u_s . However, the arc with stiff mode is clearly related to the ratio C_s/C_l . With smaller C_s/C_l , the medium-frequency voltage transients are higher (refer Section 3.4). The increased heat dissipation facilitates the next breakdown along the same path despite its complex curled shape. The influence of C_s/C_l will also be discussed in the section 5.6.

5.2.3 Arc brightness versus arc current

In a number of experiments arc interruption failed resulting in continuation of arcing after the DS blades have reached their final open positions. These failed interruptions allow to investigate the relation between entire brightness and current, since the situation with fully opened blades ensures that the arc current is the only variable factor, and not the gap spacing. The brightness at current levels between 12.5A and 27A of 90kV is displayed in Figure 5.16. It is observed that the entire arc brightness increases with increasing I_d . It is also observed from the arc video that the arc burning with fixed air distance with higher current exhibits much more curls than it does with lower current.

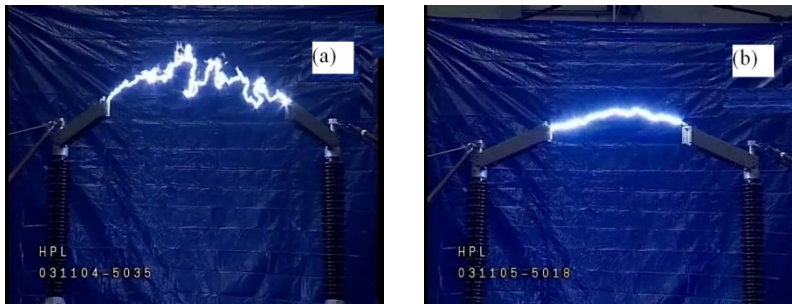


Figure 5.15. Arc in (a) erratic mode and (b) stiff mode.

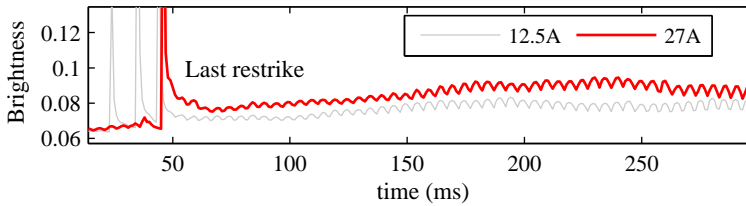


Figure 5.16. The arc brightness against time with the current as a parameter.

5.2.3 Arc movement

In absence of wind influences, the arc development upon the increasing gap distance is governed by the convection of the heated air in between. The horizontal extension depends on opening velocity of the air gap, which is in the range 0.2 to 0.6 m/s. The upward speed can be best analyzed from camera images based on failed interruptions, because of the long arc lengths. Moreover, the arc burns continuously, which is most suitable for studying its movement.

Figure 5.17 shows the arc motion from a failed interruption with $I_d = 10\text{ A}$, $E_m = 90\sqrt{2}\text{ kV}$. The height H in mm refers to the distance above the original closed position of the main blades. After about 70 half cycles, the test is stopped by the master breaker in the laboratory. For each half cycle, a single frame is selected. The sub-figures are taken at corresponding phase angles for 10 subsequent half cycles; the seven sub-figures cover the complete arc duration. The time difference between two curves therefore is 10 ms (half power cycle) and between two sub-figures it is 100 ms (ten half power cycles). It is observed, that the arc moves upwards exhibiting a seemingly random path. Arcs in successive frames are slightly vertically displaced relative to the previous one.

This behaviour suggests that the heat produced by the arc creates favourable conditions a little upward from the present position. The actual arc trajectory therefore is mainly determined by the condition of the air in the gap rather than of the actual location of the arc roots.

The last sub-figure in Figure 5.17 shows the highest point (arc reach) in each arc frame versus time for interrupted currents in the range of 12.5 A to 27 A. The height increases nearly linearly with time, approximately 2.3 m/s. This speed is rather uncorrelated with current level in the tests. Too wide extent of the arc ("reach") as a result of failed interruptions may cause dielectrically hazardous situations in substations.

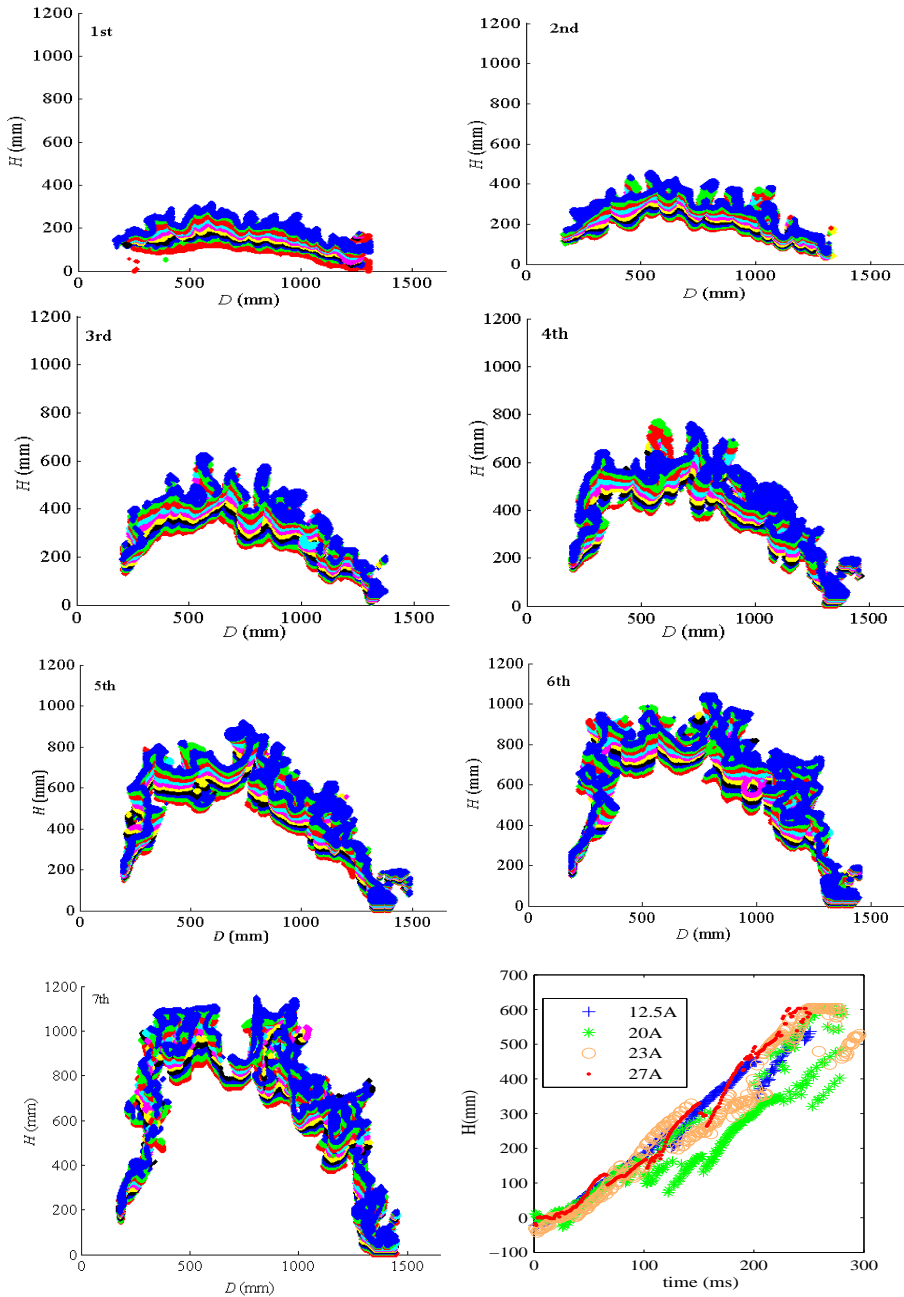


Figure 5.17. Upward arc movement (frames taken each 10 ms). The last subfigure shows the arc reach increasing with the arcing time using the interrupted current as a parameter.

5.2.4 Arc remnant decay

The light emission does not vanish immediately after final arc extinction. The decay in brightness of these arc remnants is investigated as a function of the interrupted current. The normalized brightness at four distinct values of I_d is plotted in Figure 5.18 (left) for successful interruptions. Herein, $t = 0$ is the moment of arc extinction. The curves can be fitted to match an exponential behaviour, $A\exp(-t/\tau)$, with τ the decay time constant. This time constant, plotted versus I_d in Figure 5.18 (right), scales approximately linearly with I_d : $\tau = 0.9 \cdot I_d$. The obtained result implies that with higher interrupted current, the arc afterglow decays slower. Apparently, the hot ionized discharge channel cools down more slowly after higher arc current.

5.3 Disconnecter contacts spacing

RV is the voltage impressed across the DS by the circuit after arc extinction at current zero. It possibly precedes re-strike that re-establishes the arc. This RV is maximum if it occurs at half a power-frequency cycle after interruption. Then the source voltage (at 1 p.u.) is equal but in opposite polarity with the trapped DC voltage across the load side capacitance (also at 1 p.u.). Thus, RV builds up to 2 p.u. This is also the maximum RV that the (single phase) circuit is capable to supply.

The tips between the blades of a DS can be considered as rod-rod electrodes. In the "IEEE Std 4-1995, Techniques for High voltage Testing" [2], rod-rod gap spark-overvoltages at power-frequency versus the air spacing are listed. From this standard, the required contact gap spacing based on the centre-break DS blade length [3], and its corresponding blade angle can be derived [1]. To allow for a 10% margin [4], the system voltage is taken 1.1 p.u. and thus a RV peak value of 2.2 p.u. is applicable. The condition to be satisfied for the RV no longer being able to breakdown the air gap is: $U_{gap} \geq 2.2 \times E_m$, where U_{gap} is the air gap withstand voltage and E_m is the amplitude of phase-to-ground voltage.

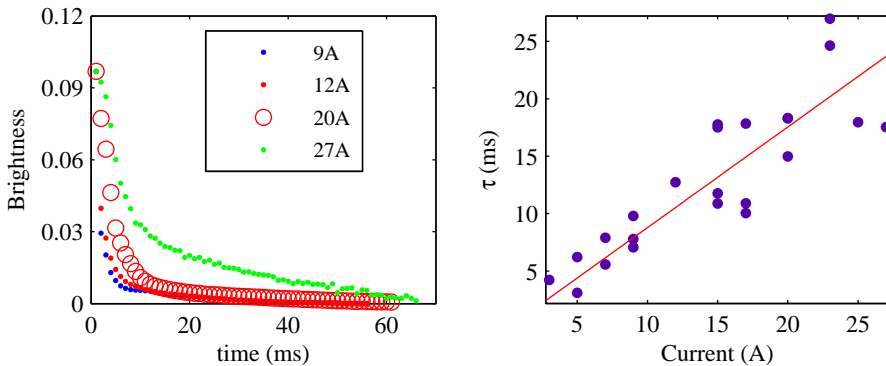


Figure 5.18. Brightness decay and its time constant τ dependency with the interrupted current.

Table 5.2 shows the minimum required gap length and blade angle with respect to the close position at different system voltage levels for a centre-break DS. The calculated results show the blade angle is less than 60 degree, considering +8% margin, taken from [2].

The blade angles obtained from experiments carried out on a 245 kV rated voltage centre-break DS differ greatly from the values in Table 5.2. In Figure 5.19, the blade angles at the moment of final arc interruption is given. All angles at final arc extinction exceed 50 degrees; some of them reach up to the final 90 degree opening angle. Evidently, the results from the experiments exceed significantly the calculated ideal values, based on (cold) air-breakdown voltage only.

For estimation of the minimum required gap distance in Table 5.2, two assumptions were made [1]:

- The thermal energy of the arc is not significant. This means that the breakdown voltage of the gap essentially is equal to a steady state, "cold" situation without arcing shortly before breakdown.
- The opening contact gap is approximated as a rod-rod type gap. In the present experiments, no corona rings or similar constructions were installed on the jaw assembly. This can cause field enhancements at the end of the contacts.

5.4 Re-strike voltage

The re-strike voltage, denoted as U_r , is defined as the value of u_d across the DS at the moment of re-strike. The re-strike voltage is mainly determined by the air gap distance, but it is also influenced by the physical air gap conditioned by the arc.

5.4.1 Re-strike voltage development

The development of U_r is analyzed for measurements with different currents I_d , and capacitances ratios C_s/C_l . The re-strike voltages obtained at a supply voltage of 173 kV are given in Figure 5.20, with C_s/C_l and I_d as parameters. The following conclusions are drawn:

- The maximum re-strike voltage level is indeed found to be twice the peak supply voltage. The re-strike voltage does not show a monotonous increase with increasing air gap length. Instead, sudden downward steps are observed at each current level. However, with higher current level the "steps" are more numerous and deeper. Apparently, besides the air gap length, also other factors should be considered.
- The re-strike voltage increases with decreasing I_d and increasing C_s/C_l . Larger I_d and smaller C_s/C_l are associated with a higher energy input into the arc upon re-strikes (Section 5.6). The arc path needs more time to recover its dielectric stress during the next RV period resulting in a lower re-strike voltage for the consecutive breakdown.

Table 5.2. Minimum contact gap distance and blade angle needed for isolating distance with a centre-break DS.

System voltage (kV)	Blade length (mm)	RV peak (kV)	Contact gap (mm)		Blade angle (°)	
			mean	+8%	mean	+8%
72.5	900	130	220	238	41	43
145	1650	260	481	519	45	47
245	2600	440	835	902	47	49
362	3500	650	1253	1353	50	52
420	4000	754	1465	1582	51	53
550	4400	988	1936	2091	56	58

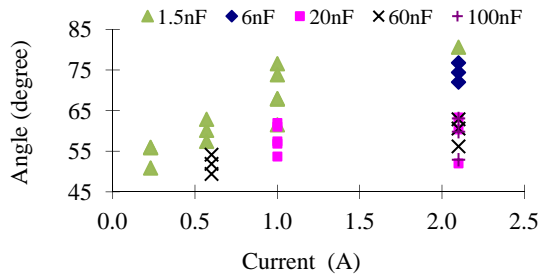


Figure 5.19. Blade angle versus I_d with C_s as parameter at 173 kV.

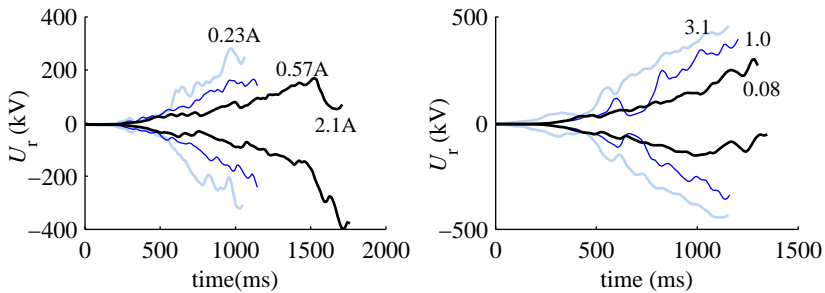


Figure 5.20. Effect of current I_d (left, with $C_s = 1.5$ nF) and capacitor ratio C_s/C_i (right, with $I_d = 2.1$ A) on re-strike voltage.

- Positive and negative re-strikes do not occur symmetrically. For example, Figure 5.20 left, most apparently at 2.1 A the positive and negative re-strike voltages differ. A re-strike usually occurs each half cycle. However, because of asymmetrical overvoltage across C_s and C_i , only one re-strike within each full power-frequency cycle may occur. It will be explained in the following subsection.

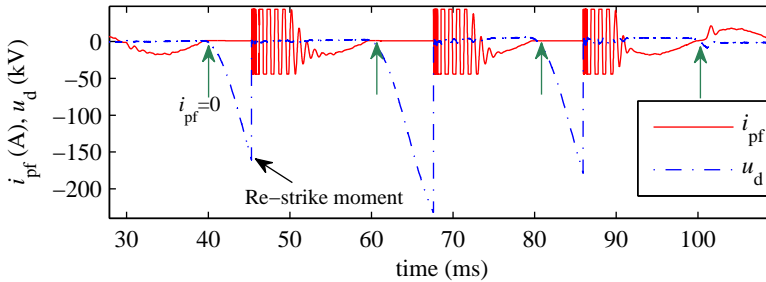


Figure 5.21. Wave shapes of u_d and i_{pf} (i_d measured at lower frequency) with only one arc extinction per power frequency cycle.

5.4.2 Unipolar re-strike voltage

Generally, once the contacts of the DS separate, re-strikes occur in each half power cycle. Figure 5.21 shows an example of the wave shapes of the voltage u_d and the current i_d versus time of an interruption process, for which the last three re-strikes are shown. Here the arc extinguishes and re-strikes only each full power cycle. According to the high-speed arc image recordings with 5000 frames per second, no arc extinctions are observed. Apparently, the arc does not extinguish as long as the high- and medium-frequency oscillation is of sufficient magnitude. The phenomenon is always observed, if the corresponding re-strike voltage exceeds the source peak voltage. Once the re-strike voltage is high enough, the medium-frequency components last sufficiently long to prevent interruption at power-frequency current zero. The oscillation in the current and voltage still continues when the power-frequency current crosses zero. In this situation, the arc can fail to extinguish. This is due to the influence of the thermal energy provided by the oscillations. If this phenomenon occurs repeatedly, re-strike will happen only at one polarity of the power-frequency, either positive or negative.

The missed arc extinction can also be observed through arc image analysis. Figure 5.22 shows the arc images corresponding to consecutive frames, taken every millisecond, within a half cycle. The x axis indicates the horizontal extension of the arc. The y axis is the arc height with respect to the main blades. In order to display the arcs distinctly, a vertical offset is added to the consecutive images. The 1st image corresponds to a re-strike moment while the 10th frame corresponds to the end of the half cycle, i.e. the moment when the arc current reaches zero again. The images after the 10th frame correspond to the next re-strike. In Figure 5.22a the 10th image shows a discontinuous arc path, whereas in Figure 5.22b this discontinuity, measured at a later stage of the same arc development, is not observed.

The polarity effect normally appears in the later stage of the interruption process. At the beginning of the interruption, the arc extinguishes at each current zero

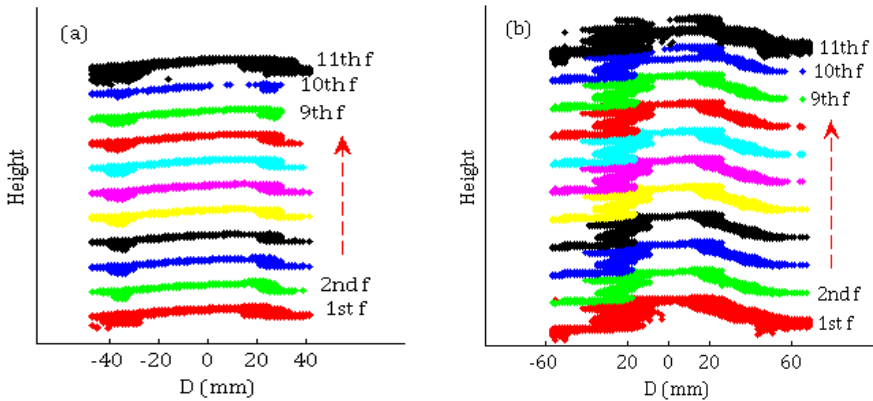


Figure 5.22. Typical arc images from experiments with $I_d = 0.7$ A and $E_m = 130\sqrt{2}$ kV at TU/e HV laboratory, (a) with obvious re-strike frame and (b) arc does not extinguish at power frequency zero crossing. $D = 0$ is the middle point of the two DS blades in a closed position.

because air gap conditions, i.e. temperature and ionization, are not sufficient to sustain arcing. However at a later stage, the gap conditions can sustain arcing during current zero without an appreciable re-strike voltage and visible interruption.

5.4.3 Re-strike voltage with air gap distance

After re-strike the arc resumes a path closely following the "traces" left by the previous arc that has just disappeared. The arc chooses the dielectrically weakest path for which the breakdown voltage is lowest. The remaining hot partly ionized air enables the arc to re-ignite at a lower breakdown voltage compared to a 'cold' situation. The measured breakdown voltage that re-establishes the arc is plotted versus the air gap spacing at $I_d = 0.3$ A and 0.7 A in Figure 5.23. The length of the arc path is estimated through the arc image frames. The reference unconditioned breakdown voltage, also plotted in Figure 5.23, is taken from the IEEE standard [2] for a rod-rod configuration. Clearly, the blade shape is much more complicated, but the comparison provides a notion to what extent the actual breakdown voltage is lowered. Despite the strong variation in breakdown voltages and the relatively rough arc path estimate (arc length is based on a 2D projection captured by the camera), the reduction in breakdown voltage by the remaining residual ionization can be observed clearly. Temporary arc extinction at current zero occurs in a situation with relatively low pre-heating and ionization of the arc channel. Continuous arcing occurs when sufficient heat and charged particles are left in the air gap. The residual gap condition has a major effect, since it lowers the re-strike voltage needed to re-establish the arc and prolongs the arc duration.

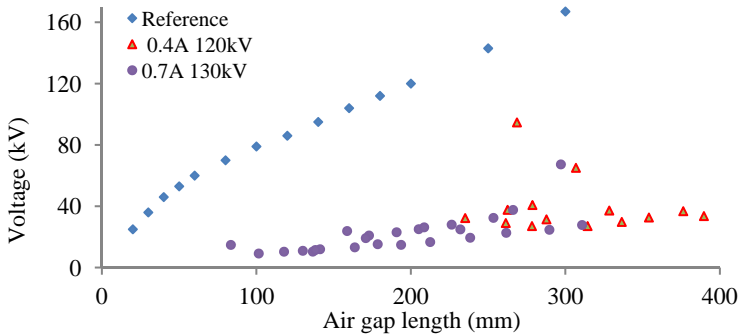


Figure 5.23. Breakdown voltage of the gap versus air gap length.

5.5 Electrical arc characteristics

The free burning arc during air-break DS interruption has a small current compared to the fault arc in circuit breakers. For understanding this type of arc behaviour, the arc current, voltage, resistance, and U-I characteristics are analyzed. Arc current (denoted as i_a) and arc voltage (denoted as u_a) are equal to the i_d and u_d waveforms, respectively, during the arcing period. Therefore, the arc voltage and current waveforms are not continuous curves, but their absence during the voltage recovery phase can be short or hardly visible when the breakdown voltage is still relatively low. This occurs at the early stage of the interruption for low currents, or during the entire arc duration with high current when the interruption fails.

5.5.1 Arc current

Figure 5.24 shows examples of arc current and voltage waveforms for a clearly visible and relatively long, a non-visible period of current zero. It is observed that when the re-strike voltage is large enough, the arc current has clear transient components at the beginning of each re-strike. When the arc is continuously burning no transient behaviour is observed in the waveforms.

5.5.2 Arc voltage

Similar to the arc current, the arc voltage exhibits an obvious transient component at the beginning of each re-strike (Figure 5.24 left). It is, however, very difficult to distinguish between the arc voltage and the induced voltage due to the severe current transients with very high di/dt . When the breakdown voltage is low, either because of a still small DS contact distance or because of a preconditioned gap, there are hardly transient voltages at the beginning of each re-strike (Figure 5.24 right). The arc voltage has a distorted shape, due to the non-linear arc

characteristic. If the median value of the voltage shape is taken as a measure of the arc voltage, it reaches up to approximately 10 kV.

For the entire interruption, the re-strike voltage does not increase monotonously as shown in Figure 5.25 (left). This is because the periodically shortening of the arc by short-circuits of loops and curls, suddenly lowering the arc voltage. In case the arc is not interrupted at full open blade position, the air gap distance is constant, and the arc keeps burning without obvious re-ignitions or re-strikes. The arc voltage continues to increase during the arcing time, which corresponds with the increasing arc length for an undisturbed arc, referring Figure 5.25 right. As shown in Figure 5.26, the arc voltage increases nearly linearly, with about 3.2 kV/m at $I_d = 27$ A.

5.5.3 U-I characteristic

The arc voltage and current are in phase (Figure 5.24), implying that the arc has a resistive nature. Since the arc voltage is in the order of a few kilovolts, and the arc current is up to 27A in this example test, the arc resistance is up to a few hundred ohms. The arc current remains constant, the arc resistance increases with increasing arc voltage. Due to the non-linear nature of the arc voltage-current (U-I) characteristic, the arc resistance varies strongly during a power cycle as shown in Figure 5.27 (left).

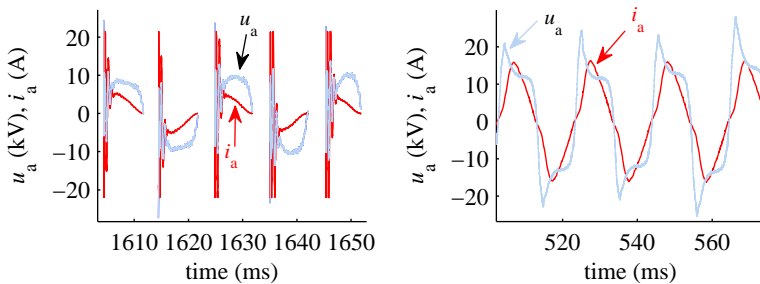


Figure 5.24. Arc current and voltage waveforms, left: $I_d = 3.9$ A with clear current zero periods; right: $I_d = 27$ A with a continuous arc current.

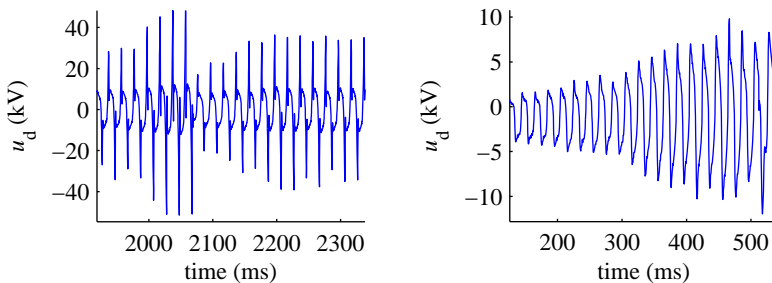


Figure 5.25. Arc voltage with and without steps in transient magnitudes at 27 A.

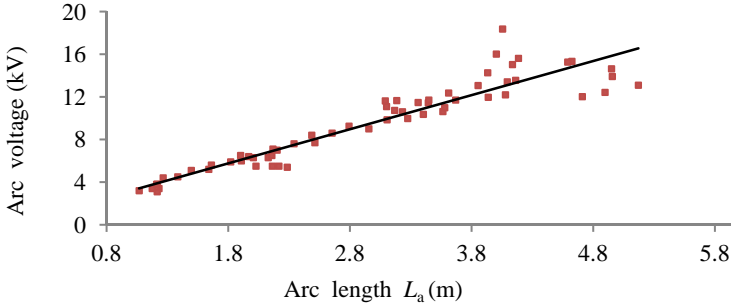


Figure 5.26. Arc voltage versus arc length at I_d of 27 A.

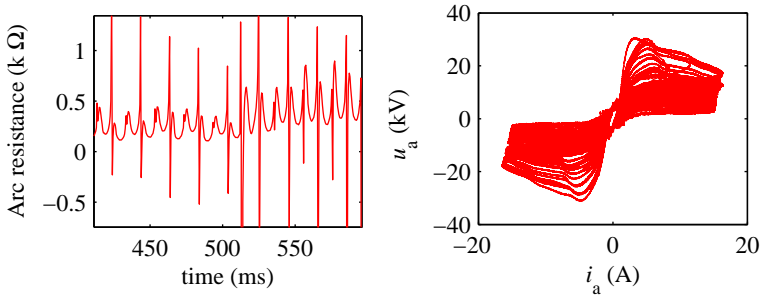


Figure 5.27. Example of the arc resistance and arc U-I characteristics at 27 A.

A typical U-I characteristic is plotted in Figure 5.27 (right), which is derived from a long duration arc at $I_d = 27$ A. It is also observed that the arc voltage increases rapidly immediately following current zero and reaches a somewhat constant value within the half cycle. The hysteresis loop confirms the typical arc U-I curve. This loop also explains that the arc voltage has variable values at identical current, but is determined by the arc length.

5.6 Energy input into the arc

The energy input w into the arc is obtained by integrating the product of the voltage u_a and the current i_a over the arcing time:

$$w = \int_{t_1}^{t_2} (u_a i_a) dt \quad (5.3)$$

Here t_1 is the moment of re-strike and t_2 is the moment of extinction at power-frequency current zero. Figure 5.28 illustrates the wave shapes of the voltage u_a , the current i_a , and the corresponding energy w over the time of a single re-strike.

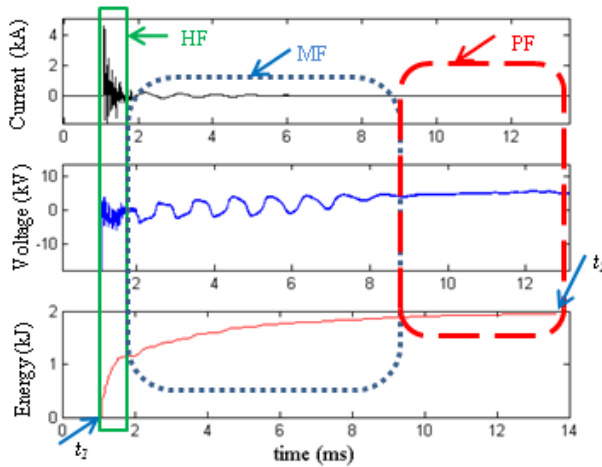


Figure 5.28. Wave shapes of u_d , i_d and the corresponding energy w ; t_1 is the re-strike moment and t_2 is the moment of temporarily arc extinction.

Upon a re-strike, three frequency components are distinguished (see Chapter 3): a high-frequency component due to charge equalization of C_s and C_l , a medium-frequency component from the oscillation between circuit inductance, both side capacitances in parallel, and the power-frequency (PF) component. The solid rectangle in Figure 5.28 indicates the duration where the HF oscillation prevails, the dotted rectangle is the duration of MF oscillation, and the dashed rectangle is the area of the remaining PF. It can be observed that the energy increases rapidly during the initial HF oscillation and continues to increase, but at a lower rate until the MF oscillation is damped. It reaches an almost constant value at power-frequency. For instance, in the example of Figure 5.28 it reaches 1.10 kJ during the first 0.3 ms, increases gradually to 2.18 kJ during the following 8 ms, until it finally reaches 2.0 kJ. The energy contributions in the shown example for the HF and MF oscillations are comparable, but the PF phase hardly contributes. Thus it may be concluded that (here) re-strike transients contribute very significantly to energy input the arc.

5.6.1 Energy distribution in transients

The energy after each re-strike in terms of percentages contributed during the phases with different dominant frequencies is plotted in Figure 5.29. The current is varied from 9 A to 27 A.

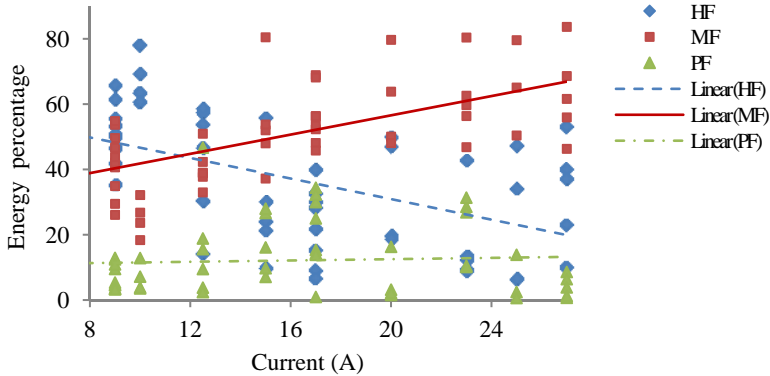


Figure 5.29. Energy contribution upon re-strike by various current frequency components (HF, MF, PF) as a function of current I_d .

The dependence on current level is roughly indicated by fitted lines. The results show that the contribution of the HF oscillation is relatively high at low values for I_d and drops at higher I_d . For instance, the HF energy contribution lies between 30% and 80% at $I_d < 12.5$ A but is less than 55% for $15 \text{ A} < I_d < 27$ A. The MF contribution increases with current level with an energy fraction between 20% and 50% at $I_d < 12.5$ A and over 40% for $15 \text{ A} < I_d < 27$ A. The energy at PF is usually smaller than 30% at all tested current levels. On average the contribution of PF is about 10%.

For the experiments with a fixed value of C_s (I_d in the range of 9 A to 27 A), the interrupted current depends on the value of C_l . Since C_l is much larger than C_s the MF contribution depends on C_l whereas the HF contribution depends on C_s , which is taken constant. Therefore, the energy input from the MF component increases with higher C_l . As a result, the relative importance of the MF component increases with I_d . The energy contribution from the power-frequency current is always relatively low. There is a large spread in the relative contribution of the HF and MF oscillations, but they both dominate the energy input.

5.6.2 Influence of C_s/C_l and I_d on energy

The relation between factors C_s/C_l , I_d and the arc energy is shown in Figure 5.30 for a current $I_d = 2.1$ A. In the upper three figures (indicated by 'a'), the development of arc energy against time with C_s/C_l as a parameter is given in each arcing period. The lower three figures (indicated by 'b'), show the arc energy against time with I_d as a parameter. It is observed that:

- The energy input into the arc upon re-strike is typically a few hundred Joule going up to a few thousands Joule at lower ratio of C_s/C_l and longer arc duration.

- It increases gradually (with occasional "steps") because of the increasing re-strike voltage caused by the motion of the DS contacts. It reaches the largest value, just before complete arc extinction.
- It is higher with higher interruption current and lower C_s .

5.6.3 Energy versus re-strike voltage U_r

The correlation between the energy w and re-strike voltage U_r at different current I_d is presented in Figure 5.31. Four different re-strike voltage (U_r) ranges are selected with I_d between 9 A and 27 A. Since C_s (50 nF) and E_m ($90\sqrt{2}$ kV) are fixed, I_d depends on C_l only. Figure 5.31 shows that at the same current level, the energy supplied into the arc increases with increasing re-strike voltage. Therefore, with higher interrupted current and higher re-strike voltage, more energy is delivered to the arc upon re-strikes. Because of the higher energy input into the arc, the breakdown voltage of the gap is lower and the gap recovers slower, the arc is not more difficult to interrupt but more easily to re-strike, even at longer gaps, indicating that the current to be interrupted and the breakdown voltage on re-strike are critical factors for interruption performance.

5.7 Transients upon re-strike

Due to the slow movement of the DS main blades an arc of a long duration arises, characterized by transient phenomena upon re-strike. The resulting transient voltage and current may endanger sensitive secondary components of the network through electromagnetic coupling.

From the frequency components initiated by re-strike, the maximum transient voltage across both capacitances, $u_{max} = |E_m| + \left| \frac{U_r}{1 + C_s/C_l} \right|$, occurs at medium-

frequency (see Chapter 3); E_m is the peak value of the power source and U_r is the re-strike voltage. Taking the re-strike voltage as a worst case equal to 2^*E_m , with $C_s/C_l \ll 1$, the maximum transient voltage may reach 3 p.u. The maximum

transient current upon each re-strike through the DS is $i_{max} = \frac{U_r}{\sqrt{L_H \left(\frac{1}{C_s} + \frac{1}{C_l} \right)}}$ with L_H

the equivalent inductance of HF loop. The maximum value of the transient current depends on the re-strike voltage and the circuit parameters of the high-frequency loop and can reach values up to a few kiloamperes within a few microseconds (7 kA in the test).

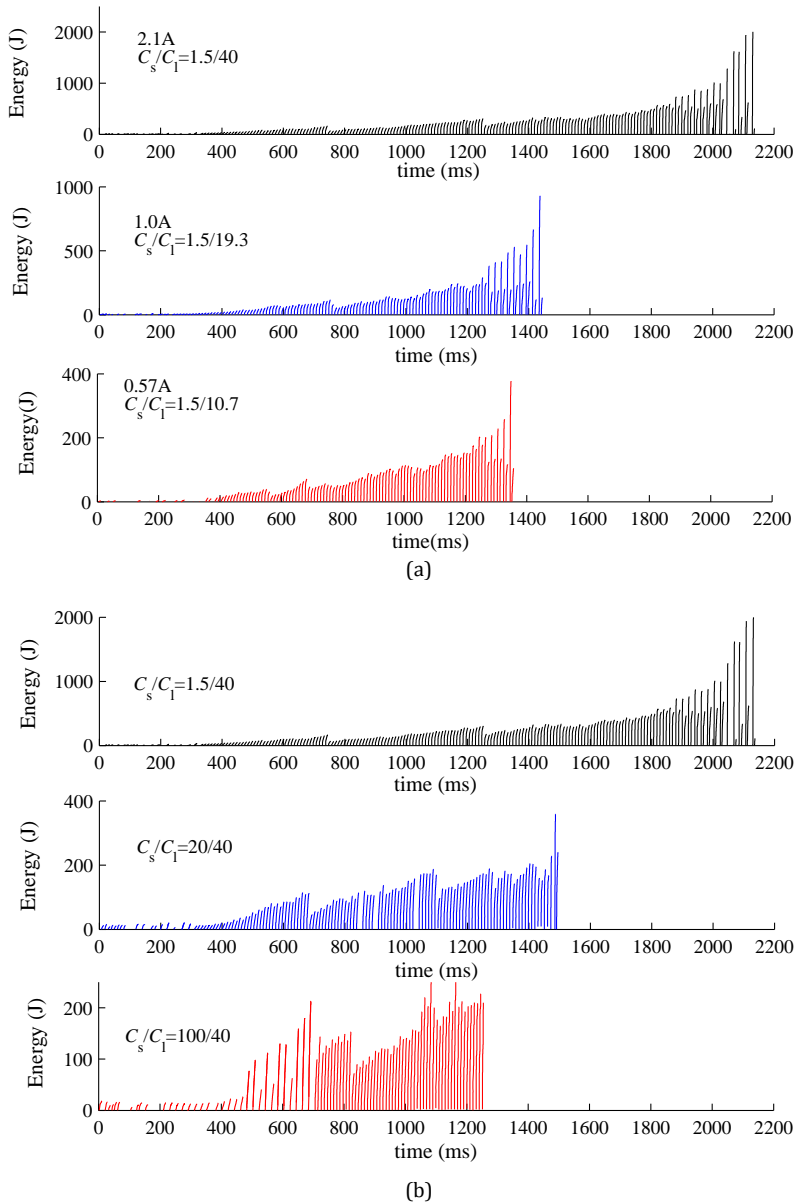


Figure 5.30. Energy input to the arc on re-strike versus time with parameter: (a) capacitor ratio C_s/C_1 at $I_d = 2.1$ A, and (b) current I_d with fixed $C_s = 1.5$ nF.

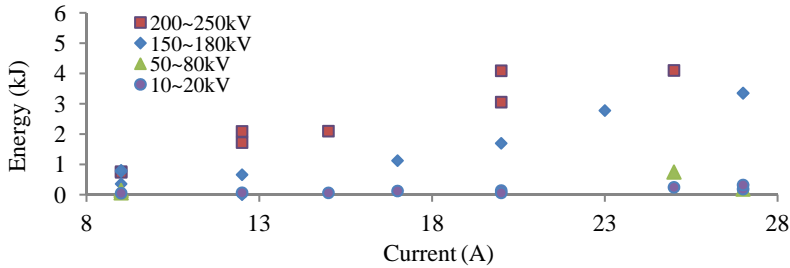


Figure 5.31. Arc energy upon re-strike at different interruption current level. Parameter is re-strike voltage interval.

5.7.1 Transient voltage upon re-strike

Figure 5.1 shows the overvoltages across the load side capacitance that appear in the end phase of the interruption process. Figure 5.32 shows the maximum observed overvoltage upon re-strike across C_l as a function of the re-strike voltage at different values of the ratio C_s/C_l , with a source voltage of 173 kV and a current of 2.1 A. The overvoltage across C_l can reach up to 2.4 p.u. It increases with increasing re-strike voltage and decreasing ratio C_s/C_l . It can also be observed that the overvoltage reaches the highest value at the lowest C_s/C_l ratio: $C_s/C_l = 0.04$.

The dominant frequency of the overvoltages is in the order of a few tens of kilohertz. Since most of the overvoltages occur at the end of the interruption, where the re-strike voltage is high, it would be advisable to put effort in interruption of the circuit at an earlier stage. At higher ratio of C_s/C_l , the overvoltages reduce significantly.

Apart from the high peak values, overvoltages are characterized by steep fronts. Although these repeated steep fronts have a lower fall-time than that observed in GIS-DS switching, the resulting travelling waves in open air stations still can lead to considerable stresses to equipment (notably transformers) directly connected to the DS [5]. The transient may reach 2 p.u. within a few tens of microseconds in the performed experiments.

5.7.2 Transient current upon re-strike

The current through the disconnector in the experiments at $9 \text{ A} < I_d < 27 \text{ A}$ are recorded with a bandwidth of 20 MHz. For the experiments, the value of C_s is 50 nF, and the source RMS voltage is taken as 90 kV. Figure 5.33 shows that the transient peak current value increases with the re-strike voltage. The dominant frequency of current transient is a few tens of kilohertz to a few megahertz, according to the measured data. It was also found that the rate of rise of the transient current is a few kiloamperes per microsecond.

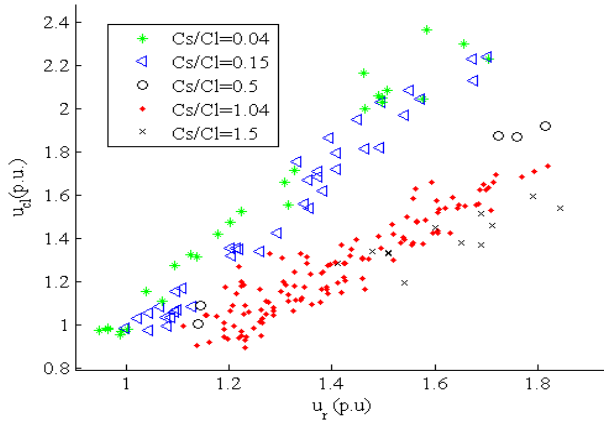


Figure 5.32. Overvoltage across C_l against re-strike voltage with the ratio of C_s/C_l as a parameter at current of 2.1 A.

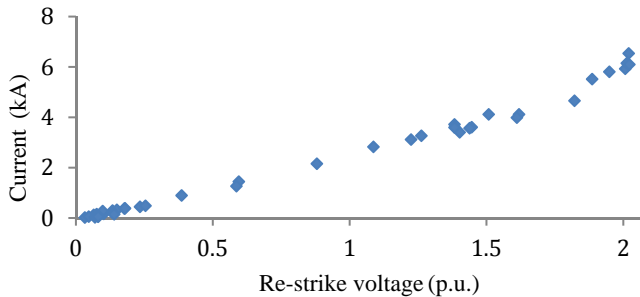


Figure 5.33. Measured HF transient current peak value against re-strike voltage.

5.8 Conclusion

Both recorded electrical and optical signals show that in the few seconds of capacitive current interruption the arc has frequent extinctions and re-ignitions. It extinguishes temporarily at the power-frequency current zero, but re-ignites by the circuit impressed recovery voltage and ultimately extinguishes when the electrical strength of the air gap is larger than the recovery voltage the circuit can provide. During this process, the breakdown voltage of the air gap along the arc path is significantly reduced due to the thermal influence of the arc. As a result, it may take seconds for the gap to recover and withstand the highest recovery voltage.

Arc behaviour and the interruption performance are highly affected by the circuit parameters. These parameters include capacitance ratio C_s/C_l , stray and short-circuit inductance and power supply voltage. All these affect the current to be

interrupted, the re-strike voltage, associated transients as well as the energy supplied to the arc and ultimately the heating of the air in close vicinity of the arc.

The source and load side capacitances are the main factors that influence the arc behaviour and the interruption performance. With lower ratio C_s/C_l , (specifically lower than 0.1 in the tests), the arc duration, overvoltage across the load side capacitance, contacts gap length, blade angle at final interruption, and the energy input into the arc are much larger, whereas the re-strike voltage is lower due to slower recovery. With higher C_s/C_l , the arc exhibits an erratic mode that either is sustained or changed to a stiff mode.

The current to be interrupted is another governing factor, which affects the interruption performance. With higher current, the arc duration, overvoltage across the load side capacitance, contacts gap spacing, blade angles and arc energy are much larger because gap recovery is slower and the re-strike voltage is lower. With higher current, the arc is brighter; the arc remnants decay slower, the arc upwards velocity is not affected much. The arc overall brightness is also increasing with the interrupted current.

With lower re-strike voltage, the energy input into the arc upon re-strike, and the overvoltage, over current are smaller. The re-strike voltage depends on the momentary air gap length and its corresponding physical conditions. The arc energy, overvoltages and the transient current in the circuit reach the largest value just before the arc extinguishes completely.

When the gap recovers relatively fast (at lower current, larger ratio C_s/C_l) the arc duration is short. When higher current thermally conditions the gap by reducing its breakdown value, the arc duration can be much longer, or even infinite.

The value of re-strike voltage can never be higher than 2 p.u., but the moment when this maximum is reached depends on the gap dielectric condition. The breakdown reduction mechanism will be discussed further in more detail in Chapter 9.

When the re-strike voltage is higher than the amplitude of the source voltage, the high and medium-frequency components are still strong when the next current zero appears. In such a case, the arc does not stop until another half cycle current zero. If this phenomenon occurs continuously, the re-strike voltage and the voltage across the load side appear unipolar.

The optical arc behaviour assists to understand the interruption mechanism more profoundly. The re-ignited arc follows the "traces" left by the just extinguished arc. That means the arc chooses the dielectrically weakest path for which the breakdown voltage is lowest. The ionization remaining after the disappearance of the past arc makes the arc re-ignite or re-strike at a lower breakdown voltage.

Ways to shorten the arc duration, or equivalently, to increase the current interruption capability, must be sought along this line.

5.9 Recommendation for standardization

The macroscopic arc behaviour is strongly dependent on the circuit as quantified by C_s/C_l . This observation implies that for testing of the DS switching capability, the circuit plays a major role (this also applies to the testing of auxiliary interrupting devices). Since no test-circuit has been defined yet, one of the tasks of the IEC maintenance team, elaborating an amendment to the IEC standard 62271-102 was to define a circuit. It was decided that 20 CO (close-open) tests have to be performed with $C_s/C_l = 0.1$, adopting a test-circuit as in Figure 3.1. Alternative, but yet adequate supply circuits, supplying much less than the short-time current are being discussed. It was decided to give the document the status of a technical report and allow time for collecting experience. The technical report IEC/TR 62271-305 was issued in 2009.

References

- [1] D. F. Peelo, "Current interruption using high voltage air-break disconnectors", Ph.D. dissertation, Dept. Electrical Engineering, Eindhoven Univ. of Technology, Eindhoven, 2004.
- [2] *IEEE Standard Techniques for High voltage Testing*, IEEE Standard 4-1995, Aug. 1995.
- [3] [Online]. Available: <http://www.hapam.nl/>.
- [4] IEC Standard on "IEC standard voltages", IEC 60038: Jun. 2009.
- [5] S. Arigye-Mushabe, K. A. Folly, "Evaluation of switching capacitive currents by disconnect switches using DIgSILENT software tool", in *Proc. 2005 The Australasian Universities Power Engineering Conf.*, vol.1, paper nr: S036, Sept. 2005.

Chapter 6

Interruption with Air Flow Assistance

Air flow is an effective approach for arc quenching during current interruption with air-break DSs, as already reported in [1]-[3]. Research on forced air injection into the arc ("air flow device") is rather old, and the studies were exclusively based on the air flow in a vertical direction facing the arc body from underneath a vertical-break DS. The test results proved this method to be effective. However, all literature only focused on the basic macroscopic test results. A detailed analysis on the mechanisms improving the interruption capability is lacking. In this chapter an experimental study is presented, specifically focusing on arcing time, re-strike voltage, re-strike frequency and derivative of interrupted current (di/dt). The mechanisms through which air flow assists the interruption are discussed.

6.1 Experimental setup

The test circuit depicted in Chapter 4 is extended with air flow outlets as shown in Figure 6.1. The air flow is controlled through two separate nylon air hoses ending at each tip of the main blades, directed towards the arc roots. The hose opening area is approximately 50 mm², directed about 5 cm from the expected arc root. The outlet is mounted on the moving blades, ensuring a steady air flow towards both arc roots. Two levels of air flow have been injected into the arc: 215 litre/minute and 325 litre/minute. The experiments are conducted with current values I_d of 0.5 A, 1.4 A, 2.6 A, 3.9 A, 5.0 A, 6.3 A and 7.5 A at 90 kV. The value of C_s is taken as 50 nF and C_l ranges from 18 nF to 265 nF. The value of I_d is determined by C_l and the other parameters in the circuit are fixed.

Switching operations are performed for each applied current level:

- without air flow (denoted as case A).
- with air flow rate 215 litre/minute, air velocity 72 m/s (denoted as case B).
- with air flow rate 325 litre/minute, velocity 108 m/s (denoted as case C).

The air flow rate on each side is measured by an air flow meter. Three opening operations are performed at each current level and each air flow level. However, case A was not applicable at 7.5 A, because the DS main blades reached the maximum position just after final arc extinction already at 6.3 A, which implied that interruption at 7.5 A without air flow would fail. Case B tests were not performed for current levels above 2.6 A, because of laboratory time restrictions.

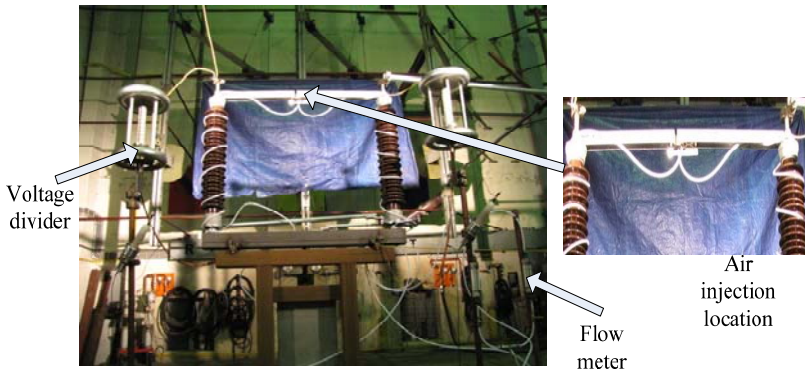


Figure 6.1. DS including voltage dividers and nylon hoses injecting air flow from underneath the DS blades at both sides.

In all switching operations, the arc extinguished completely before the main blades of the DS reached the final opening position. The voltages across the source and load-side capacitors (u_{cs} , u_{cl}), and the current flowing through the DS i_d were recorded. The measuring and data acquisition systems are described in detail in Chapter 4. The experiments were performed at KEMA High Power Laboratory Arnhem, where a strong voltage source is available.

6.2 Effect of air flow on arcing

The effect of air flow on the interruption is strongly reflected in the measured current and voltage wave shapes, and in the repetitive re-strike patterns.

6.2.1 Measured current and voltage

The current and voltage wave shapes from case A (no flow) differ significantly from cases B (moderate flow rate) and C (high flow rate). Figure 6.2 illustrates the wave shapes of the voltages u_d across the DS ($u_d = u_{cs} - u_{cl}$) and the current i_d through the DS for the three different cases at current $I_d = 2.6$ A. Experiments at other current levels show similar qualitative behaviour in spite of a varying arc duration. Figure 6.3 contains the expansions of the wave shapes taken over the period $t = 1000 \sim 1150$ ms ($t = 0$ indicates the arc start). The air gap length hardly changes during this 150 ms time span.

In all cases it is observed that: (i) the arcing duration is in the order of seconds; (ii) the entire interruption consists of numerous interruptions and re-strikes/re-ignitions; (iii) the electrical transients occur at each re-strike/re-ignition, which causes overvoltages and (local) current spikes in the local circuitry. However, differences between the interruptions with- and without air flow are apparent.

Looking at Figure 6.2, in case A, the arc duration is 2.3 s. Mostly, there is only a single re-strike within each half power-frequency cycle as shown in Figure 6.3. Once the re-strike occurs, the arc continues till the next power-frequency current zero. The arrows in Figure 6.3 illustrate re-strike and subsequent arc extinction. Compared to the wave shapes obtained with air flow (cases B, C) the re-strikes for case A occur at lower breakdown voltage and are associated with smaller transients. For instance, in Figure 6.2 the re-strikes between 0 and 1000 ms for case A are hardly visible (re-strike voltage remains below 20 kV); the re-strikes after 1000 ms are less frequent compared to cases B and C. These observations reflect the slow recovery of the dielectric strength of the air gap.

Compared to case A (2.3 s arc duration), the arc duration is much shorter in both case B and C (1.6 s for case B and 1.4 s for case C); in the later situations, there are multiple re-ignitions occurring within each half power cycle (compared to only one re-strike following current zero); the re-ignitions occur more frequently and show higher voltage transient amplitudes.

Compared to case B the arc duration in case C is even shorter; the re-ignitions occur more frequently and the breakdown voltages are higher (see the period from 0 to 500 ms in Figure 6.2). The expanded wave shapes of voltage u_d between 800 ms and 950 ms are plotted in Figure 6.4. Compared to case A the breakdown voltages in case B and C are much higher for identical air gap length. The breakdown voltages for case C are usually larger than for case B as well. This means that applying a higher amount of air flow helps to interrupt the circuit more successfully. The air flow cools the former arc path and removes localized patches of ionization and thereby increases the dielectric strength of the same volume of air in the gap. This will be explained further in Chapter 9. On the other hand, the number and magnitude of transients in current and voltage are higher.

6.2.2 Recovery voltage

Recovery voltage is the difference between the voltage across the source and load side capacitance after arc extinction at current zero. Without air flow RV rises right after current zero as a $(1-\cos)$ wave shape in one polarity until re-strike occurs, as discussed in Chapters 3 and 5. If the arc is forced to extinguish before power-frequency current zero, as in the presence of air flow, RV will maintain its original polarity before re-ignition and cannot reach the maximum value of 2 p.u. as in the case of interruption at current zero. Figure 6.5 shows a single recovery event in both situations. Without air flow, the RV increases directly to negative values (Figure 6.5 left). With air flow, the RV may first change polarity before re-ignition (Figure 6.5 right). Without air flow, at current zero the arc extinguishes at the maximum voltage across the load side. However, the arc can be forced to extinguish before power-frequency current zero because of super-imposed high-frequency oscillations, which are more apparent in arc interruption with air flow.

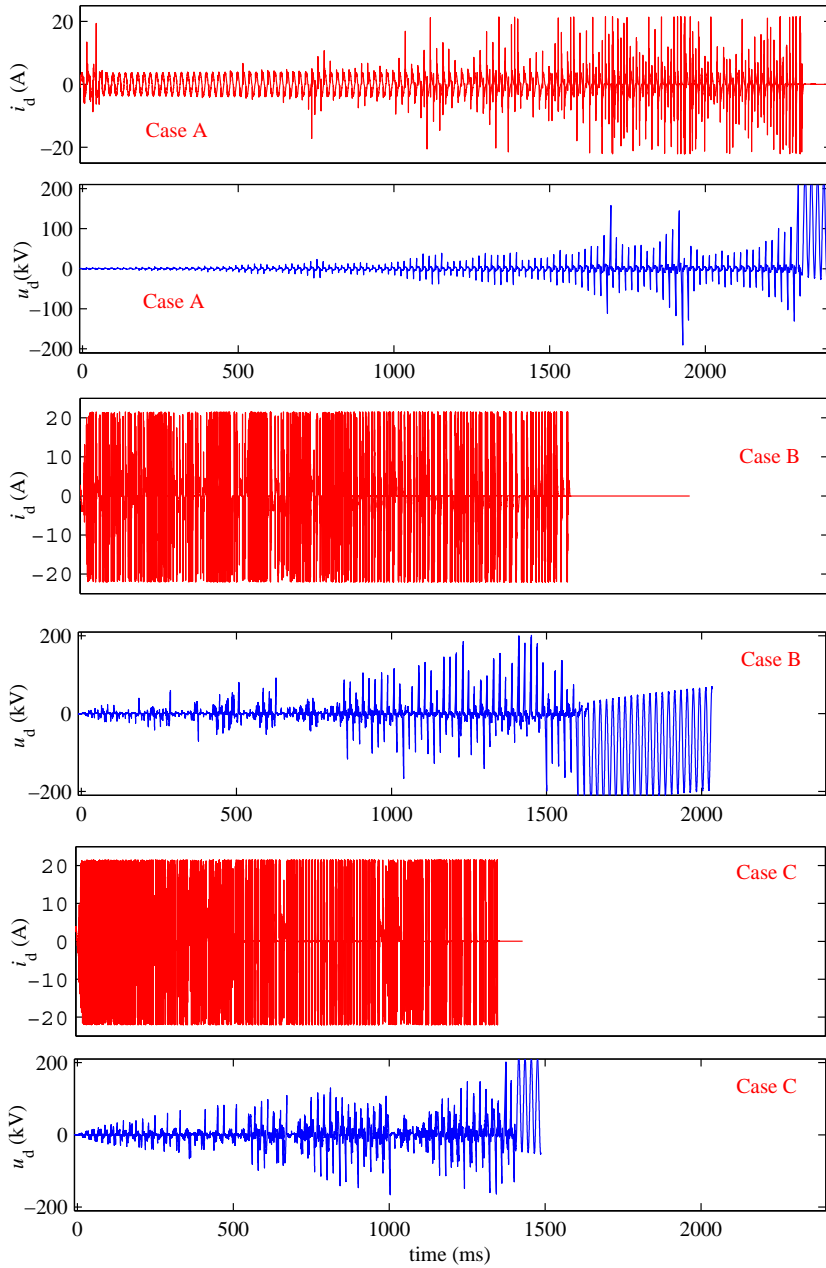


Figure 6.2. Wave shapes of i_d , u_d for cases A (no flow), B (215 litre/min) and C (325 litre/min).

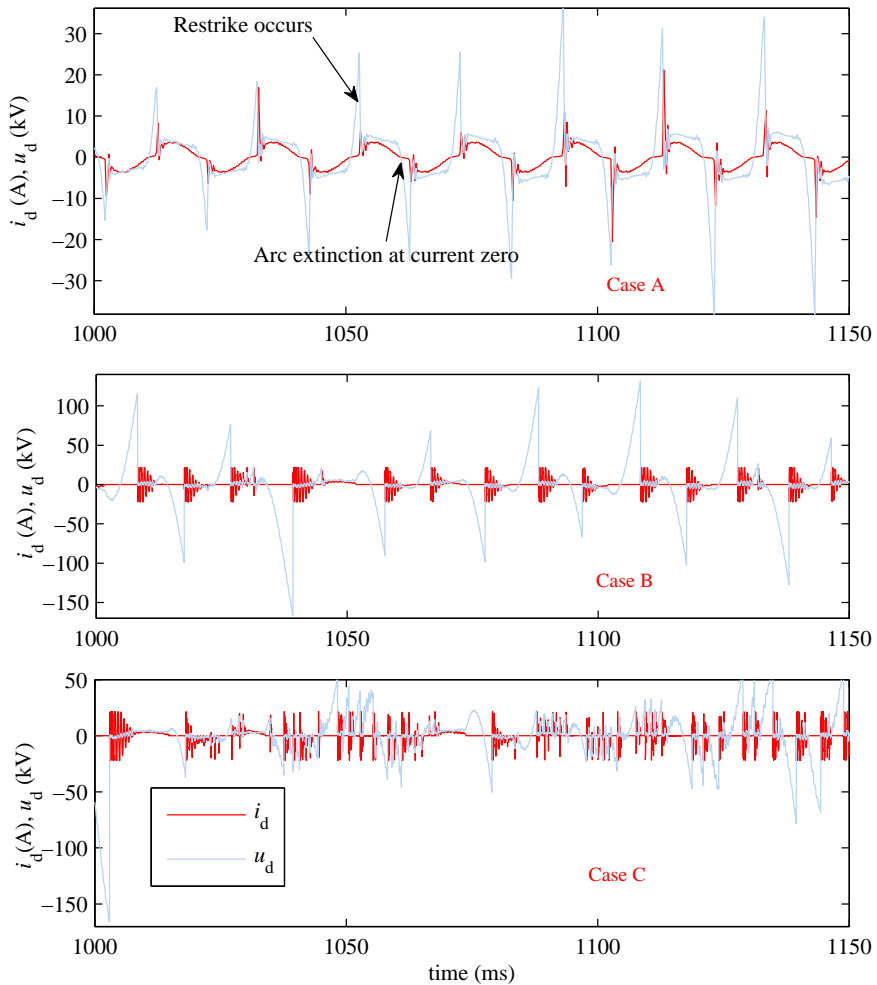


Figure 6.3. Expansion over the range 1000~1150 ms in Figure 6.2.

The voltage across the load capacitance may not have reached its maximum value (the source voltage amplitude).

Figure 6.6 presents results from simulations, showing the wave shapes of i_d and u_d assuming various power-frequency phase angles where the arc current is chopped. At $t = 20$ ms the arc current is at maximum. At $t = 25$ ms the arc current crosses zero. The currents $i_{di(i=1\dots6)}$, and voltages $u_{di(i=1\dots6)}$ are the simulated results when the arc is chopped at 20 ms, 21 ms, 22 ms, 23 ms, 24 ms, 25 ms.

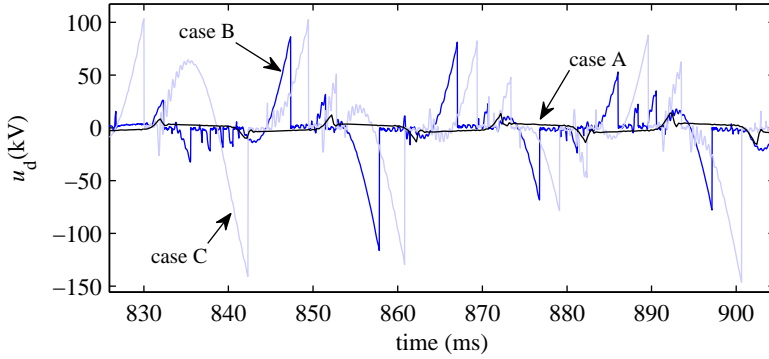


Figure 6.4. Expansion of u_d between 800 ms ~ 950 ms for cases A, B and C.

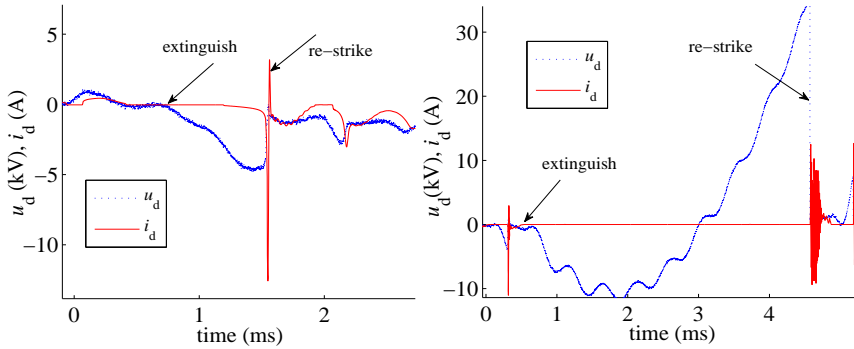


Figure 6.5. Single recovery event, (left) without air flow, (right) with air flow.

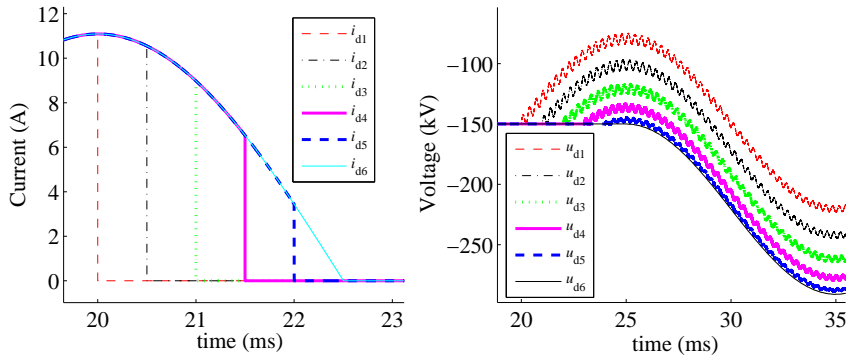


Figure 6.6. Simulated wave shapes for i_d and u_d at various arc-chopping phase angles.

The simulated results show that the RV across the DS reaches lower values when arc current is chopped closer to its peak value. The RV is equal to u_{cs} plus the offset U_{cl} . Since the source side u_{cs} remains nearly equal to u_s , it means that the RV depends on U_{cl} . The larger the arc current at chopping, the smaller U_{cl} is, and the smaller the maximum value that the RV may reach. With air flow, the arc is

chopped at various phase angles apart from the power-frequency arc current zero. Thus, the values the RV can reach are smaller than without air flow. With a smaller RV, it is more difficult to break down the air gap for the next re-strike.

6.2.3 Arc modes

Based on the previous observations, it might be stated that the arc appears in two distinct modes. One mode is referred to as "thermal arc", usually occurring for case A. It is associated with a sequence of arc extinctions at (power-frequency) current zero and re-strikes until sufficient gap distance has been reached. During every half cycle the arc remains stable. Transients are limited to re-strikes that occur every half cycle. The other mode is referred to as "dielectric arc", usually occurring in cases with sufficient air flow (cases B and C) or other cooling. Here, the arc is a very concentrated succession of arc interruptions (mostly away from natural current zero) and re-ignitions. The arc is chopped at various phase angles within a power cycle. Apparently, the air gap dielectric recovery speed is greatly increased compared to case A, because of cooling of the (former) arc path by the air flow. Visually, the "thermal" arc duration is longer, contains more curls than the dielectric arc, has a less violent appearance and audible noise than the arc in the "dielectric" mode. Examples of arcs in both modes and their re-strikes are shown in Figure 6.7.

6.3 Interruption data analysis

For the analysis of the experimental data the main focus will be on the arc duration, which is obviously different for the cases with and without air flow. The re-strike voltage, the number of re-strikes per cycle, and the interrupted current derivative di/dt are studied as well in order to understand the effect of air flow on the interruption mechanism.

6.3.1 Arc duration

The arc duration is influenced significantly by the interrupted current I_d and the air flow rate in the experiments. Figure 6.8 presents the arc duration as a function of the interrupted current with the air flow as a parameter for all interruption operations. Obviously, the arc duration for case A is much longer than for cases B and C; the arc duration in case C is nearly 50% reduced with respect to case A. In addition, at identical interrupted current level, the arc duration decreases with a higher amount of air flow rate. It should be noted that the case B tests were only performed up to 2.6 A. The linear interpolation lines for cases A and C show that the arc duration tends to increase with increasing interruption current I_d in both cases (however with a large spread). This is in agreement with the results presented in Chapter 5 for interruptions without air flow.

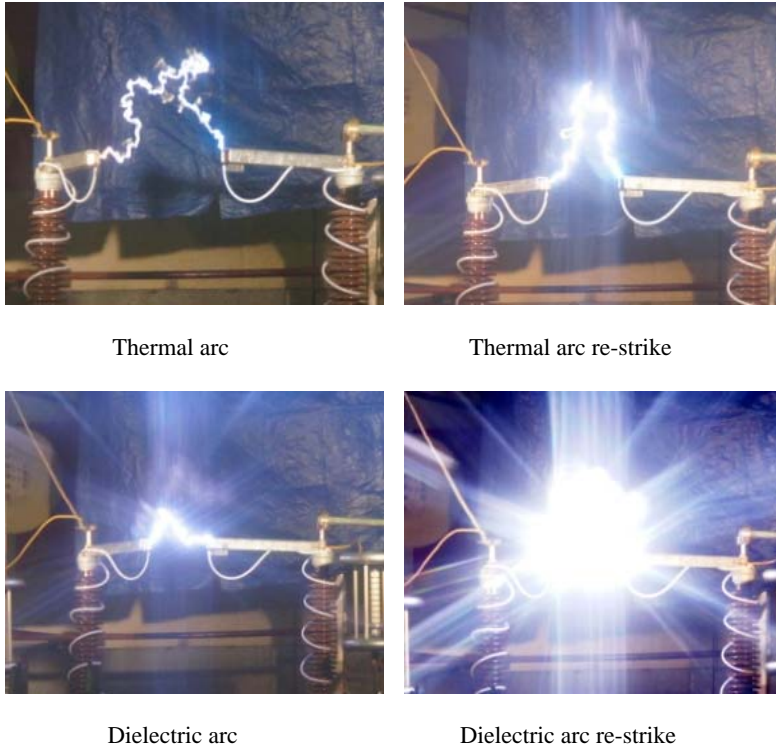


Figure 6.7. Arc modes: (left) steady state operation; (right) at their re-strike moments.

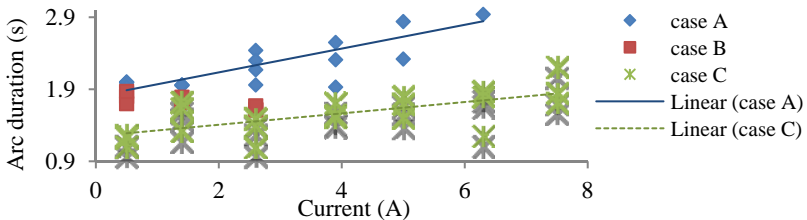


Figure 6.8. Arc duration versus the current I_a with air flow rate as parameter.

6.3.2 Re-strike voltage versus time

Measured values from three repeated operations at the same current level and air flow rate are combined to get statistically relevant re-strike voltage values in order to detect a possible trend. The values of the re-strike voltages are divided into 10 time intervals (bins), equally distributed over the interval from the moment that the arc starts until the moment that the arc extinguishes completely.

The median values of the positive re-strike voltages in each bin versus time using air flow level as a parameter are presented in Figures 6.9 and 6.10. Negative re-strike voltages show similar behaviour. Time $t = 0$ is the moment of arc initiation.

From Figures 6.9 and 6.10, the following conclusions are drawn:

- For a given time (or DS gap length), normally the re-strike voltages in cases B and C are much higher than in case A for every current level.
- At a low current (0.5 A in these tests), however, the re-strike voltage for the cases with- and without air flow are similar. The air flow does not affect the interruption as much as it does for a current of 1.4 A or higher. The re-strike voltage at 0.5 A for the three cases increases approximately linearly with time (i.e. with the air gap length). This suggests that thermal influences on the recovery do not play a main role yet due to the small current.
- For current levels up to 2.6 A, where experiments for both case B and C are carried out, the re-strike voltages of cases B (moderate air flow rate) and case C (high air flow rate) are similar.
- The re-strike voltage is mainly determined by the interrupted current in case A. With higher current, the re-strike voltage is lower, which was also observed in Chapter 5, where the interrupted current was below 2.3 A.
- Without air flow, the re-strike voltages clearly depend on the current level during the entire interruption process. On the other hand in cases B and C, during the first 1500 ms of the interruption process, the influence of the current is limited since the difference between re-strike voltages at different current levels is hard to be observed (in particular for case C in Figure 6.10). However, at the end of the interruption process, the re-strike voltages correlate better with current level. It is also observed that the influence of the current is not so obvious for case C as it is for case B; this implies that with higher air flow rate, the current influence is smaller.

It is concluded that both air flow and interrupted current play key roles in the interruption process. For rather small current (roughly < 1 A), the thermal influence does not affect the re-strike voltage value significantly, and the air gap recovers mainly dielectrically. When the current is larger (roughly > 2 A in these experiments), the thermal influences start to dominate the interruption. If the air flow rate is high, the re-strike voltage values at different current levels are similar at the most stages of the interruption, which means that the air flow mainly dominates the interruption, and the current level plays a less prominent role in current range chosen in these experiments.

6.3.3 Breakdown frequency

Obviously the number of breakdown events per unit time (breakdown frequency) depends on air flow rate and interrupted current. Figures 6.11 and 6.12 show the Cumulative Number (CN) of breakdown events versus time at all applied current

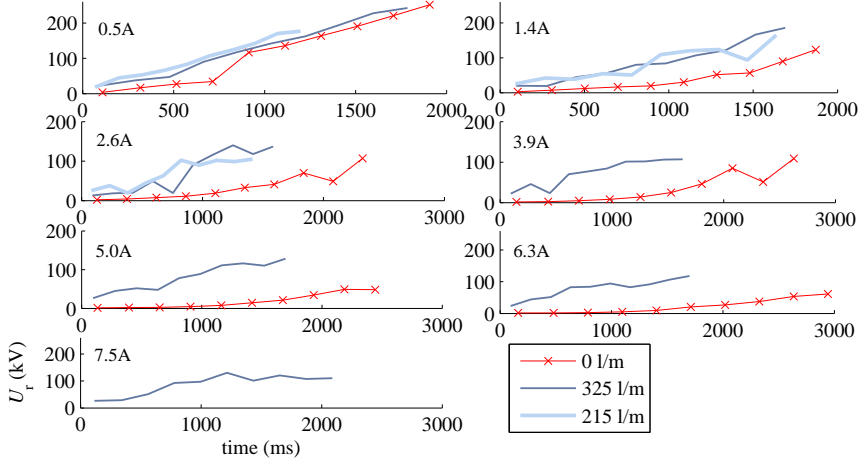


Figure 6.9. Re-strike voltage (in kilovolts) versus time (milliseconds) with air flow rate as a parameter at current range 0.5~7.5 A.

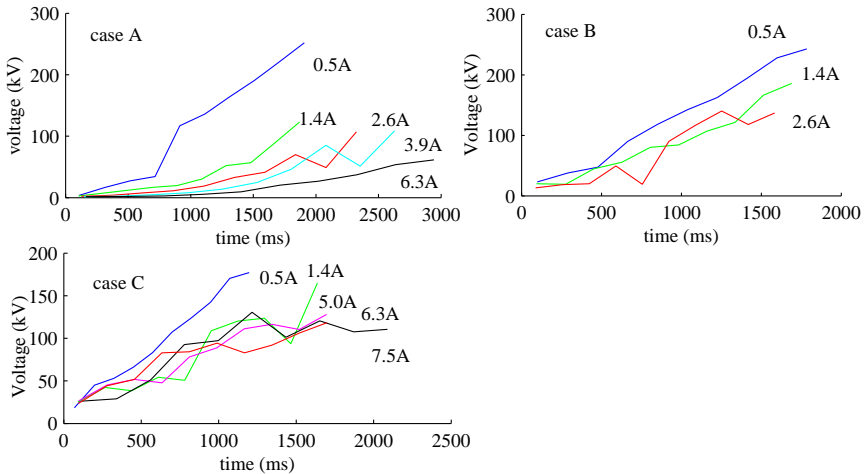


Figure 6.10. Gap recovery reflected in re-strike voltage (kilovolts) versus time (milliseconds) with current I_d as a parameter for cases A, B and C.

levels. A continuous theoretical CN line of one re-strike per 10 ms as a reference is added at the bottom of Figure 6.12. The following behaviour is observed:

- Since the arc does not only extinguish at power-frequency current zero, but is also chopped at other phase angles, at an identical arcing time the CNs for cases B and C are much larger than for case A, at every current level.
- At 0.5 A, the CN per unit time is more or less similar for cases B and C. However, at 1.4 A and 2.6 A the CN for case C is larger than for case B. A high air flow rate results in more frequent breakdown events.

- At all current levels for case A, the CN increases rapidly at the very beginning of the interruption process. This rapid increasing stage lasts longer in case the current is low compared to higher current. After this stage the CN increases more slowly and linearly. The rate of increase is about 0.1 per millisecond. The initial high re-strike frequency is because the thermal influence plays no major role yet. Later on, the arc exists continuously till the next current zero crossing due to the thermal influences.
- For case C in Figure 6.12 the CN is decreasing with the increasing current level. This implies that the effect of the current becomes more pronounced at higher current level.

As a conclusion, at a low current (0.5 A in the test) and in the very early stage of the interruption processes at higher currents, the current influence on breakdown frequency is relatively small. The interruption mode is mainly dielectrically determined. In a later stage of the interruption process with higher current, the current level dominates the interruption in absence of air flow. However, at higher current levels (> 1.4 A), the air flow becomes a key mechanism. Both air flow and current level determine the arc duration.

6.3.4 Current derivative di/dt

The current derivative di/dt at the moment of current zero is (for circuit breakers) a key factor to evaluate the interrupting performance. Since the arc extinguishes temporarily when the current crosses zero at each half cycle in case A, the derivative di/dt is calculated from the current waveform $i = \sqrt{2} I \sin(\omega t + \theta)$ where I is the rms value of the arc current; ω is the angular frequency ($2\pi * 50$ Hz), and θ is the initial phase angle. The derivative di/dt at current zero is $\frac{di}{dt} = \sqrt{2} I \omega$. In case A, the current ranges from 0.5 A to 6.3 A, hence $\frac{di}{dt} = (0.2 \sim 3)$ A/ms. However, the arc can be chopped at any moment for case B and C, which means that current zeros, leading to interruption, are caused by the high-frequency current transients with much higher di/dt than quoted above.

di/dt is calculated from the measurements at each arc extinction point. The calculated di/dt values are statistically distributed variables. Their properties are analyzed with the aid of Figures 6.13 and 6.14. Results are shown for different current levels and for the cases A, B and C. Noticeably, the di/dt values at 0.5 A are

not depending on the air flow rate, which confirms the conclusion drawn earlier on thermal influences not being relevant yet. When the current exceeds 1.4 A, di/dt is higher with air flow than without air flow at each current level. At 1.4 A and 2.6 A, the di/dt in case B is lower than that in case C, which means di/dt is larger with higher air flow rates.

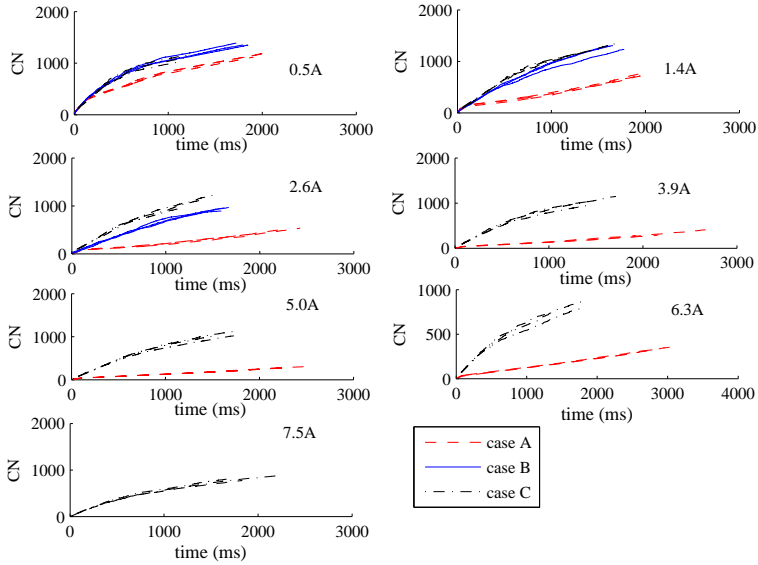


Figure 6.11. Cumulative number of breakdown events versus time with the current as parameter for cases A, B and C.

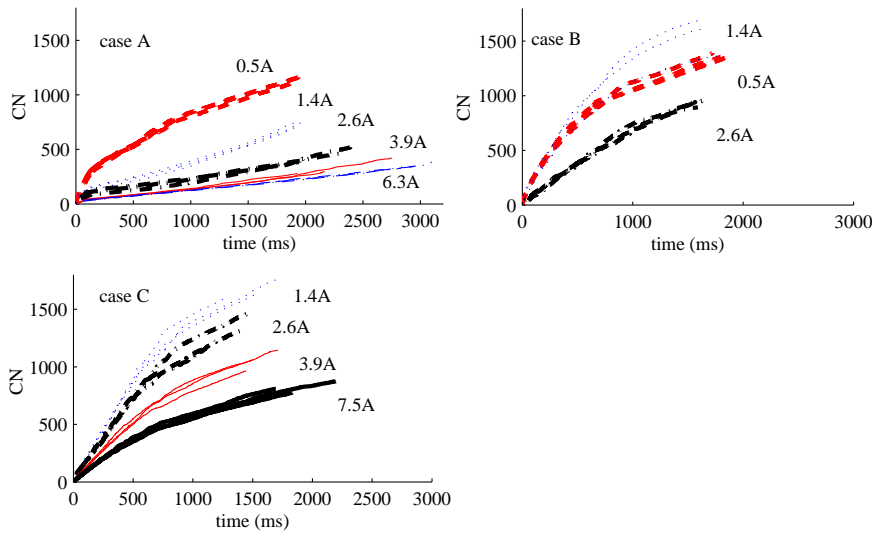


Figure 6.12. Number of re-strikes versus time for cases A, B and C at different values of I_d .

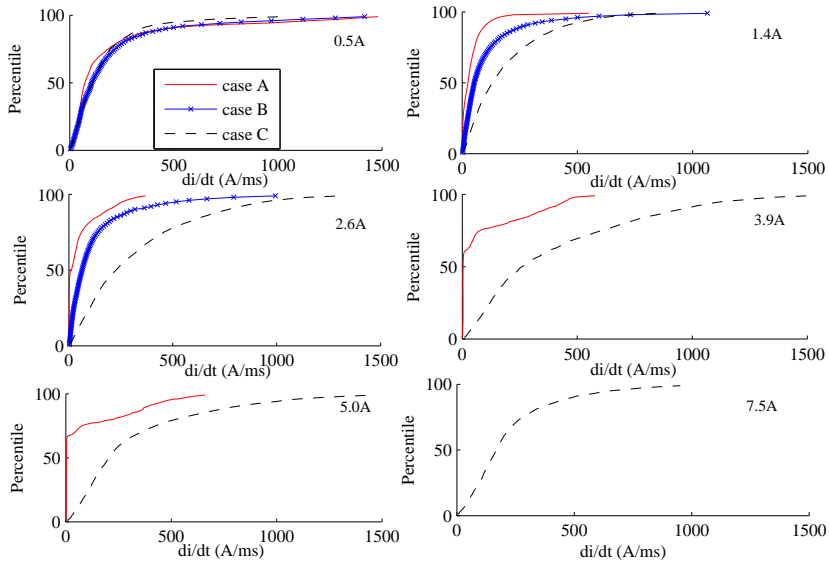


Figure 6.13. Cumulative distribution of interrupted di/dt for the cases A, B and C at different current values.

Since the tests for case B are not done at current above 2.6 A, the value of di/dt is only evaluated for cases A and C. The 50-percentile (median value) di/dt value for case A, is in the range 4 to 25 A/ms (with low current of 1.4 A). This value is comparable with the estimated values before, assuming only arc extinction at power-frequency current zero. The median values of di/dt in case C range from 100 to 300 A/ms, several ten times higher than for case A. Obviously, the interruptible di/dt with air flow is drastically higher than without air flow. This again confirms the strong influence of air flow on the interruption process.

6.4 Conclusion

Two interruption modes are observed, a dielectric and a thermal mode. The dielectric mode interruption mainly occurs in the case with a high air flow rate (here 315 litre/minute) and with arc current roughly below 1 A. The thermal mode occurs in the case without air flow at higher interrupted current (> 1.4 A in the present experiments). The main differences between these modes can be summarized as follows:

During the dielectric mode, the arc current may be chopped at any moment in the power-frequency cycle for the case with sufficient air flow. Multiple breakdown

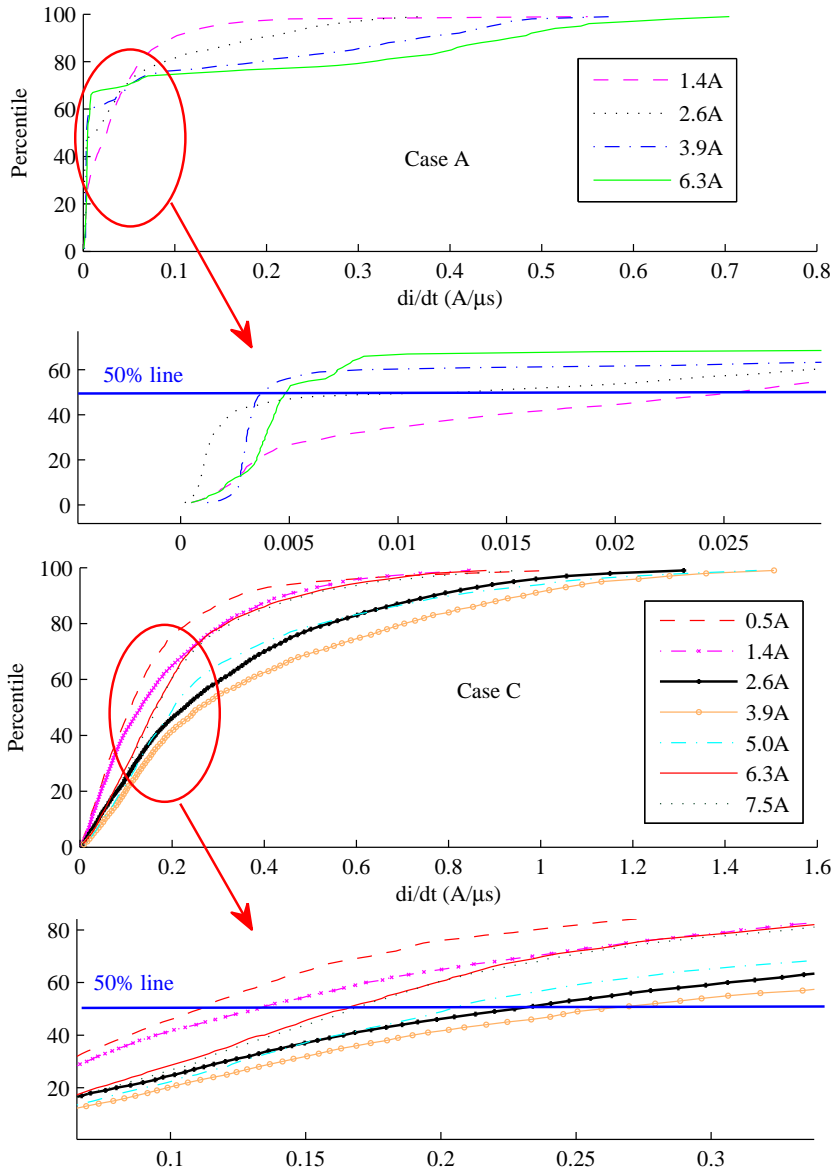


Figure 6.14. Cumulative distribution of interrupted di/dt for cases A and C with I_d as a parameter.

events within a half power-frequency cycle are very likely and the number of the breakdown events per unit time is much higher compared with the thermal mode interruption. At the same interrupted current level the breakdown voltage, mainly dominated by the air gap length, is higher than for the thermal interruption mode.

Both the higher breakdown repetition frequency and the higher value of the breakdown voltage make this mode potentially more hazardous for neighbouring substation equipment (specifically power transformers). The interrupted current derivative di/dt at the current zero is much higher (about a factor 20) than for the thermal interruption mode. This implies that the arc current can also be interrupted at current zero from higher frequency oscillations than power-frequency, caused by the transients in the circuit.

During the thermal interruption mode, the arc can initially be chopped at any moment at the very beginning of interruption process due to the very short air gap length. However, after (1-2 half cycles), the arc extinguishes at the power-frequency current zero only. The interrupted current derivative di/dt increases roughly linearly with the interrupted current, except in the small gap initial arc phase. Due to thermal influences, the breakdown voltage is much lower than in the case of the dielectric interruption mode at the same air gap distance. This is, in principle, less hazardous for voltage transients striking nearby equipment. However, ultimately the overvoltage is at the same level, but reaches at a much longer gap than in the dielectric mode and occurs less frequently.

Since air flow may convert thermal interruption into dielectric interruption, the dielectric strength of the air gap increases, as well as the corresponding interruptible di/dt . The air flow is an effective method to improve the interrupting capability of the air-break DS to interrupt small capacitive currents. However, significant values (here 315 litre/minute) at both arc roots during the complete arcing process have to be realized. This limits its practical application because compressors and high-pressure containers should be available. Alternatively, one could imagine creating the necessary pressure simultaneously with the blade rotating motion. A better directed air flow could reduce the necessary air flow rate.

References

- [1] E. C. Rankin, "Experience with methods of extending the capability of high voltage air-break switches", *AIEE Trans. on Power Apparatus and Systems*, vol.78, pp. 1634-1636, Dec. 1959.
- [2] I. W. Gross, C. Killian, J. M. Sheadel, "A 330- kV air switch", *AIEE Trans. on Power Apparatus and Systems*, vol.73, pp. 264-270, Jan. 1954.
- [3] A. Foti, J. M. Lakas, "EHV switch tests and switching surges," *IEEE Trans. on Power Apparatus and Systems*, vol.83, pp. 266-271, Mar. 1964.

Chapter 7

High-velocity Opening Auxiliary Interrupter

A device with fast opening contacts called high-velocity auxiliary interrupter, attached to the main blades of the DS, has been increasingly employed since the 1950s. This device has been used mostly on vertical-break DS and mainly in North America. According to [1] a high-velocity interrupter using a mechanical spring can greatly reduce the arcing time by achieving a large air gap in a short time interval starting at the instant the auxiliary contacts release.

7.1 Operating principle

The working principle of a centre-break DS with high-velocity auxiliary interrupter is illustrated in Figure 7.1. In parallel to the main contact blades of a DS, there are two auxiliary steel springs, which are also referred to as "whips". They are short-circuited by the main contacts when the DS is in closed position. When the DS main contacts separate the current commutates from the main blades to the auxiliary contacts and the arc does not yet start. The whips bend (thereby tensioning the springs) during opening until the contact at the hook releases. At that moment, the whips act as released springs and the arc arises between the auxiliary contacts. The potential energy stored in the bended "spring" contacts, together with their low mass, cause a fast acceleration and provides for a rapid opening. Because of the high opening speed the arc extinguishes rapidly. The circuit is interrupted and a visible contact separation is provided [2].

The increased interruption capability by the high contact opening speed of quick-break devices can be explained qualitatively. Assuming the arc re-strikes at the moment of maximum RV and continues to burn for another half cycle ($T_{\frac{1}{2}c}$) till the next current zero crossing, the arc duration T_{arc} can be estimated roughly with:

$$T_{arc} = \frac{2.2 \times U_{line}}{\sqrt{3} v_{air} E} + T_{\frac{1}{2}c} \quad (7.1)$$

Here, v_{air} is the opening velocity of the air gap; E is the electric field strength the air gap can withstand; U_{line} is the phase to phase voltage. To allow for a 10% margin, the system voltage is taken to be at 1.1 p.u., so a RV peak value of 2.2 p.u. is adopted [3]. Equation (7.1) shows that with larger E and v_{air} , the arc duration becomes shorter. The breakdown field strength E is affected by many factors, such as thermal effects from the arc current, blade geometry, gap distance, and so forth.

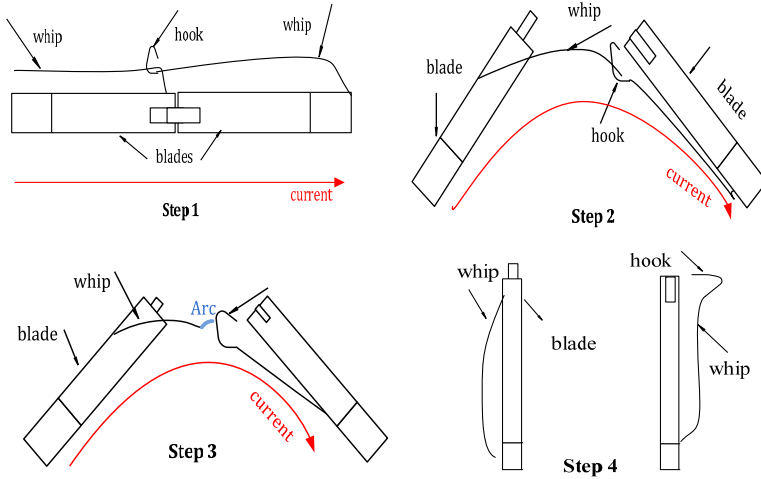


Figure 7.1. Operating principle of a centre-break DS with a high-velocity auxiliary interrupter.

With higher v_{air} the required air gap distance is reached faster and the arc duration is shorter.

There are only a few publications related to the innovation by the high-velocity auxiliary interrupter [2], [4]. Moreover, there is hardly any information on the interruption process itself and on potential causes of occasional failures since the limited available literature merely focused on test results rather than their explanations. In this chapter a series of experiments is described in order to understand the interruption phenomena. The reason for occasional interruption failure is discussed in terms of arc energy and re-strike voltage.

7.2 Experimental setup

The experimental setup, together with the measuring system is identical to the simplified circuit diagram depicted in Chapter 4. The setup and a close-up of the DS, with the attached auxiliary interrupter, are presented in Figure 7.2. The tested DS is a centre-break type with a rated voltage of 145 kV. The experiment is performed at 90 kV and a fixed value for C_s of 50 nF. The current I_d is controlled with the value of C_i and its range is chosen between 5.3 A and 27 A.

The opening velocity of the auxiliary contacts is derived from the momentary distance of the separating contacts as a function of time by analyzing the arc image frames. Figure 7.3 (left) shows the determination of the air gap length d by comparing distance D_1 between the contacts in each image with the known distance D_2 between the fixed sides of the DS (1650 mm: a centre-break DS from

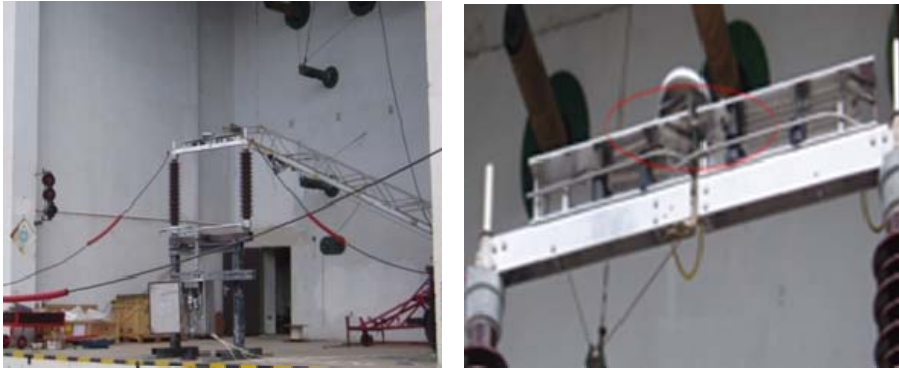


Figure 7.2. Laboratory setup (left) and DS (right) with high-velocity auxiliary device (its contacts are inside the drawn ellipse).

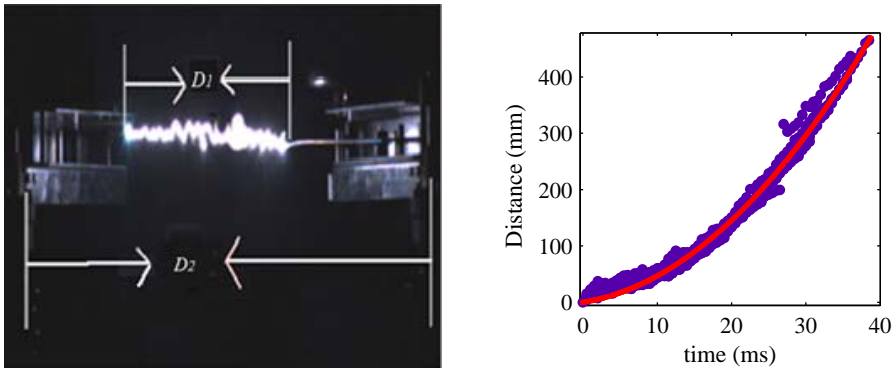


Figure 7.3. Distance between the auxiliary interrupter contacts; arc image example (left), and contact distance as a function of time (right, releases at $t = 0$).

HAPAM). Data obtained from all experiments are combined in Figure 7.3 (right) together with a quadratic regression according to $d = 1/2 at^2 + v_0t$, where a is the acceleration and v_0 is the initial velocity when the interrupter contacts release. The fit results in an acceleration of 260 m/s^2 and an initial velocity of 2 m/s . The average speed during the complete opening process is 11 m/s , more than ten times higher than the separation velocity of the DS main blades (refer Chapter 4, and [2]).

7.3 Overview of the experimental results

The experiments have been arranged such that there are at least three times repeated (closing and) opening operations performed for each current level. Only the opening operation is studied. The results are summarized in Table 7.1. Successful interruption means that the arc only burns between the auxiliary

Table 7.1. Summary of the experiments at 90 kV on interruption with rapid auxiliary contacts.

CO I_d (A)	1st	2nd	3rd	4th	5th	6th
5.3	✓	✓	✓	✓	-	-
8	✓	✓	✓	-	-	-
9.5	✓	✓	✓	-	-	-
10	✓	✗	✓	✓	✗	✓
12.5	✓	✗	✓	-	-	-
15	✓	✓	✓	-	-	-
17	✓	✓	✓	-	-	-
20	✓	✗	✓	-	-	-
23	✗	✓	✓	-	-	-
25	✓	✓	✗	-	-	-
27	✗	✓	✗	-	-	-

Note: 'CO' means close-open operation, ✓: successful interruption; ✗: failed interruption; -: no test.

contacts and extinguishes before they return to their original positions, parallel to the main blades. An interruption fails when the arc commutates from the auxiliary contacts to the main blades and the arc does not extinguish.

Table 7.1 shows that the interruption has a higher likelihood to be successful at lower current levels. Below 10 A the interruptions always succeeded. However, the failure probability does not relate directly to the current I_d . For example, interruption sometimes failed at 10 A and 12.5 A, but always succeeded at 15 A and 17 A. In addition to the tests indicated in Table 7.1, a series of 20 repeated CO tests was performed at 7 A with 100 kV supply voltage. All interruptions are successful, but for 10 A current only one out of six is successful at 100 kV. With increasing I_d , there is an overall tendency of current interruption to fail. The reasons for failure will be discussed in the following sections.

7.3.1 Electrical and optical observations

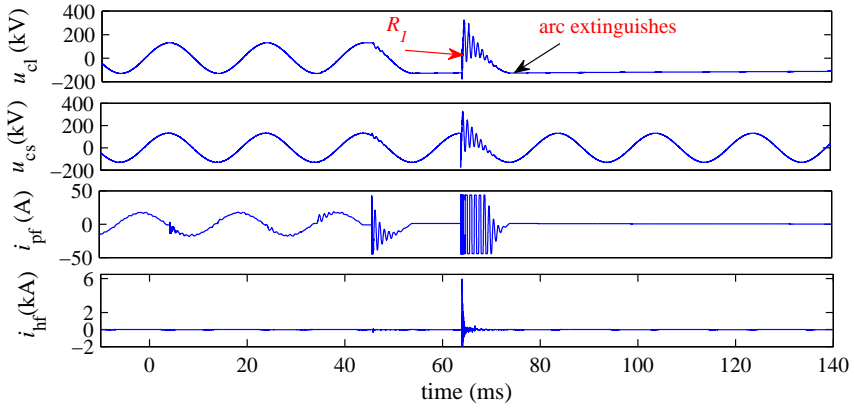
Figure 7.4a shows the wave shapes of the voltages u_{cs} , u_{cl} and the current i_d (with low and high-frequency bandwidth, denoted as i_{pf} and i_{hf} respectively) for a successful interruption at $I_d = 12.5$ A. The voltage u_d across the DS is shown in Figure 7.4b together with the current i_d in high vertical resolution. Time $t=0$ is the moment when the auxiliary contacts release and the arc ignites. The arc does extinct after 73 ms. It is observed that there are several re-strikes with the usual high-frequency oscillations during the arcing period. A few re-strikes with clear oscillations are indicated with '1', '2', '3' in Figure 7.4b. The maximum amplitude of the transient current reaches 5.9 kA as shown in Figure 7.4. The overvoltages across C_s , C_l and the DS are 2.6 p.u., 2.5 p.u. and 2.0 p.u., respectively.

The arc image is recorded with a speed of 1000 frames/s. A few frames from characteristic instances directly after the arc initiation are shown in Figure 7.5 with the time indication inside of the pictures. The images show that the arc mainly extends straight between the auxiliary contacts. The frame at 63 ms with the highest brightness corresponds to the most severe re-strike, indicated by R_1 in Figure 7.4a. The frame taken at $t = 73$ ms, about a half cycle later, shows the last frame before the arc extinguishes definitely and the frame taken at $t = 83$ ms, again a half cycle later, shows the afterglow at the arc remnants.

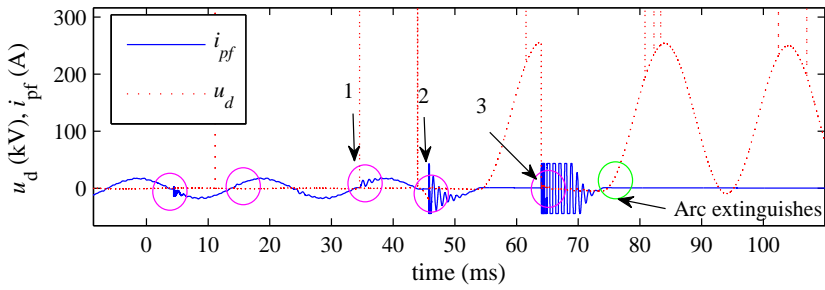
Figure 7.6a presents the wave shapes of the voltages u_{cs} , u_{cl} and the arc current (i_{pf} , i_{hf}) for a failed interruption at $I_d = 27$ A. Figure 7.6b zooms in on the wave shape of u_d together with the current i_{pf} . Preceding the severe re-strike at $t = 88$ ms, there are several re-strikes after the auxiliary contacts are released, indicated with the numbers '1', '2', '3'. The RV before the last re-strike, indicated by R_2 , is close to the maximum RV of 254 kV ($2E_m$) followed by a transient current peak at 6.5 kA. The overvoltages across C_s , C_l and the DS reach 2.6 p.u., 2.6 p.u., and 2.0 p.u., respectively. After that, the arc is re-established between the main blades (not between the auxiliary contacts) until it is finally interrupted by the master breaker after 600 ms. After the severe re-strike at R_2 there are no apparent re-strikes and no obvious arc current-less periods are observed; the arc burns continuously, implying thermal re-ignition after every current zero, with no measurable voltage needed to re-ignite the arc. The average arc voltage increases gradually with time (and arc length) up to a level of 10 kV.

Images taken at instances directly after the arc initiation are shown in Figure 7.7, where the arcing time is indicated. It is observed that the arc is first burning in a more or less straight appearance between the auxiliary contacts and then transfers suddenly to the main blades of DS after a severe re-strike (R_2) (brightest frame in Figure 7.7). At that instance the stiff, linear arc is converted to an erratic, curling arc moving upwards, driven by the upward motion of the heated air.

While burning between the auxiliary contacts, for both successful and failed interruptions, the arc tends to follow the shortest, straight path between the (fast moving) auxiliary contacts. It gets a complex erratic three-dimensional structure after commutating to the (slow moving) main blades of the DS in a failed interruption. Comparing successful and failed interruptions, the transient current and overvoltage values amplitudes hardly differ. The over current and overvoltage also show no significant differences between a DS equipped with fast opening contacts and a DS only having the main blades. The observed overvoltages reported in [4] reach 2.3 p.u., but this value was obtained at lower interrupted currents $I_d \leq 2.3$ A. That means the high-velocity interrupter does not contribute to a reduction of the overvoltage and transient current. However, since the duration of a successful interruption is an order of magnitude shorter even at significantly higher current, the number of re-strikes is much lower.



(a)

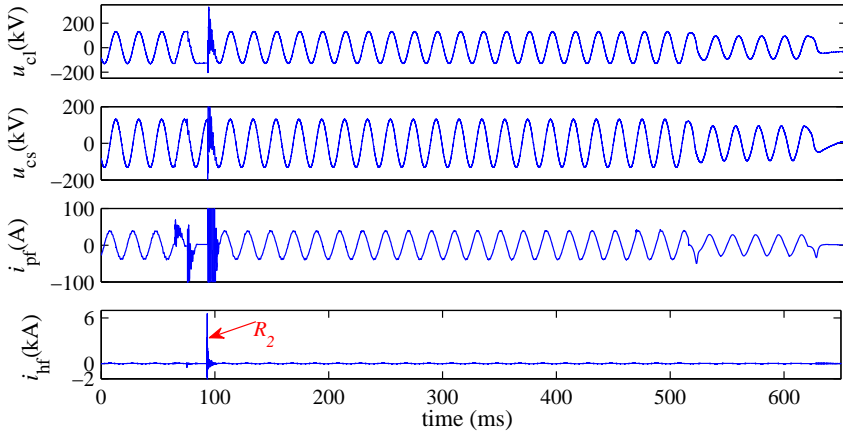


(b)

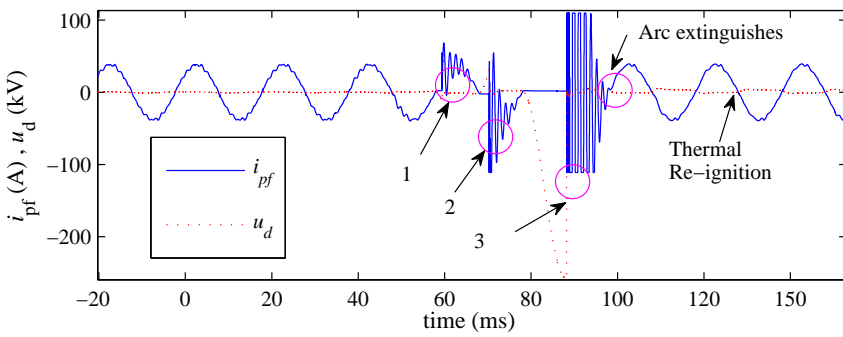
Figure 7.4. (a) Wave shapes of u_{cs} , u_{cl} , i_{pf} , i_{hf} and u_d for a successful interruption. R_1 indicates the most severe re-strike; (b) '1', '2', '3' indicate clearly observable re-strikes just before arc extinction. The circles in the lower figure indicate the re-ignitions/re-strikes.



Figure 7.5. Arc images at characteristic instances from a successful current interruption. The time of the Figure 7.5 corresponds to the time of Figure 7.4a.



(a)



(b)

Figure 7.6. (a) Wave shapes of u_{cs} , u_{cl} , i_{pf} , i_{hf} and u_d for a failed interruption. R_2 indicates the most severe re-strike; (b) '1', '2', '3' are the re-strikes before the arc transfers to the main contacts.

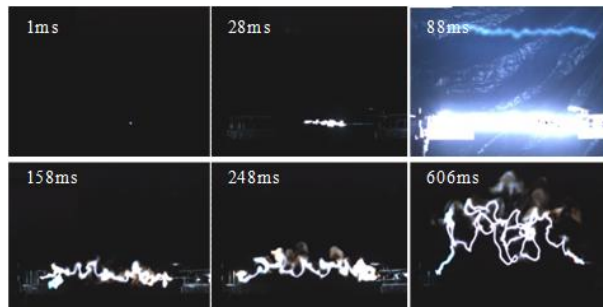


Figure 7.7. Arc images from a failed interruption. The time of the Figure 7.7 corresponds to the time of Figure 7.6a.

Two distinct types of arc continuation are distinguished. One is defined as dielectrically dominated re-strike, which means that the breakdown of the air gap occurs in (largely) unconditioned air (degree of ionization and thermal effects hardly affect the dielectric strength of the gap) at a high field stress. The second type is defined as thermally dominated re-ignition, which means that the breakdown occurs at a lowered voltage due to a relatively high thermal energy density in the arc region. Therefore, the dielectric re-strike voltage is much higher than the thermal re-ignition voltage for an identical air gap distance. The clearly visible re-strikes with numbers '2', '3' in Figure 7.4b and '1', '2', '3' in Figure 7.6b are dielectrically dominated. Thermally dominated re-ignition appears in the failed interruptions at higher current. Thermal re-ignition occurs in failed interruptions after the arc has transferred to the main blades. There are no further clear observable re-ignitions or re-strikes, while the arc continues burning between the slowly opening main blades (see Figure 7.6a). Although the arc current periodically crosses zero, the arc continues to exist, sustained by thermal energy. The arc always re-ignites immediately along its prior path just after the current zero crossing.

7.3.2 Arc duration

Figure 7.8 shows the arcing time versus the current I_d for all successful interruptions. There is no obvious correlation between arc duration and DS current I_d (up to the maximum tested current level $I_d = 27$ A). The arc duration ranges from 40 ms to 90 ms, comparable with similar experiments reported in [6] for $I_d = 7.3$ A, where the arc duration was in the range of 40 to 70 ms. The reason is related to the rapid cooling of the arc path thanks to the very fast elongation of the opening gap. Breakdown voltage reduction due to ionization is therefore believed to be of minor importance in the entire interruption process because of the rapid mixing of cool air with the pockets of ionized air.

7.4 Re-strike voltage

The analysis of re-strike voltage is based on the last three re-strikes before the final interruption, since they are clearly observable in all cases. For each single experiment, the values of the re-strike voltages U_r are plotted versus the current I_d in Figure 7.9. The filled bars belong to failed interruptions and the open bars correspond to successful interruptions. The numbers on the right side of Figure 7.9 indicate the experimental sequence. From the results summarized in Figure 7.9 the following observations are made:

- In all experiments clear (at least three) observable re-strikes occur, although they can differ greatly in magnitude of the re-strike voltage. The earlier re-strikes, indicated with '1', usually occur at low voltage because the air gap is still short. The re-strikes can be qualified as thermally influenced with reduced re-strike voltage due to hot air left by the arc. On the other hand, the

final breakdowns, indicated with '3', usually have high re-strike voltages (up to 2 p.u.), since a large air gap is reached and the re-strike is dielectrically dominated, which will be discussed later in this same section.

- Considering only successful interruptions (open bars in Figure 7.9), the probability of occurrence of re-strike voltage (U_r) higher than 1 p.u. decreases with increasing I_d . For $I_d < 10$ A, most of the three consecutive re-strikes have values above 1p.u. However, only a single high U_r value is observed (in each test series) for $I_d > 12$ A. This suggests that for higher interrupted currents, the thermal influence on the interruption process becomes more prevailing, causing a lower re-strike voltage. This phenomenon was also observed in previous experiments for a DS without auxiliary contacts during the entire interruption process [2], [5]. However, here it mainly occurs at the end phase of the interruption process. Apparently, despite the rapidly increasing air gap, the accumulated thermal

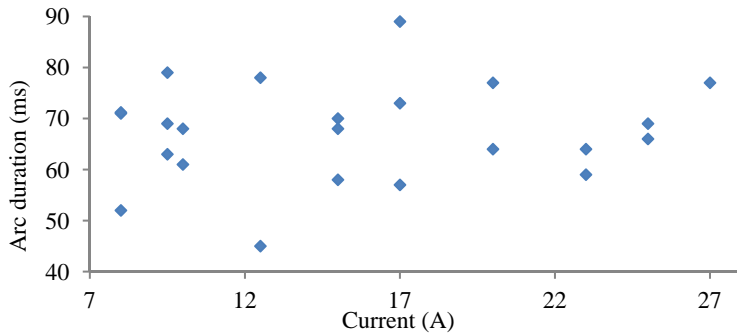


Figure 7.8. Arc duration versus the current I_d at 90 kV supply voltage.

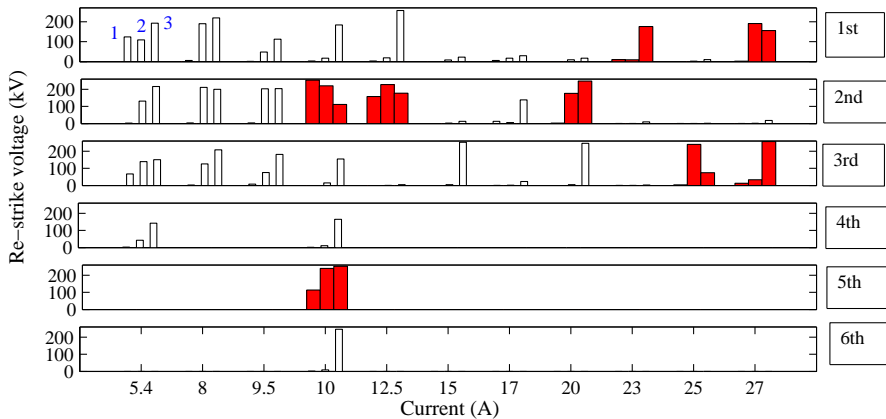


Figure 7.9. Re-strike voltage U_r versus the interrupted current I_d for successive tests (at least three for each current level).

energy from the previous arc re-strike still affects the next one, especially at relatively high I_d (≥ 10 A). This suggests that the interruption capability can be further improved with a higher opening velocity, since faster opening reduces the number of re-strikes further and helps cooling the arc remnants during recovery.

- Considering only failed interruptions (filled bars in Figure 7.9), the last three consecutive values of U_r always exceed 1 p.u. at $I_d = 10, 12.5$ A (even reaching 2 p.u., the maximum value according to [7]). However, only two re-strike voltage values exceed 1 p.u. for I_d larger than 17 A. This implies that at a lower I_d (< 12.5 A), higher (consecutive) re-strike voltages need to occur to cause a failed interruption. At larger I_d (> 20 A), only a single dielectrically dominated re-strike can already result in an interruption failure. Therefore, avoiding even a single dielectric re-strike at larger interrupted current is needed for the interruption to be successful. Most of the dielectric re-strikes occur at the end of the interruption process, so it is important to interrupt the circuit successfully already quickly after contact separation by realizing a long gap in a very short time.

The measured re-strike voltage versus the air gap length is plotted in Figure 7.10. The results are obtained from both the experimental series at 7 A, 100 kV with a total of 20 operations, and the experiments summarized in Table 7.1 with 9 A to 27 A at 90 kV utilizing the same DS with the same auxiliary device. Similar as in Chapter 5, the plotted reference breakdown voltage as a function of gap length is taken from the IEEE standard [8]. It shows that, although the breakdown voltage from the experimental results increases with increasing gap length, they are considerably lower than the reference values. Up to a distance of around 350 mm, the reference electric field strength (0.5 kV/mm) exceeds 10 times the experimentally obtained results (up to 0.05 kV/mm). For an air gap length above 550 mm, the reference electric field increases approximately linearly with increasing air gap length. However, the measured values tend to rise much more steeply and are much closer to the reference values. Probably, while the distance between the auxiliary contact tips becomes larger, the influence of the residual ionization is smaller, causing the re-strike voltage to be in the order of half of the reference values.

The values of the re-strike voltages suggest a break up into two regions: thermal re-ignition breakdown region and dielectric re-strike region, indicated in Figure 7.10 by a horizontal dashed line. In the dielectric re-strike region, the voltages are larger than roughly 0.5 p.u. (45-50 kV), and for the thermal breakdown region they are below this value.

Figure 7.11 shows the relation between re-strike/re-ignition voltage, current I_d , and air gap length. The dashed line separates the thermally and the dielectrically dominated regions.

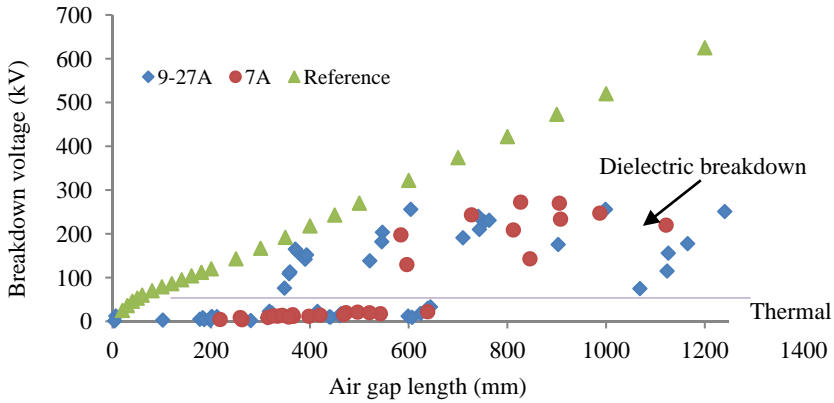


Figure 7.10. Breakdown voltage versus air gap length.

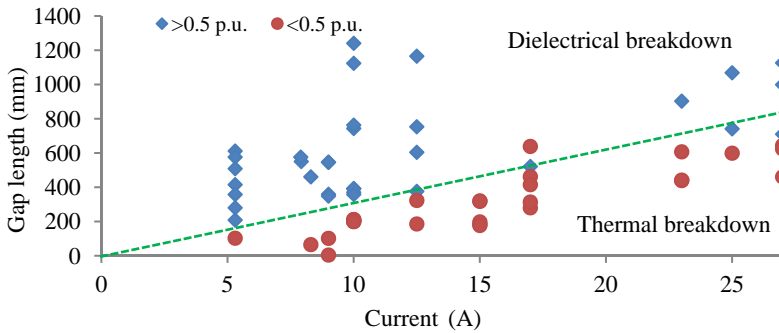


Figure 7.11. Relation between breakdown voltage and current I_a , air gap length.

Figure 7.11 suggests that the distinction between thermal and dielectric breakdown is related to the energy input per volume. Both higher current and smaller gap distance favour thermal breakdown.

In Figure 5.22 with 0.7 A, 130 kV and 0.4 A, 120 kV, 99% of the observed breakdown voltage levels are below 40 kV within 400 mm air gap length. In Figure 6.10 with experiments up to 6.3 A, the breakdown voltages are lower than 100 kV (1.1 p.u.) in the entire interruption process. In contrast to this situation with no fast opening device, most breakdown voltages values with the high-velocity interrupter are in the region of dielectric regions (see Figure 7.10), although the number of breakdowns is relatively small.

7.5 Energy input into the arc

The energy input into the arc is compared for failed and successful operations, and its dependency on re-strike voltage and currents is studied.

7.5.1 Energy upon re-strike for failed and successful interruptions

In order to compare the energy supplied to the arc upon re-strike in failed and successful interruptions, the arc energy associated with the last three consecutive re-strikes is calculated (see Figure 7.9). The method to calculate the arc energy has been described in Section 5.6. Taking $I_d = 12.5$ A as an example, the energy calculated for the three experiments is shown in Figure 7.12. The energies w_1 , w_2 , w_3 correspond to the 1st, 2nd, 3rd re-strike in each test. Among these three interruption experiments, the 1st and 3rd succeeded, but the 2nd one failed. The energy input into the arc at the 2nd experiment is much larger than for the other two; in the 2nd experiment the total energy input by the three re-strikes is almost 4 kJ compared with approximately 2 kJ and 40 J at the 1st and the 3rd experiment, respectively.

The total arc energy supplied into the arc resulting from the last three re-strikes versus the current I_d is depicted in Figure 7.13. The cumulated arc energy for the failed interruptions clearly exceeds the values for successful interruptions. The energy correlates only marginally with current level. This observation aligns with the observation in Section 7.3 on the weak relationship between current and likelihood of failure in case of auxiliary contacts providing interruption.

7.5.2 Energy versus re-strike voltage

The energy input to the arc is determined by the (transient) voltage and current, the latter depending on the current I_d (through the circuit parameters) and the re-strike voltage (refer to Section 5.6). The calculated energy is plotted versus re-strike voltage and current in Figure 7.14. The energy is calculated from the experimental series with I_d from 5.3 A to 27 A summarized in Table 7.1.

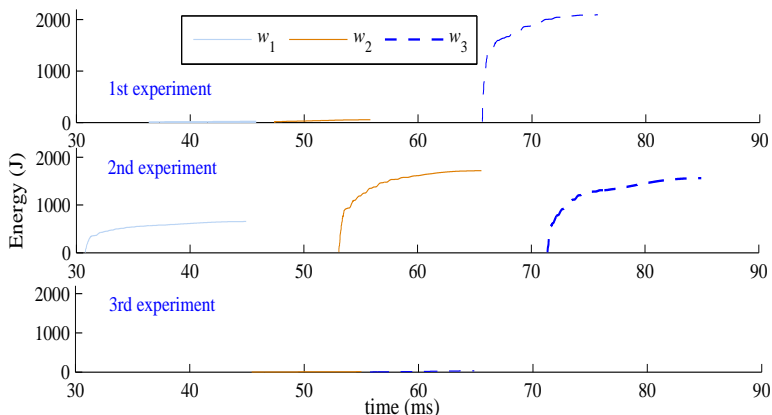


Figure 7.12. Temporal development of the energy w input into the arc upon re-strike for the three experiments at $I_d = 12.5$ A. The vertical scales are taken equal to indicate the wide range in energy supply by different re-strikes.

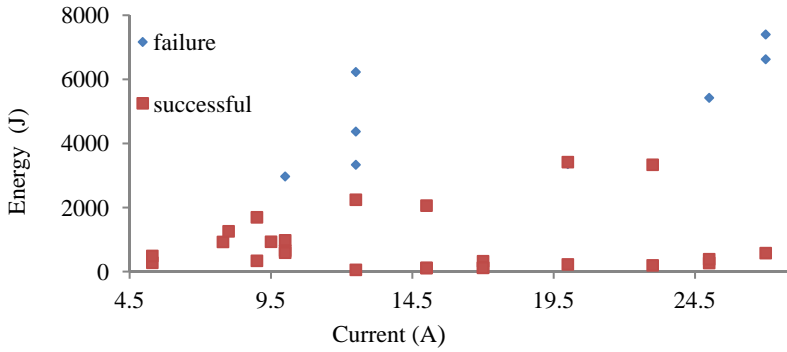


Figure 7.13. Arc energy by last three re-strikes versus current for failed- and successful interruptions.

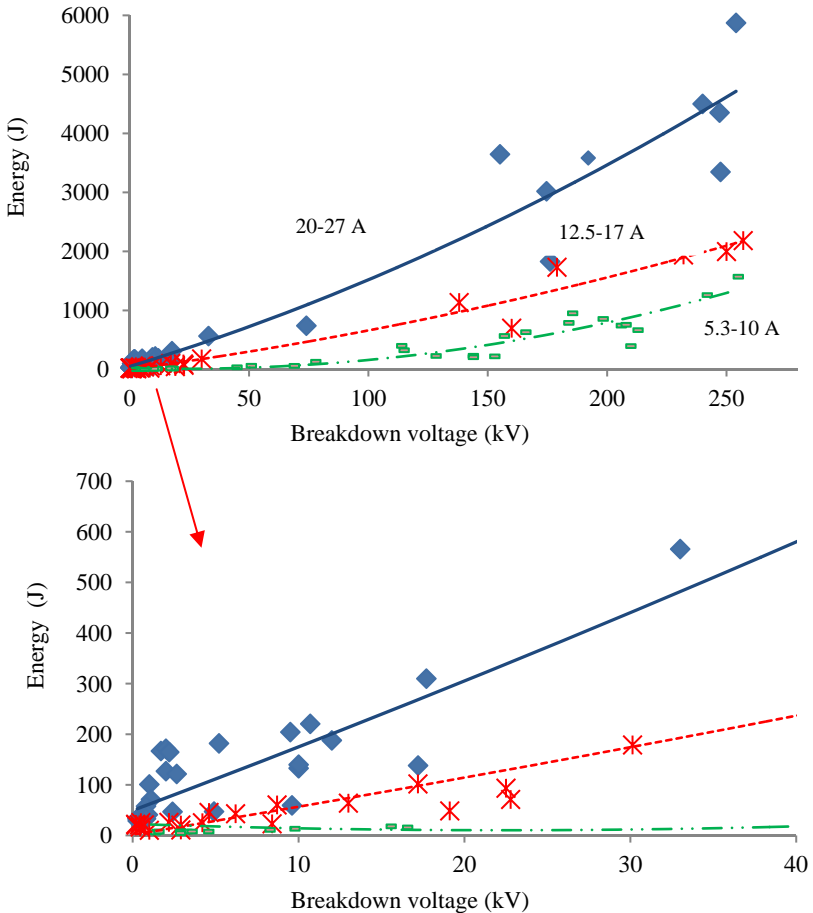


Figure 7.14. Arc energy versus re-strike voltage (U_r) with I_d as parameter and its expansion up to 40 kV.

The current values are grouped in three ranges. With identical re-strike voltage, however, it depends on the interrupted current. That may explain why the interruption has the tendency to be more likely to fail at higher I_d .

7.6 Conclusion and recommendation

Compared to the interruption without high-speed auxiliary contacts, the arc duration is significantly reduced and the number of re-strikes during the entire interruption is limited to only a few re-strikes or re-ignitions. The arc is burning between the auxiliary contacts, which exhibits a "stiff" arc for successful interruption. Application of fast opening contacts does not reduce the transient overvoltage and current amplitudes. However, the number of voltage transients is much smaller.

The energy, supplied to the arc upon re-strike, is closely related to re-strike voltage and current. Thus, both re-strike voltage and current determine the failure or success of interruption. This implies that reducing the re-strike voltage and avoiding the breakdown at larger air gap can enhance the interruption capability.

The experiments show that the DS with fast opening auxiliary contacts is very effective in increasing the DS current interruption capability. It can interrupt currents up to 7 A at 100 kV safely and 9 A at 90 kV in our experiments and the arcing time has dropped significantly to only a several tens of milliseconds instead of several seconds.

Residual ionization has a major effect, since it lowers the breakdown voltage needed to re-establish the arc and prolongs the arc duration. Fast opening of the gap mixes cold air with the arc residue and reduces the thermal energy density by diluting the ionized air. Also it cools down the air gap, which increases the gas molecule density and thereby reduces the mean free travelling path for free electrons.

It is recommended that the contact opening speed must be as fast as possible without any bouncing and that it is maintained as long as possible. This reduces accumulation of heat in the air gap. The length of the straight arc before the arc starts an upward motion depends only on the air gap between the tips of the auxiliary contacts. That means the higher the contact separation speed, the faster the arc is forced to elongate, and the faster the arc extinguishes, because recovery of the gap breakdown voltage towards the unconditioned "cold air" situation is fast.

The moment that the whip releases, however, should be chosen such that dielectric re-strike of the arc between the main blades is avoided. Before the auxiliary contacts release, the distance between main blades must meet the requirement in Table 5.2 in Chapter 5. Due to these various factors, it is

recommended to test the specific auxiliary interrupter before it is put into practice.

References

- [1] E. L. Luehring, J. P. Fitzgerald, "Switching the magnetizing current of large 345- kV transformers with double-Break air switches", *IEEE Trans. on Power Apparatus and Systems*, vol. pas-84, pp. 902-906, Oct. 1965.
- [2] Y. Chai, P. A. A. F. Wouters, S. Kuivenhoven, P. van der Wal, M. Vanis, R. P. P. Smeets, "Current Interruption Phenomena in HV DSs with High-Speed Opening Auxiliary Contacts", in *Proc. IEEE PES General Meeting Conf.*, 2010, pp.1-8.
- [3] Y. Chai, P. A. A. F. Wouters, R. T. W. J. van Hoppe, R. P. P. Smeets, D. F. Peelo, "Experiments on capacitive current interruption with air-break high voltage DSs", in *Proc. Asia-Pacific Power and Energy Engineering Conf.*, 2009, p. 1-6.
- [4] D. F. Peelo, "Current interruption using high voltage air-break DSs", Ph.D. dissertation, Dept. Electrical Engineering, Eindhoven Univ. of Technology, Eindhoven, 2004.
- [5] Y. Chai, P. A. A. F. Wouters, R. T. W. J. van Hoppe, R. P. P. Smeets, D. F. Peelo, "Capacitive current interruption with air-break high voltage DSs", *IEEE Trans. Power Delivery*, vol. 25, pp. 762-769, Apr. 2010.
- [6] KEMA test report 411-05, KEMA, Arnhem, the Netherlands, Dec. 2005.
- [7] L. van der Sluis, *Transients in Power Systems*, New York: Wiley, 2001, p. 49.
- [8] *IEEE Standard Techniques for High voltage Testing*, IEEE Standard 4-1995, Aug. 1995.

Chapter 8

Interruption with Inserted Resistors

In addition to the methods discussed in the previous chapters, the option of inserting a resistor will be discussed in this chapter. The resistive device is used to dissipate arc energy. The approach will be discussed based on its mechanism and applicability. Less attention is paid to practical realization and on the economics of the considered solutions.

Insertion of a resistive component into the circuit aims to reduce switching overvoltage, e.g. a closing resistor often applied in a circuit breaker. Several comparable approaches are reported in [1]-[9]. According to [1], an inserted resistor improves the damping of the oscillations in capacitive circuits. References [2]-[4] focus on the application of a resistor in series with DSs in GIS. References [5]-[8] point out that inserted resistors are able to reduce the duration of the DS switching arc. In [6], linear and nonlinear resistors are adopted to reduce switching surges. Both nonlinear and linear resistors are reported to have a similar beneficial effect on switching capacitive currents for gas-blast switches (which are not employed at the present time) although without any details provided.

In this section, the interruption performance of a DS having a resistor inserted in series with the main blades contacts is discussed first: 1) simulations show the potential effect on the interruption of parameters such as arc current, RV, high-frequency oscillation, and energy dissipation by the resistor; 2) laboratory experiments on the effect on overvoltage damping are presented. Next, interruption performance of a DS having a resistor inserted in parallel to the main blades contacts is discussed as well. Finally, some remarks are made on selection criteria for resistive elements.

8.1 Series resistor

Assuming that in the circuit of Figure 8.1, a resistor R is inserted in series with the DS just before the DS starts opening. The parameters taken for simulations are: source voltage $u_s = E_m \sin(\omega t + \theta)$ (where $E_m = \sqrt{2}/\sqrt{3}U_{line}$ with U_{line} system voltage in rms: ranging from 72.5 kV to 550 kV), $R_s = 50 \Omega$, $L_s = 480$ mH, $C_s = 10$ nF. The initial current to be interrupted in absence of R is taken 10 A. The effect on interrupted current, RV, transient and energy dissipation are studied.

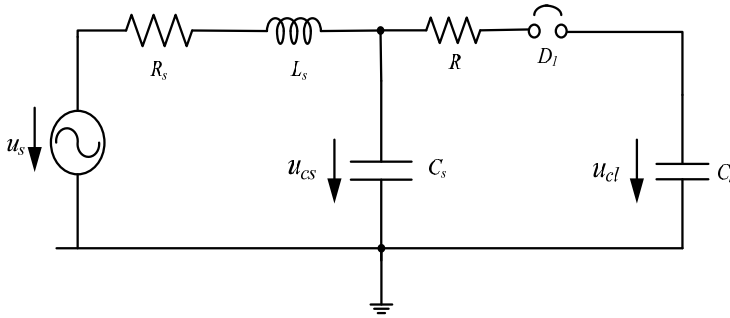


Figure 8.1. Equivalent circuit for a DS with a resistor inserted in series.

8.1.1 Effect on current I_d

The impedances of C_s and C_l applied in the test circuits are much larger than the source impedance of R_s and L_s . The DS current I_d reduces according to:

$$I_d \approx \frac{U_{line}/\sqrt{3}}{\sqrt{R^2 + 1/(\omega C_l)^2}} \quad (8.1)$$

Figure 8.2 shows this current as a function of R for different system voltage levels. The horizontal line indicates the value of the resistor to limit the current to 1 A.

Since the value for the capacitance at DS load side is in the range of tens to hundreds of nanofarad, the current I_d does not decrease significantly below a resistance value of 10 k Ω . On the other hand, not much is gained by using values exceeding 100 k Ω . These values determine the resistance range if a reduction of the power-frequency current during switching is aimed for. Obviously, the effect of inserting a resistor also depends on the system voltage level.

8.1.2 Effect on recovery voltage

For a source voltage given by $u_s = E_m \sin(\omega t + \theta)$, the RV and its maximum value RV_{\max} are given by (8.2) and (8.3), respectively.

$$RV = E_m \sin(\omega t + \theta) + E_m \frac{1}{\sqrt{1 + R^2 \omega^2 C_l^2}} \quad (8.2)$$

$$RV_{\max} = E_m + E_m \frac{1}{\sqrt{1 + R^2 \omega^2 C_l^2}} \quad (8.3)$$

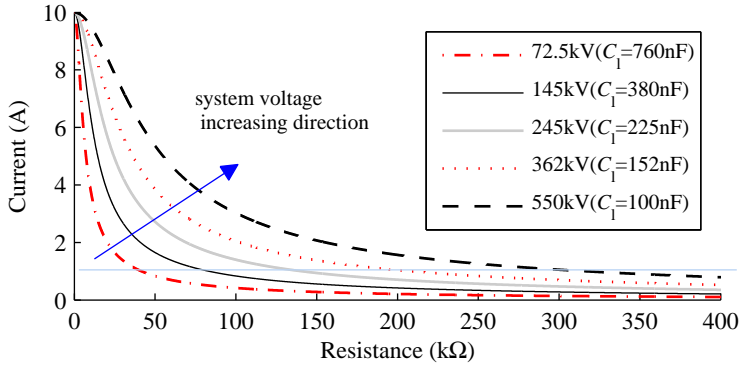


Figure 8.2. Interruption current I_d versus inserted resistance value.

With a fixed voltage E_m , the maximum RV_{max} across the DS decreases with increasing resistance because part of the voltage drops across R . Compared to the situation without inserted resistor, the RV_{max} is halved when $R\omega C_i \gg 1$, because no trapped charge is accumulated in C_i . In the simulation of Figure 8.3, five values of R (0.1 kΩ, 1 kΩ, 10 kΩ, 100 kΩ, 1000 kΩ) are considered, showing the wave shapes of RV at system voltages of 72.5 kV and 550 kV. The RV amplitude reduces with increasing R . At 72.5 kV the effect on RV becomes significant as from 10 kΩ and for 550 kV as from 100 kΩ. Therefore, the inserted resistor should have a value between a few tens of kilo-ohms and a few hundred of kilo-ohms, depending on the voltage level.

8.1.3 Effect on transient oscillation upon re-strikes

A resistor may have a significant effect on high and medium-frequency components. The effectiveness of its value depends on the inductance and capacitance in the high and/or medium-frequency loop. For the damping high-

frequency component, the resistance R should exceed $2\sqrt{\frac{L_H}{C_H}}$, where L_H and C_H are

the equivalent inductance and capacitance of the HF loop, indicated in Figure 3.1. Since L_H is in the order of tens of microhenry range and C_H is the series value of C_s and C_b , a value typically of a few hundred ohms is sufficient to avoid the high-frequency oscillation. To avoid medium-frequency oscillations, typical values as from a few kilo-ohms are needed since the source side inductance in the circuit usually is tens of milohenries and the equivalent capacitance is the parallel value of C_s and C_i .

Figure 8.4 shows simulations of oscillations for various values of the inserted resistor. The simulation parameters are: $E_m = 300\sqrt{2}$ kV, $I_d = 2$ A, $C_s = 18.4$ nF, $C_i = 36.8$ nF, $L_H = 20$ μH, $L_s = 13.8$ mH, $R_s = 1$ kΩ, the values of R are taken as 0.01kΩ,

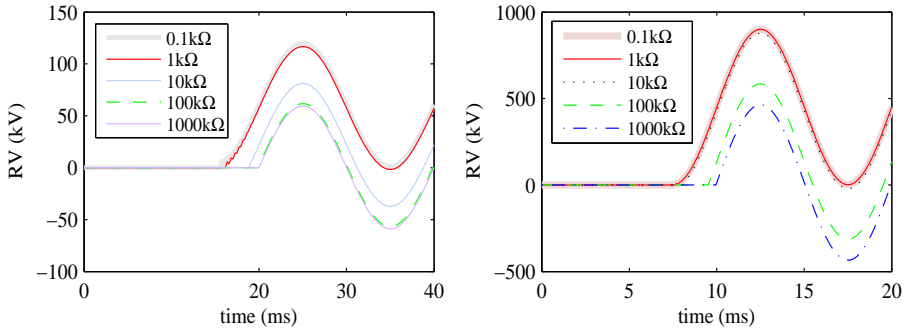


Figure 8.3. RV wave shape for various resistor values (left) at 72.5 kV and (right) at 550 kV.

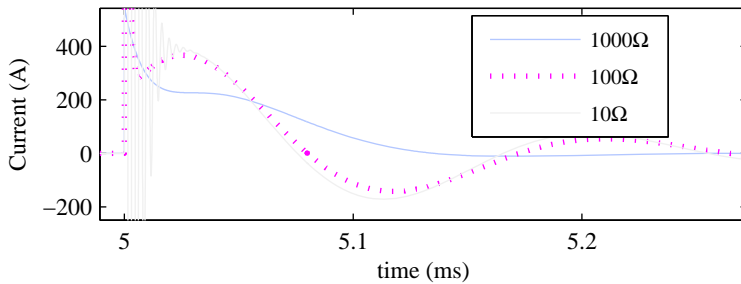


Figure 8.4. Wave shapes of i_a for different resistance values showing its effect on damping of the high and medium-frequency components.

0.1 kΩ, 1 kΩ. For $R = 0.01$ kΩ oscillations are observed in the medium and high-frequency range; at $R = 0.1$ kΩ the high-frequency component has disappeared, but the medium-frequency component still remains; at $R = 1$ kΩ all oscillations are damped.

8.1.4 Energy dissipation through resistor during interruption

The energy dissipated in the inserted resistor by the DS current is obtained from

$$w_R = \frac{\left(\frac{1}{\sqrt{3}}U_{line}\right)^2}{R^2 + (1/\omega C_l)^2} \cdot R \cdot t \tag{8.4}$$

The relationship between the dissipated energy (over 1 second) and the resistor value is shown in Figure 8.5. The energy dissipation, i.e. the energy the resistor should be capable to withstand, has a maximum when the impedance of C_l equals R , i.e. when $R = 1/(\omega C_l)$.

Taking an example, supposing the initial current is 10 A at 145 kV system voltage ($C_l = 380$ nF), R is 8.4 kΩ. With the value of $R = 8.4$ kΩ, the current reduces from

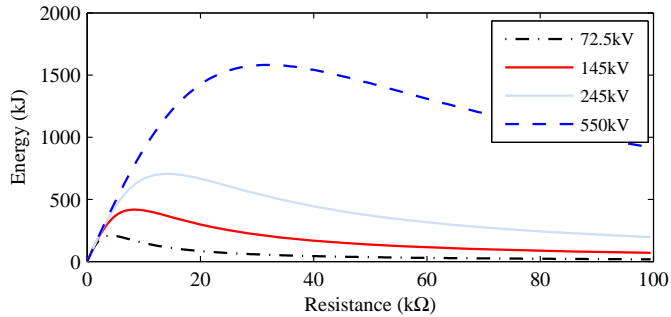


Figure 8.5. Energy dissipation versus inserted resistor value at C_l listed in the Figure 8.2.

10 A to 7 A, RV reduces from $2E_m$ to $(1+1/\sqrt{2})E_m$. Obviously it is not possible to interrupt successfully when $I_d = 7$ A at 145kV. Similar results may be obtained from other system voltage levels. Therefore, a resistor is recommend with a value larger than $1/(\omega C_l)$, but required dissipation energy lower the maximum value of energy in Figure 8.5. In such a case, the supply voltage will mainly drops across the resistor.

It should also be mentioned that insertion of a high-ohmic current limiting resistor just before DS opening creates difficulties that are, in fact, comparable to those associated with the opening of the DS itself. Therefore, how to insert such high resistor into the circuit is motivation for further work. On the other hand, resistor values suitable to damp the switching oscillations have much smaller value and limited dissipation. Insertion of low-ohmic resistors is therefore easier to achieve.

8.1.5 Experimental results

A series of experiments to verify the effect of an inserted series resistor on oscillation damping is carried out at the TU/e HV laboratory. The chosen parameters are: $E_m = 100\sqrt{2}$ kV, $C_s = 4$ nF, $C_l = 32$ nF, $I_d = 1$ A, $L_H = 17$ μ H. Figure 8.6 presents the wave shapes of the current i_d and their expansions around a single re-strike for $R = 0$ Ω , 200 Ω and 1 k Ω . The oscillations observed with inserted resistor disappear for 200 Ω , which can be expected since the corresponding quality factor of the HF circuit is 0.4. The amplitude of the transient currents is reduced drastically, up to a factor 10, for $R = 1$ k Ω .

The optical observations of the arc are presented in Figure 8.7, showing the cumulated arc brightness (see Chapter 5) with and without series resistor. "Stars" indicate the arc brightness with $R = 200$ Ω and "Dots" show the result with $R = 0$ Ω . Without damping resistor a higher brightness tends to occur, especially at the end of the interruption. The damping resistor prevents severe re-strikes, not only from the perspective of arc brightness, but also from the audible noise associated

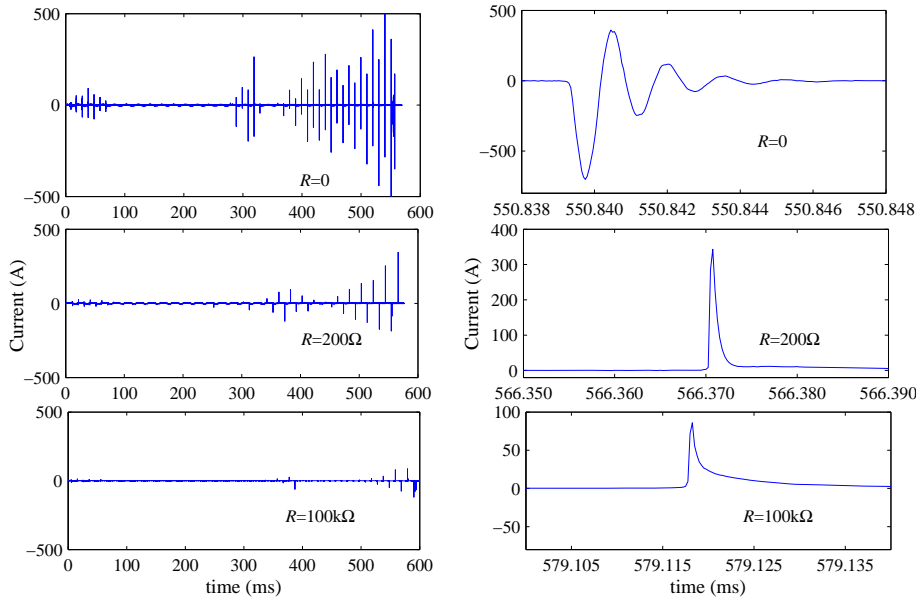


Figure 8.6. (left) Wave shapes of current i_a and (right) their final re-strikes zoomed in for different resistor values.

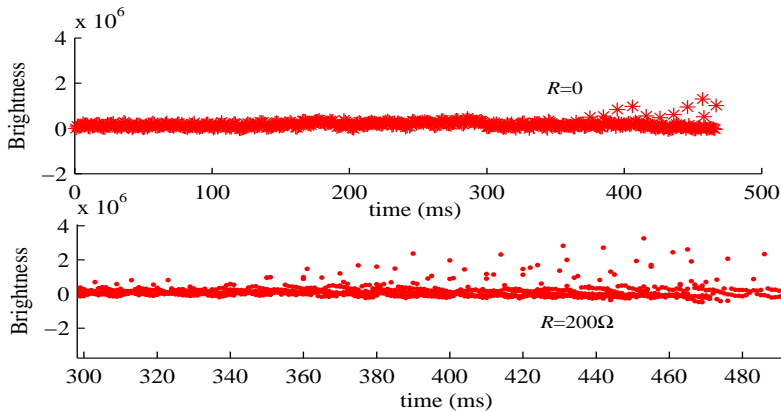


Figure 8.7 Arc brightness against time with and without series resistor.

with these re-strikes. However, the effect on arc duration could not be analyzed due to the gradual voltage decay.

8.2 Parallel resistor

Figure 8.8 shows the circuit with a resistor including an additional switch, indicated by D_1 , in parallel to the DS main blades. In closed position, the resistor

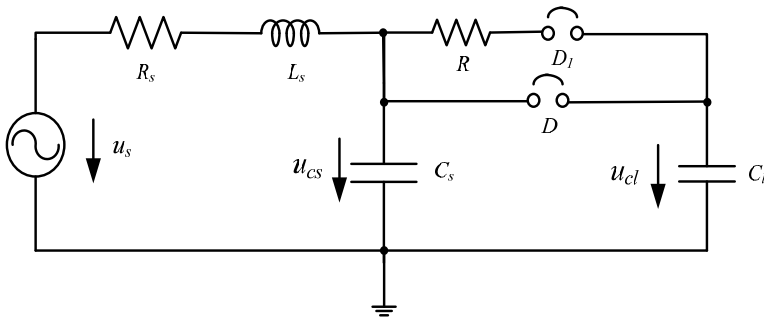


Figure 8.8. The circuit for a parallel inserted resistor.

branch is short-circuited by the main blades. When the DS starts to open, an arc arises between its contacts. However, once the arc extinguishes at the next current zero, the voltage across R that equals the voltage across the air gap, determines the possibility of subsequent re-strikes. In case the voltage across the resistor R is lower than the momentary breakdown voltage of the air gap, there will be no re-strikes between the contacts of the main blades. The current will flow through R and its series switch D_1 . The resistor has to be disconnected from the circuit after commutation, a situation similar to the circuit of Figure 8.1. Putting a resistor in parallel to the DS initially may be a practical way to insert a resistor, which after current commutation becomes a series component. For this series resistor, a relatively large value is needed for an appreciable reduction in interruption current. For preventing re-strikes between the main contacts, a lower value is required. These opposing requirements prevent this method to be effective for practical application.

It is also possible to put a nonlinear resistor, such as MOV, a component with a nonlinear current–voltage characteristic, in parallel to the disconnector. Obviously the current to be interrupted is similar to the situation without the nonlinear resistor. Figure 8.9 shows the simulation results of the voltages wave shapes of u_{cs} , u_{cl} and the voltage across the disconnector. The simulation parameters are $u_s = 120\sin(\omega t + \theta)$, $C_s = 10 \text{ nF}$, $C_l = 380 \text{ nF}$. The voltage at 1mA for the nonlinear resistor is 70kV. The results give the basic idea that the MOV could fix the voltage across the disconnector, which reduce the RV. As a consequence the chance to be restrike is less. However, further investigation is recommended as future work.

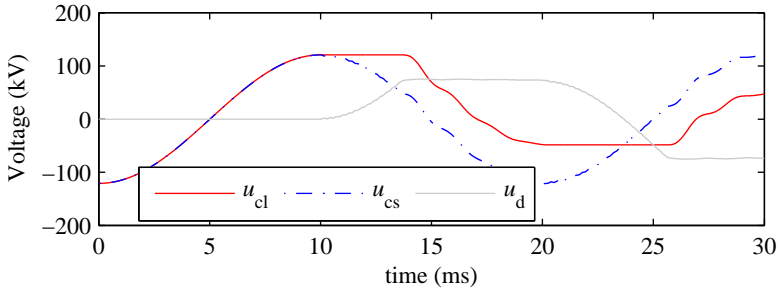


Figure 8.9. Simulated results of the wave shapes of u_{cs} , u_{cl} and their difference.

8.3 Discussion

An inserted resistor can theoretically facilitate current interruption by reducing the current and lowering the RV (relatively high values needed), or by suppressing transient currents during DS re-strike (lower values of resistances). The high value of the resistor needed for limiting the current and RV causes heat dissipation issues as well as commutation problems and therefore is in question for practical application. The dissipation requirements to suppress transients are much easier to comply with, but have not proven to be effective in shortening arc duration. An inserted resistor in parallel to the main contacts of the DS may improve the current interruption capability by limiting the RV across the DS, but only relatively low values can be applied for successful commutation. Nonlinear resistor is also a potential choice.

Resistor type and value strongly depend on the current the DS is intended to interrupt. A resistor with a value sufficient to reduce the interruption current and the RV should be capable to dissipate energy in the order of tens of kilojoule during the time the current flows through the resistive element. This is in the order of a few seconds. The allowed temperature rise during that time is an important design criterion, which determines the size and material of the resistor. Considering the high-frequency phenomenon, a resistor with low inductance is preferred which at the same time is capable to dissipate sufficient energy. Resistors should have high heat capacity and low thermal expansion coefficient to limit the thermal and mechanical stresses on the component. Ceramic resistors are a preferred option, but they are rather expensive.

References

- [1] R. C. Van Sickle, "Influence of resistance on switching transients", *AIEE Trans.*, vol. 58. pp. 397-404, Aug. 1939.
- [2] Y. Hiroshi, M. Tetsuo, "Disconnecting switch", U.S. Patent 5225642, Jul. 1993.
- [3] H. Yamamoto, J. Hirata, "Disconnecting switch", U.S. Patent 5091614, Feb. 1992.

- [4] Y. Yamagata, K. Tanaka, S. Nishiwaki, "suppression of VFT in 1100 kV GIS by adopting resistor-fitted disconnecter", *IEEE Trans. on Power Delivery*, vol. 11, pp.872-880, Apr. 1996.
- [5] M. S. Savic, "Suppression of the high-frequency disturbances in low-voltage circuits caused by disconnecter operation in high voltage open-air substations", *IEE Proceedings*, vol. 133, pp. 293-297, Jul. 1986.
- [6] A. Foti, J. M. Lakas, "EHV switch tests and switching surges," *IEEE Trans. on Power Apparatus and Systems*, vol. 83, pp. 266-271, Mar. 1964.
- [7] D. F. Peelo, "Current interruption using high voltage air-break disconnectors", Ph.D. dissertation, Dept. Electrical Engineering, Eindhoven Univ. of Technology, Eindhoven, 2004.
- [8] R. P. O'leary, R. H. Harner, "Evaluation of methods for controlling the overvoltages produced by the en-generation of a shunt capacitor bank", in *Proc. Large High Voltage Electric Systems international Conf.*, Aug. 1988.
- [9] J. Tao, S. Chen, C. Yang, "Simulation of disconnect switch operation of air insulated Substation", In *Proc. the XIV international Symposium on High Voltage Engineering*, Aug. 2005.

Chapter 9

Pre-breakdown Phenomena in Disconnecter Interruption

Small current interruption with DSs is a succession of arcing and breakdown (re-strike/re-ignition). The physics behind the interruption process occurring in switching with an air-break DS is strongly related to repetitive breakdowns, thus to the breakdown mechanisms in air gaps with presence of pockets of hot, ionized air. The AC recovery voltage during the blades opening results in a varying electric field over a gradually increasing gap length. This chapter gives a qualitative discussion on the breakdown processes, during the conditions present in the air gap. The basic breakdown mechanism, and its application to a non-uniform field, will be described first. Next, experimental evidence will be presented related to current interruption, mainly focusing on the pre-breakdown current. Finally, the implications for understanding of the current interruption behaviour with air-break DSs will be discussed.

9.1 Classical modelling of breakdown

At ambient temperature and pressure, air is an excellent insulator. It is commonly used in power system components such as overhead lines, switch yards, etc. Electric breakdown in air occurs when the dielectric strength of the air is exceeded; it is an evolution from non-conductive to conductive status.

Gas breakdown mechanisms have been investigated over more than a century and most phenomena can basically be understood in terms of the Townsend and streamer discharge model [1].

9.1.1 Townsend discharge

The current through the air gap between two parallel plate electrodes as a function of the applied DC voltage was investigated by Townsend in the early 20th century. It was found that initially the current increased proportional with the applied voltage and then remained approximately constant at a value i_0 . As the applied voltage was increased further, the current started increasing exponentially until complete breakdown of the gap. The general pattern of the current-voltage relationship is sketched in Figure 9.1 [1]. Up to the voltage u_1 the current increases, because of an increasing drift velocity of the charged particles inside the gap under the influence of the applied electric field, until a background current (saturation current) i_0 is reached. The rate of continuously created free electrons and ions by e.g. natural radioactive decay, cosmic and UV radiation

limits the current. The increase in the current past u_2 up to the breakdown at u_3 is ascribed to ionization of the insulating gas molecules by electron impact.

With an electric field applied across the gap, an initial free electron will accelerate and gain kinetic energy. Upon impact with a gas molecule, if the kinetic energy exceeds the ionization energy of the molecule, there is a probability that an electron is liberated. The energy gained between two successive collisions is proportional to the electric field and the travelled distance between consecutive collisions, which is denoted as the free travelling path. Its mean value is inversely proportional to the concentration of gas particles, i.e. the gas density. This free electron generating process is called "Electron Impact Ionization" [2]. Both electrons will accelerate and may gain sufficient energy for further ionizing collisions, resulting in an avalanche of free electrons. This process is quantified by the first Townsend coefficient, representing the average number of electrons produced by one electron per unit length in the direction of the electric field.

A complete breakdown requires secondary processes. In the Townsend discharge model, the positive ions left behind drift to the cathode. If sufficient energy is released upon their impact and neutralization at the cathode, there is a probability that a secondary electron is released from the cathode. Alternatively, photons emitted by neutral gas particles, which are excited upon the electron impact, can account as well for secondary electrons. The second Townsend ionization coefficient gives the probability that an ion or photon results in a secondary electron. The Townsend criterion for complete gap breakdown states that, if on average per initial free electron more than one secondary electron is liberated, the gap ionization grows to a full breakdown.

Paschen studied experimentally the breakdown voltage of a gas in a homogeneous field as a function of gas pressure and gap spacing in 1889. His findings are nowadays referred to as the well-known Paschen law, stating that the breakdown voltage U_b is a function of the product gas pressure p and gap length d : $U_b = f(pd)$. Figure 9.2 depicts the Paschen curve for air at a temperature of 20 °C. The minimum of this curve can be understood in terms of the Townsend model. At the left side of the minimum either the pressure or the gap length has become so low, that few ionizing collisions occur during the crossing of the gap. The electron avalanche is too small to have sufficient probability of creating secondary electrons to continue the breakdown process. At the right side, the energy gained by free electrons is low, either due to a reduced mean free travelling path at higher pressure (i.e. higher density) or low electric field because of large gap length. Thus, also the electron impact ionization is reduced.

The pressure of an ideal gas in equilibrium is described by its state equation $p = N T k_B$, (p : gas pressure, N : gas density, k_B : Boltzmann constant; T : absolute temperature). This relation shows that pressure is affected by the density or temperature of the gas. Therefore sometimes the Paschen law is presented such

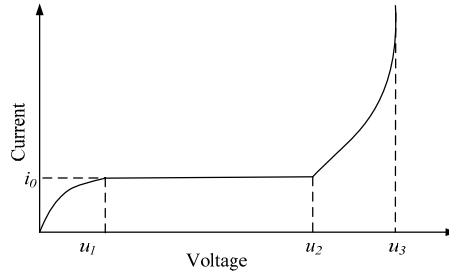


Figure 9.1. Relationship between the current and the voltage in pre-breakdown region.

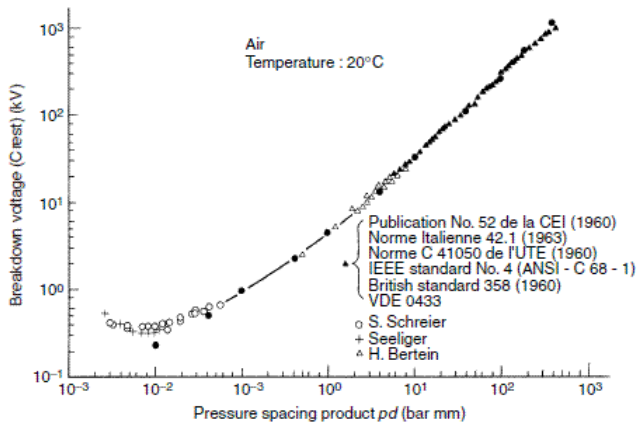


Figure 9.2. Paschen curve for air in log-log scale, copied from [2].

that the breakdown voltage is a function of the product of gas density and gap length.

Although the Paschen law was derived from experiments on uniform electric field, it does not really apply for the non-uniform field between the DS main blades with concentrated field at the tips. However, the impact ionization by accelerated free electrons influenced by the electric field strength is also here considered as a main mechanism.

Deviations from predictions based on the Townsend model were observed for large air gaps with inhomogeneous fields or at high pressure. It also fails to explain the electron transit time in practice often being shorter than can be expected from the avalanche model.

9.1.2 Streamer breakdown

The streamer breakdown mechanism is an alternative approach, also based on primary electron avalanches. It was proposed by Raether, Meek, and Loeb, based

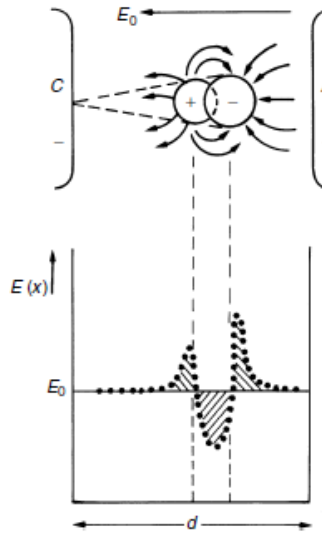


Figure 9.3. Field distortion in a gap caused by space charge of an electron avalanche (copied from [5]), E_0 is the applied electric field, $E(x)$ is the electric field after distortion.

on numerous experiments [3], [4]. In the streamer model the effect of the space charge field by the avalanche electrons and photon ionization in the gas volume is taken into account. As the electrons move to the anode, the positive ions are left behind in a relatively slow-moving tail. The avalanche has accumulated, especially in the head of the avalanche, negative space charge. The tail contains positive ions. These space charges distort the applied electric field distribution, i.e. enhancing the electric field in front of the head and behind the tail of the avalanche; in between the electric field is reduced as shown in Figure 9.3. Electrons will gain more energy because of the enhanced field, causing increased ionization and also more energetic (UV) electrons from highly excited gas atoms. These UV-photons start new avalanches further on by photo-ionization. This significantly accelerates the breakdown development. A streamer is a thin channel formed from the primary avalanche. When streamers bridge the gap with plasma, the breakdown occurs. The streamer mechanism is specifically important in an inhomogeneous field, where in regions with field enhancement also relative large local ionization occurs, causing high space charge fields.

In a non-uniform gap, there is a divergent field. The electric stress near one or both electrodes with high curvature is enhanced with respect to the remainder of the gap [5]. Consequently the ionization is enhanced. Partial ionization starts in the gas with highest electric field intensity, but does not directly cause complete breakdown. At higher applied voltage the field strength over the complete gap reach a value sufficient to initiate complete breakdown.

9.2 Pre-breakdown current in disconnecter interruption

The experimental data presented in Chapter 5 showed that each interruption involves numerous repetitive arc extinctions and re-ignitions. For the study of the pre-breakdown process of current interruption with a DS, the focus is on the arc current after arc extinction at the power-frequency current zero until the succeeding breakdown.

Typical wave shapes of the current i_d through the DS at I_d of 2.6 A and its expansions at different stages of the interruption process are plotted in Figures 9.4 and 9.5, respectively. Four examples, each indicated by a circle, are extracted from the full current waveform shown in Figure 9.5. Duration Δt_1 denotes the period after current zero crossing, the measured current remains zero (below the measurement threshold of 0.5 mA). After this period, a small "step" in the current is observed (see Figures 9.5b and 9.5c). The period Δt_2 denotes the duration between the moment of starting the "step" until the moment of complete breakdown. Regarding the intervals Δt_1 and Δt_2 the following observations are made:

- The current zero duration Δt_1 decreases gradually with time, i.e. with increasing gap distance (compare Figures 9.5a, b, c and d). In the final stage of the interruption, the current zero period is even hardly discernible (Figure 9.5d).
- At the beginning of the interruption, after Δt_1 the breakdown occurs without an observable pre-breakdown current (Figure 9.5a). In the later stage of the interruption process, there is a "step" in the current, followed by a gradually rising current (Figure 9.5b, c). In the end stage of the interruption, the "step" is also not clearly visible, but instead directly after interruption a pre-breakdown current arises (Figure 9.5d). As the RV increases further, the gap breaks down completely.
- The period Δt_2 changes also with increasing air gap length. In early stage of interruption, Δt_2 is not noticeable; in the end stage, it nearly occupies the entire period between current zero crossing and breakdown.

Many factors are involved determining the development of the entire breakdown, such as the electric field, residual charges and temperature inside the gap (degree of ionization of the air). The electric field in between the main blades, resembling a rod-rod electrode configuration, is inhomogeneous. Further fragments of residual plasma are left in the hot air gap from previous arcing. This is exemplified in Figure 5.18 showing light emission from hot spots in the arc path after current interruption.

The observed "steps" in the current occurring after a few cycles (about 10 cycles at I_d of 2.6 A) after the operation starts can be understood in terms of the electric and thermodynamic condition of the arc path. Once the current crosses zero, the

residual plasma gradually vanishes as the gap is cooling down. At the same time the RV starts rising. The conductivity of the plasma of the previous arc path is too weak for a detectable current, resulting in a measured current zero stage (Δt_1). With increasing RV, the electric fields at the blade contacts (the arc roots) are enhanced by the non-uniform field. Near the DS blades roots the situation is most favourable to initiate new ionization, apparently via a sudden onset of a current resulting in a step-wise increase. The current path will follow the previous arc route because of the still present charge carriers and the enhanced temperature. The electric field increases with the further RV. In addition, the dissipated energy by the current heats the channel. This leads to re-ionization until complete breakdown occurs after time Δt_2 .

Δt_1 decreases with the gap length means the "step" is initiated earlier with the same RV even with longer arc route. The reason can highly probably be attributed to the remaining partly ionized hot air. There is more accumulative residual charge (ionized hot air) after longer time because the hot air needs long duration for diffusion. In Figure 9.6 the duration Δt_2 is plotted versus the arcing time during which the interruption develops. Measurements at three interruption current levels (I_d of 1.4 A, 2.6 A, 5 A) are compared. The time Δt_2 is lower for larger current I_d and smaller arcing time (smaller gap length). It may be explained:

- Δt_2 is larger for larger gap length. Longer arc length at larger gap length, resulting in lower air density. In such a case, it required longer duration to accomplish full breakdown.
- With higher current, the path left by a previous arc has a higher temperature. As the gas temperature is inversely proportional to the gas density at constant pressure (assuming the ideal gas law still applies), higher temperature means lower density, resulting in longer free travelling path for electrons, stronger ionization, and consequently lower breakdown voltage. Lower breakdown voltages correspond to shorter time Δt_2 for the RV to reach the breakdown value.

The influence of temperature on the breakdown voltage can roughly be estimated using the factor $293/T(K)$ correcting the density for temperature [6]. From Figure 5.23 it was concluded that the actual observed breakdown voltage was about a factor 6 lower than expected for unconditioned air at the same gap distance according to IEEE Standard. If this difference could be exclusively ascribed to temperature a value of 1500°C is obtained. This temperature is not arc temperature, but the channel temperature at the breakdown.

9.3 Discussion

The pre-breakdown process of the small current interruption with a DS is qualitatively analyzed along the classical electron avalanche breakdown theory. A pre-breakdown current of a few amperes can be observed with duration of several

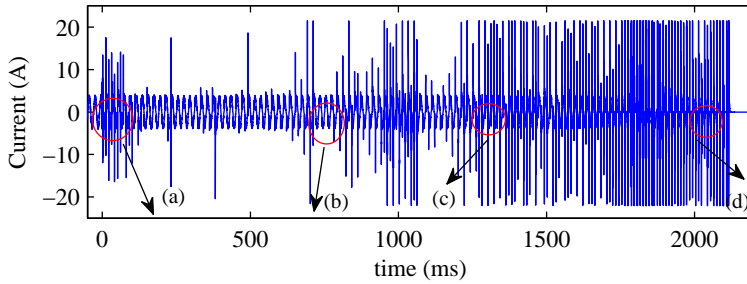


Figure 9.4. Wave shape of the current through the DS at I_d of 2.6 A; circles indicate the instances where expansions are taken for Figure 9.5.

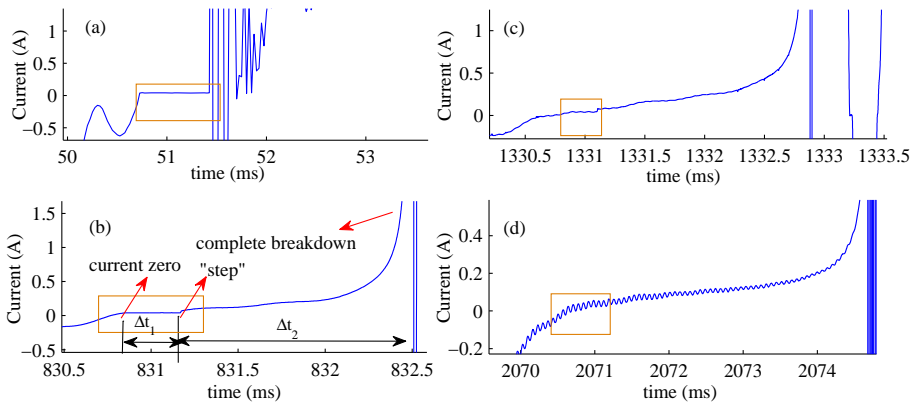


Figure 9.5. Pre-breakdown current at different moments of the current interruption process through the DS at I_d of 2.6 A, see Figure 9.4.

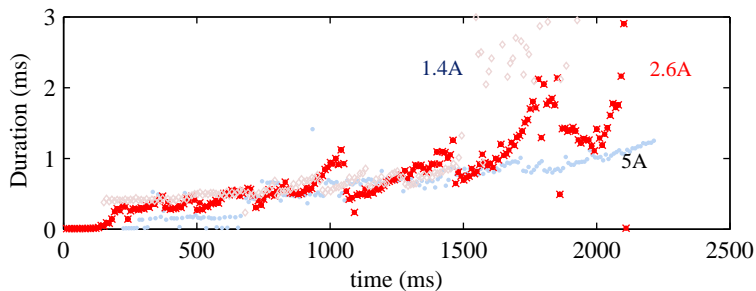


Figure 9.6. Breakdown development duration Δt_2 against time for I_d of 1.4 A, 2.6 A and 5 A.

hundreds of microseconds prior to breakdown. This current is initiated by the E-field at the arc root, but drawn through the still weakly conducting former arc channel, and supplies energy to it. If this supply of energy exceeds the loss of energy mainly by natural (or forced) convection cooling, the former arc channel

will become highly conductive again and breakdown follows. Practical examples of forced convection are air flow and whip, dragging the arc fast into cool ambient air. For instance, there is no “steps” phenomenon observed for the entire interruption with air flow because residual charges are forced to leave the air gap by the air flow. Instead the complete breakdown occurs suddenly (see Figure 9.4a). The pre-breakdown discharge develops faster with increasing current I_d (or shorter distance) into breakdown. This is related to higher temperature in the arc path giving rise to a larger mean free travelling path for liberated electrons and the higher residual ionization. The pre-conditioned path from an earlier breakdown is therefore a preferred path for subsequent re-strikes. This model is consistent with the observed beneficial effect of an applied air flow through cooling the breakdown channel and removing ionized gas remnants.

References

- [1] J. S. Townsend, *Electricity in gases*, Oxford University Press, p.2, 1915.
- [2] E. Kuffel, W. S. Zaengl, J. Kuffel, *High Voltage Engineering Fundamentals*, Second Edition, Newnes, Aug. 2000.
- [3] H. Raether, *Electron avalanches and breakdown in gases*, S.I.: Butterworth, 1964.
- [4] J. M. Meek, J. D. Craggs, *Electrical Breakdown of Gases*, John Wiley & Sons, Chichester, 1978.
- [5] G. J. J. Winands, *Efficient streamer plasma generation*, Dissertation, Eindhoven Univ. of Technology, Eindhoven, 2007.
- [6] C. L. Wadhwa, *High Voltage Engineering*, 2nd edition, New age international limited publisher, 2007.

Chapter 10

Conclusions and Recommendations for Future Research

Limited literature sources recognize that disconnector requirements should include the capability of interrupting capacitive currents up to a certain current level. For safety and economical reasons, it is desirable to find approaches to improve the current interrupting capability. For this, it is indispensable to understand the related interruption phenomena and its influencing factors profoundly. This is the main objective of this thesis.

Capacitive current interruption by a disconnector involves the interaction between the arc and the circuit. The transient phenomena caused by this interaction, cover different frequency ranges. Transient voltages and currents, that may have an impact on neighbouring equipment, arise during the interruption.

A variety of experimental setups were designed and installed in this study. They include the test disconnector, high-resolution and wide-band optical and electrical measurement and data acquisition. The high voltage sources used a resonant generator for detailed observation of the arcing process as well as high voltage power transformers in two different power laboratories to make quantitative analysis during the entire interruption process. Aided by computer modelling, experimental data obtained from three different test-sites have been analysed in order to better understand the interruption in terms of repetitive arcing and breakdown phenomena. This understanding can be exploited to improve the interruption capability of a disconnector with the assistance from auxiliary means such as air flow, high-speed contact separation and damping resistors.

The main conclusions of this thesis and recommendations for future work will be addressed in this chapter.

10.1 Conclusions

Recorded electrical and optical signals show that in the few seconds of capacitive current interruption, the arc has frequent extinctions and re-ignitions/re-strikes. It extinguishes temporarily at the (power-frequency) current zero crossing, but re-ignites due to the recovery voltage impressed by the circuit. This process comes to a halt when the dielectric stress of the air gap exceeds the recovery voltage value. During this process, the breakdown voltage of the air gap along the arc path is significantly reduced due to the thermal influences caused by the arc,

and is lower than the direct shortest distance connection between the disconnecter blades. For slow opening main blades (as usual in a standard disconnecter), it may take seconds to reach sufficient gap distance to withstand the highest recovery voltage. The associated transient overvoltage has reached a value up to 2.5 p.u. in the experiments, and could theoretically reach 3 p.u., with the rate of rise in the order of tenths per unit per microsecond. Current transients with peak values up to a few kiloamperes were observed, rising with a few kiloamperes per microsecond.

The observed arc behaviour, transients, re-strike voltage and so forth, are highly affected by the circuit parameters. These parameters involve the capacitances C_s and C_l at both sides of the disconnecter, stray and short-circuit inductance, and the power supply voltage. These factors all affect the current to be interrupted, the re-strike voltage with associated transients as well as the energy supplied into the arc, which ultimately heats the air in the vicinity of the arc.

The source and load side capacitances are the main circuit factors that influence the interruption performance. With a ratio C_s/C_l , smaller than 0.1 in the presented experiments, the arc duration, overvoltage in the circuit, contact gap length and blade angle at final interruption, and energy input into the arc are increasing. Slow dielectrically recovery of the (former) arc trajectory against circuit impressed recovery voltage is ultimately the cause for long arc duration.

The current to be interrupted is another governing factor. With higher current, the arc duration, the magnitude of overvoltage and the energy dissipation upon re-strike increase, resulting in larger blade contact gap spacing when final interruption is achieved. With increasing current, the gap recovery becomes slower and the re-strike voltage decreases, until a current level is reached beyond which interruption is no longer possible and the arc re-ignites purely thermally. In that mode, the arc will generally no longer extinguish, irrespective of the gap space. It has been observed that at increasing current the overall arc brightness increases, the decay of arc remnant light emission is slower, and the post arc energy input during recovery is larger.

With decreasing re-strike voltage, the energy input into the arc on re-strike reduces. The arc energy, overvoltages and transient current in the circuit reach their maximum (during the interruption process) just before the arc extinguishes completely. Therefore interrupting the circuit successfully at an early stage at a relatively short gap implies a lower re-strike voltage, lower transients, and lower energy input into the arc.

It is observed that the re-ignited arc follows the "traces" left by the just extinguished arc. The arc prefers the dielectrically weakest path for which the breakdown voltage is lowest. The ionization left behind from the arc in the previous power-frequency cycle makes the subsequent re-ignition or re-strike to

occur at a reduced voltage, compared to the actual cold-air contact distance. A pre-breakdown current, drawn through the still weakly conducting former arc channel, is supplied by the rising recovery voltage. It supplies energy to the channel, creating the conditions for pre-breakdown until complete breakdown. Upon re-strike, there is energy input from the transient components heating the arc further. By this the subsequent level of voltage at which re-strike/re-ignition will occur is affected.

With the purpose of removing the residual charges from previous arc path, thus avoiding space charge to accumulate at all, two approaches are investigated in detail experimentally: removal of residual plasma by air flow and drawing the residual plasma into cooler air flow by a high-speed auxiliary interrupter. Two interruption modes are observed, indicated as a dielectric and a thermal mode.

The dielectric mode mainly occurs in the case with a high air flow rate (directed to the arc foot points, in the tests up to 315 litre/minute) and with low arc current (roughly below 1 A). In this mode, thermal effects play a very limited role. During the dielectric mode, the arc current may be chopped at any phase angle of the power-frequency cycle. Multiple breakdown events within a half power-frequency cycle are common and the number of the breakdown events per unit time is significantly higher than in the thermal mode interruption. At the same level of the interrupted current, the breakdown voltage (mainly dominated by the air gap length), is higher than for the thermal interruption mode. Both higher breakdown repetition frequency and higher value of the breakdown voltage makes this mode potentially more hazardous for neighbouring equipment due to the frequent transients. The interrupted current derivative (di/dt) at current zero is much higher (about a factor 20) than in the thermal mode. This implies that the arc current can also interrupt at current zero by high-frequency oscillations, caused by the transients in the circuit.

The thermal mode occurs at higher interrupted current (>1.4 A in the present experiments) without air flow. During thermal interruption, the arc in principle extinguishes at every power-frequency current zero. The interrupted current derivative increases roughly linear with current. Due to the residual ionization from previous arcs, the breakdown voltage is much lower ("thermally reduced") than in the dielectric interruption mode. In principle, the voltage transients are less hazardous to nearby equipment. However, eventually the overvoltage reaches a very high level, but at a much larger gap distance than in the dielectric mode. Re-strikes occur less frequently (one per power frequency loop).

Figure 10.1 depicts qualitatively the frequency of re-strikes versus the duration of the interruption process for the standard centre-break disconnecter with and without air flow. The continuous thin lines indicate the successful interruptions without air flow. The continuous bold line indicates the case of a failed interruption in which the arc continues "forever" in the thermal mode. The dashed

lines indicate interruptions with air flow assistance. At the earliest stage of the interruption, with and without air flow, the frequency of interruption is higher than during the remainder of the interruption process. With increasing arcing time, the frequency of re-strike decreases until 100 Hz, i.e. once per half 50 Hz power-frequency cycle. The decrease is faster with higher current. With air flow and also at low current, the frequency is always higher than 100 Hz until final interruption. The air flow results in the overall effect of increasing the re-strike frequency at the same current. Three regions can be defined:

- A region where the frequency clearly exceeds 100 Hz. Re-strikes are less influenced by the residual plasma. The re-strike voltage is mainly determined by the gap length (left region in Figure 10.1).
- A region where the frequency is 100 Hz. The re-strikes are increasingly influenced by the residual plasma (depending on the current level). High re-strike voltage is still required in order to breakdown the air gap, but the current plays an important role in the recovery (centre region in Figure 10.1).
- A region where no re-strikes occur. The breakdown is thermally dominated completely. Re-strike voltage is not necessary in maintaining of arcing. This situation appears when the interruption fails (right region in Figure 10.1).

Application of high-speed auxiliary contacts reduces the arc duration significantly and the number of re-strikes during the entire interruption is limited to only a few. The arc is burning between the auxiliary contacts, bridging the gap in a straight manner ("stiff arc"). This is different from interruption with a disconnecter with slow moving main contacts, where thermally dominated breakdown occurs during a major period of the entire process with an "erratic" arc shape containing significant upward motion and curling. Application of fast opening contacts does not reduce the transient overvoltage and current amplitudes. However, the number of voltage transients is much smaller, because of the very short arc duration.

It is recommended that the contact opening speed is as fast as possible without any bouncing. With higher contact separation speed, the arc is forced to elongate, cooling will be more efficient, and it will extinguish in a shorter time. The moment of the whip release, however, should be chosen such that dielectric back re-strike of the arc between the main blades is avoided.

Actually the effect of a high-speed interrupter and the air flow can also be understood from the breakdown voltages (see Figures 5.20 and 6.10). Figure 10.2 conceptually depicts the breakdown voltage versus time with high-speed interrupter, and with cold and hot air qualitatively at the same gap length.

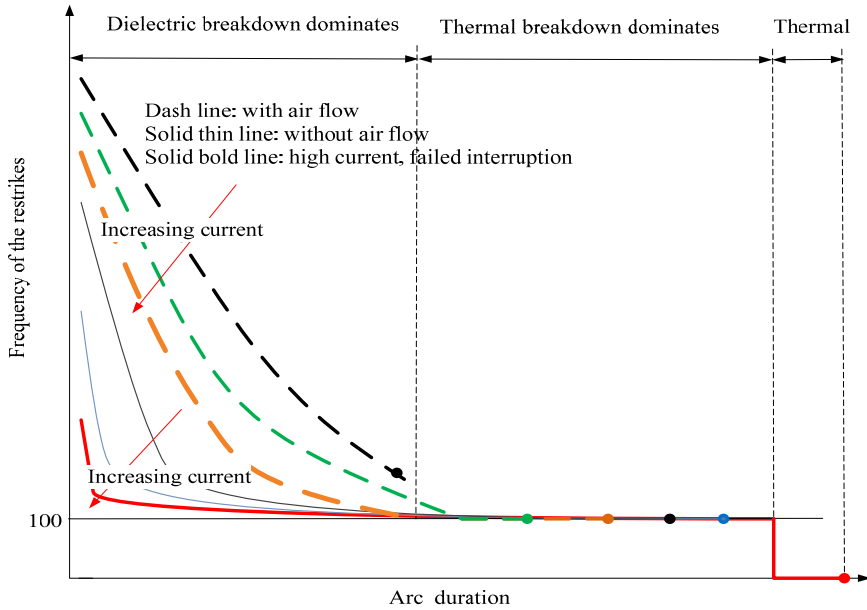


Figure 10.1. Frequency of re-strikes with and without air flow with the interrupted current as a parameter.

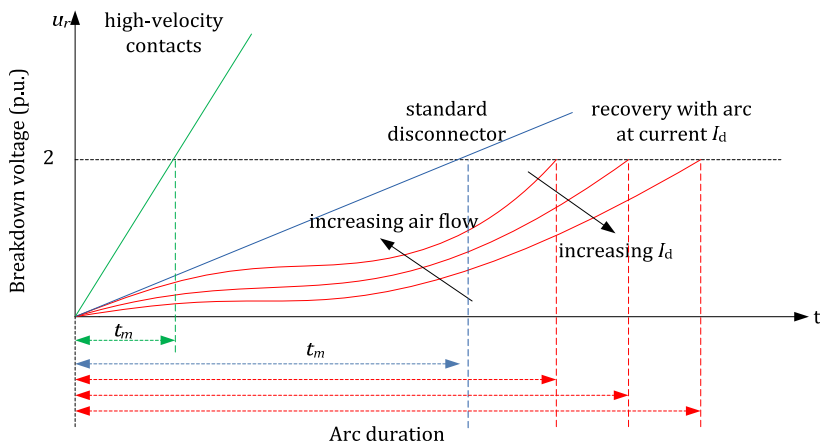


Figure 10.2. Breakdown voltage against time with high-velocity contacts, standard disconnector and recovery with arc at varying currents.

In the cold air, the dielectric recovery voltage increases with cooling and removal of the residual plasma by convection. The breakdown voltage is proportional to the gap distance. However, for higher currents the breakdown voltage is lower due to the influences from a previous arc. With air flow, the breakdown voltage is

higher due to the stronger convective plasma removal (see Figure 6.10); with the assistance of a high-speed interrupter, the dielectric recovery develops even faster because of forced convection coming from the surrounding cool air in a very short time. In this sense, cooling the arc either by dragging it into a cold environment (high-speed auxiliary switch) or by supplying cold air (air flow) is the essential process.

Since the maximum recovery voltage the circuit is able to supply is limited to 2 p.u., the arc will stop when the breakdown voltage of the medium has reached this voltage. There is minimum arc duration (t_m) for high-velocity and standard disconnector, shown in Figure 10.2. For the interruptions with disconnecting under arcing, the arc duration increases with higher interrupted current.

10.2 Proposed future research

The condition of the (ionized) air left from previous re-strikes is a main issue in understanding capacitive current interruption with a disconnector. The physical phenomena discussed in Chapter 9 only provide a rough background.

Quantitative understanding of the influence of arc temperature, degree and amount of ionization in the air gap on the breakdown development and the dielectric recovery could be worthwhile for further investigation.

For the free burning arc in air there is no proper arc model covering the range of currents occurring in the disconnector. This point is addressed in Chapter 5 but research, e.g. along the line of the approach proposed in the review given in Chapter 2 may be carried out further.

Interruption with the assistance of a pre-inserted resistor is theoretically and experimentally only basically studied in Chapter 8. Future experimental work could be carried out in order to address the resistance value in terms of current reduction, heat dissipation and difficulties related with the insertion of (high value) resistors into the circuit. The merits of applying non-linear components could also be considered.

Ablation assisted arc extinction is presently only used for relatively high current interruption. The feasibility for low current levels, studied here, can be investigated. Such study could include new materials, which suit best with the application on disconnectors for relatively low capacitive currents.

Publications related to this work

- [1] Y. Chai, P. A. A. F. Wouters, R. P. P. Smeets, "Capacitive Current Interruption by HV Air-Break Disconnectors With High-Velocity Opening Auxiliary Contacts", *IEEE Trans. on Power Delivery*, vol. 26, pp. 2668-2675, Oct. 2011.
- [2] Y. Chai, P. A. A. F. Wouters, R. T. W. J. van Hoppe, R. P. P. Smeets, D. F. Peelo, "Capacitive current interruption with air-break high voltage disconnectors", *IEEE Trans. on Power Delivery*, vol. 25, pp. 762-769, Apr. 2010.
- [3] Y. Chai, P. A. A. F. Wouters, R. P. P. Smeets, "Arc imaging on capacitive current interruption using a disconnector with an auxiliary interrupter", in *Proc. IEEE Asia-Pacific Power and Energy Engineering Conf.*, Wuhan, 4p, Mar. 2011.
- [4] Y. Chai, P. A. A. F. Wouters, R.T.W.J. van Hoppe and R. P. P. Smeets, "The influence of air flow on current interruption with air-break HV disconnectors", in *Proc. the 17th International Symposium on High Voltage Engineering Conf.*, Cape Town, 6p, Aug. 2011.
- [5] Y. Chai, P. A. A. F. Wouters, S. Kuivenhoven, P. van der Wal, M. Vanis, R. P. P. Smeets, "Current interruption phenomena in HV disconnectors with high-speed opening auxiliary contacts", in *Proc. IEEE Power and Energy Society GM Conf.*, Minneapolis, 8p, Jul.2010.
- [6] Y. Chai, P. A. A. F. Wouters, R. T. W. J. van Hoppe, R.P.P. Smeets, "Arc images during small capacitive current interruption with HV air-break disconnectors", in *Proc. the 18th International Conference on Gas Discharges and Their Applications Conf.*, Greifswald, pp. 158-161, Sept. 2010.
- [7] Y. Chai, P. A. A. F. Wouters, R. T. W. J. van Hoppe, R. P. P. Smeets, D. F. Peelo, "Experiments on capacitive current interruption with air-break high voltage disconnectors", in *Proc. IEEE Asia-Pacific Power and Energy Engineering Conf.*, Wuhan, 6p, Mar. 2009.
- [8] Y. Chai, P. A. A. F. Wouters, R. T. W. J. van Hoppe, R. P. P. Smeets, "Arc behaviour in small capacitive current interruption with high voltage air-break disconnector", in *Proc. the 16th International Symposium on High Voltage Engineering Conf.*, Hannover, paper nr. G-19, 6p, Aug. 2009.

Nomenclature

Abbreviations

AC	Alternating current
CT	Current transformer
CVT	Capacitive voltage transformer
CN	Cumulative number
CO	Close and open
DS	Disconnecter
DSs	Disconnectors
DC	Direct current
HF, MF, PF	High-, medium-, power-frequency
HV	High voltage
GIS	Gas insulated substation
G	Short-circuit generator
M	Master breaker
p.u.	Per unit
Rms	Root mean square
RV	Recovery voltage
S	Make switch
TR	Short-circuit transformer

Symbols

ω	Angular velocity
ω_p	Angular power-frequency of u_s
ω_H, ω_M	Oscillation angular frequency at HF, MF
δ_H, δ_M	Damping constant at HF, MF
θ	Initial angle of u_s
θ_1	Rotation angle of the frame related to the position parallel of the DS blades
θ_2	Rotation angle of the strip related to the position parallel of the DS blades
$\theta_{1,0}$	Initial value of the θ_1
$\theta_{2,0}$	Initial value of the θ_2
τ	Time constant of the decay of hot gas left from arc
a	Acceleration of the released whip
Δt_1	Current zero lasting period
Δt_2	Current (not zero values) lasting period before the breakdown occurs
C	Capacitance

C_H	Capacitance of C_s, C_l in series
C_s, C_l	Capacitance at the source and load side
$C_{1...10}$	Capacitors for voltage divider
B_k	Sum of the brightness of a frame
$B_{(ij)}^{(k)}$	Brightness of the k^{th} frame
$CH_{1...4}$	FrontEnd channels
d	Whip contact separation
$D_{1...4}$	Voltage divider
di/dt	Current derivative at current zero crossing
E_m	Amplitude of u_s
E	Electric field strength of the air gap
f	Frequency
H	Arc height of the against the blades at original position
I_{sc}	Short-time withstand current of a circuit breaker
i_d	Current through the disconnecter
i, j	Coordinates of a image pixel
I_d	rms of i_d
I_{max}	Amplitude of the current through the DS
i_H, i_M	Current through the disconnecter at HF and MF
i_{pf}	Current through DS measured at a low bandwidth
I_{hf}	Current through DS measured at a high bandwidth
i_a	Arc current
k_B	Boltzmann constant
L_s	Inductance at the source
L_H	Equivalent inductance of HF loop
L_a	Arc length
N	Gas density (specify moles per volume or number of molecules per volume)
N_k	Normalized brightness of a frame
N_0	Normalized brightness of the first frame in a video recording
N_{arc}	Brightness of the arc after correction with a background frame
P	Pressure
RV_{max}	Peak of the recovery voltage
R_s	Resistance at the source
R_H	Equivalent resistance of HF loop
R	Resistor
T_{arc}	Arcing time
T	Absolute temperature
u_{cs}, u_{cl}	Voltage across C_s and C_l

u_d	Voltage across the disconnecter
U_r	Re-strike voltage of the air gap
U_{line}	rms value of the system voltage
U_E	Equalization voltage after HF oscillation
u_{CM}	Voltage across C_s and C_l at MF
U_{cs}, U_{cl}	Voltage across C_s, C_l at the moment of a restrike
U_{gap}	Gap withstand voltage
u_i	Input voltage of the voltage divider of D_1 during calibration
u_{in}	Input voltage of the adjustable transformer
u_o	Output voltage of the voltage divider of D_1 during calibration
u_{out}	Output voltage of the adjustable transformer
U_{oc}	Voltage across the disconnecter after switching off
u_a	Arc voltage instantaneous value
U_a	Arc voltage mean value
v_{air}	Opening velocity of the air gap
u_s	Instantaneous source voltage value, phase-to-ground voltage
v_0	Initial speed of the released whip
w	Energy input the circuit upon restrike
w_R	Energy dissipation of the resistor

Acknowledgement

This thesis would not have been finished without the efforts from many people. I would like to make use of this opportunity to show my personal gratitude to those who supported me during the course of this work.

First of all, I am indebted to my promotor, prof.dr.ir. René Smeets for accepting me as his Ph.D. student. I am very much appreciative for his enthusiastic encouragement, guidance and support from the very beginning to the final stage of this work and my stay at TU/e. He is intelligent, analytical, constructive, as well as diplomatic, kind, considerate and caring in social life.

I also owe my deepest gratitude to my co-promotor dr. Peter Wouters. His down-to-earth attitude, high level knowledge, always fast and very carefully reviewing all my paper work within last four years are indeed remarkable. On many weekends, holidays, twilight hours, I saw the light on in his office which was such an inspiration to me. I enjoyed a lot working with him, travelling and even sharing some important festivals. I also thank his wife Fen for her fabulous food and their daughter Yan for taking care of Ruirui.

I thank the sponsors for this project: IOP-EMVT for funding, HAPAM for contributing test objects and allowing to measure during testing in Prague, Enexis for its generous supply of capacitors loads and KEMA for supplying laboratory test space.

Further, I would like to thank all the committee members, prof. dr-ing. V. Hinrichsen, prof. ir. L. van der Sluis, prof. dr. E. Lomonova, dr. D. F. Peelo and prof. ir. W. L. Kling. Thanks for their time on reading my thesis and giving me very constructive feedbacks. Special thanks go to dr. David Peelo for his recommendations and his two visits all the way from Canada.

Furthermore, a lot of thanks go to ing. René van Hoppe. He did a lot of work for my experimental setup. Without his smart ideas and great help the experiments would not be fulfilled. I also thank Nilles Vrijssen for his interest in calculating the disconnecter blades moving speed during his internship with me. Special thanks go to ir. Sander Kuivenhoven from KEMA, ing. Paul van der Wal from HAPAM, Sjoerd van Driel from TU/e for their help during the tests in KEMA laboratories and other suggestions for this project. I also thank ir. Ad van Venrooij for his help on the circuit drawings in the last moment of finalizing the thesis.

It is an honour for me to show my thankfulness to many colleagues and staff from the EES group for their general suggestions and caring the progress of this thesis from time to time. I thank all my (former) fellow Ph.Ds., Sharmistha, Shima, Zhen,

Rong, Vlada, Petr, Peter, Totis, Lei, Jasper, Anton, Paul, Arjan, Geesje, Glenn, Pavlo, Phuong, Vuong, Ioannis, Yan, Yu, Jin, Ballard, Jerom, Helder and many I still have forgotten to mention, I enjoyed very much to the time spent with you not only in our official coffee room but also in the external coffee corner. Thank you guys for being part of my Ph.D. life.

Big thanks go to my personal friends from TU/e, and also those friends I met at Regional International School in Eindhoven. Thank you for sharing all useful and 'gossipy' information about everything. You know how important it is to have all of you around.

Finally I am grateful to my Chinese and Serbian family, especially my beloved husband Miloš for his never-ending love, support, understanding and encouragement. Of course, our always positive and joyful daughter Ruirui is a powerful source of inspiration and energy. Life becomes so colourful being with you two together.

Yajing Chai

24th, Jan. 2012

Curriculum Vitae

Yajing Chai was born on 08-01-1975 in Hubei, China. She received her B.Sc. and M.Sc. degree from Wuhan University in 1996 and 2001 respectively at the High Voltage Group of Electrical Power Engineering. From 1996 till 2004, she was a laboratory assistant and a lecturer with the Department of Electrical Engineering of Wuhan University. She was an exchange young scholar at Belgrade University, Serbia between 2004 and 2005. From 2005 to 2007, she was a researcher with the High Voltage Institute of Wuhan University. In 2008 she joined the Electrical Energy Systems group at Eindhoven University of Technology, the Netherlands, as a Ph.D. candidate under the supervision of prof.dr.ir. R.P.P. Smeets and dr. P.A.A.F. Wouters.